



Ph.D. Thesis by
Antje Fitzner

Modeling the tidewater glacier Kangiata Nunaata
Sermia and the freshwater flux into
Godthaabsfjorden



The PhD School of Science,
Faculty of Science,
University of Copenhagen
Denmark.

Submitted: September 2014

Advisor: Dorte Dahl-Jensen
University of Copenhagen, Denmark

Antje Fitzner
Niels Bohr Institute
University of Copenhagen
Juliane Maries Vej 30
DK-2100 København Ø
Denmark

fitzner@gfy.ku.dk
<http://www.gfy.ku.dk/fitzner>

This Ph.D. thesis has been submitted to the PhD School of The Faculty of Science,
University of Copenhagen, in September 2014.



Figure 0: The calving front of Kangiata Nunaata Sermia. Picture taken by Peter S. Mikkelsen.

Abstract

The Greenland ice sheet loses mass due to changing surface mass balance, direct melting on the surface, ice flow through the numerous outlet glaciers, and basal melt. This Ph.D. thesis focuses on the outlet glaciers terminating in Godthåbsfjord near Nuuk in West Greenland, with Kangiata Nunaata Sermia (KNS) being the main contributing glacier. The mass loss of this glacier forms a small contribution to the total mass loss of the Greenland ice sheet, but it will have a large impact on the local ecosystem when there is a large freshwater flux into the fjord. Here, two independent methods are used to estimate the total mass loss by KNS and its neighboring outlets, namely an ice sheet model applied to KNS and stable oxygen isotope measurements in the fjord.

The Parallel Ice Sheet Model (PISM) is applied to model current and future mass loss. A parameter study is conducted to select the best parameter settings matching observed surface velocities and observed ice thickness. A monthly mean climatic forcing is applied to these best settings to investigate the individual components of the total fluxes. The model reproduces the present behavior of KNS. Also, seasonal variations are modeled. The modeled solid ice flux, surface velocities, and total mass flux agree well with the observed surface velocities, calving flux estimates, and elevation changes.

The glacier is currently losing mass and will continue to lose mass. Using present day climate without additional warming, the KNS drainage basin will likely suffer a mass loss of (4.2 ± 2.9) km³/yr water equivalent (w.e.). The best model run suggests a mass loss of 3.0 km³/yr w.e. until 2050. Adding an increase in temperature, following the Representative Concentration Pathway (RCP) scenarios, the expected mass loss is (10.3 ± 2.6) km³/yr w.e until 2050.

Due to the lack of successful bed elevation measurements, the bed topography underneath KNS is basically unknown. Here, a simple iterative method is presented to adjust the bedrock map using observed surface velocities. This method is tested on Greenland's largest outlet glacier, Jakobshavn Isbræ, and applied to KNS afterwards.

Also, available data on freshwater fluxes from land and glaciers and measurements of salinity and stable oxygen isotopes in Godthåbsfjord, taken between 2007 and 2010,

are used in order to determine the relative contribution from the various freshwater sources into the fjord. To this end, the seasonal signal of salinity and stable oxygen isotopes is analyzed.

A box model is used to compute the freshwater contributions from the glaciers from oceanographic measurements. The model identifies critical parameters for quantifying glacial meltwater and run-off into the fjord system. These critical parameters include the stable oxygen isotope composition of glacial ice, run-off and seawater, and transport in the surface layer. With a better knowledge of the discussed parameters, such as the velocity in the surface layer and the isotopic signature of glacial ice, the uncertainties in the estimates of the various freshwater sources can be reduced significantly.

According to this study, there is (11.5 ± 2.3) km³/yr freshwater entering the fjord, (7.8 ± 6.4) km³/yr of which from glacial meltwater (excluding surface melt) and (3.8 ± 8.7) km³/yr of which from run-off of surface melt water. Downscaling the modeled results allow us to estimate the individual glacier contributions. KNS contributes 4.8 km³/yr glacial meltwater and 1.4 km³/yr run-off. Hence, the total freshwater coming from this glacier is 6.2 km³/yr.

Dansk Resumé

Den grønlandske indlandsis oplever et massetab på grund af ændringer i overfladens massebalance, direkte afsmeltning af overfladen, isflydning fra talrige gletsjere og smeltning ved bunden. Denne Ph.D. afhandling fokuserer på de udløbsgletsjere der flyder ud i Godthåbsfjorden ved Nuuk i Vestgrønland, hvor Kangiata Nunaata Sermia (KNS), er den primære udløbsgletsjer. Massetabet fra denne gletsjer udgør en lille del af det samlede massetab fra Grønlands indlandsis, men det kan have en stor indflydelse på det lokale økosystem når store mængder ferskvand tilføres fjorden. I denne Ph.D. anvendes to uafhængige metoder for at estimere det samlede massetab fra KNS og dens nabogletsjere: en isflydemodel af KNS og målinger af stabile ilt-isotoper i fjorden.

Det nuværende og fremtidige massetab modelleres med isflydemodellen “Parallel Ice Sheet Model” (PISM). Effekten af aktuelle parametre er undersøgt og de optimale parameterindstillinger er valgt på baggrund af overensstemmelse med overfladehastigheder og den observerede istykkelse. Parameterindstillingerne bliver forceret med et gennemsnitligt, månedligt klima for at undersøge de individuelle komponenter af den totale flux. Modellen reproducerer den nuværende tilstand af KNS. Sæsonmæssige variationer bliver også modelleret og den modellerede isflux, overfladehastigheder og totale masseflux stemmer overens med observationer af overfladehastigheder, fluxen fra kælving ved isfronten samt højdeændringer.

Gletsjeren mister i øjeblikket masse og vil fortsætte med at miste masse. KNS dræningsbassinet vil sandsynligvis opleve et massetab på (4.2 ± 2.9) km³ vand pr. år for et klima svarende til det nuværende uden øget opvarmning. Den bedste modelkørsel antyder et massetab på 3.0 km³ vand pr. år ind til 2050. Hvis temperaturen derimod følger “Representative Concentration Pathway (RCP)” scenarier er det forventede massetab (10.3 ± 2.6) km³ vand pr. år.

Bundens topografi under KNS er stort set ukendt på grund af manglende succes med topografi målinger. Her præsenteres en simpel, iterativ metode til at modellere bundtopografien ved brug af observerede overfladehastigheder. Metoden er testet på Grønlands største udløbsgletsjer: Jakobshavn Isbræ. Herefter er metoden også benyttet for KNS.

Herudover anvendes data fra målinger af ferskvandsflux fra land og gletsjere, samt

målinger af salinitet og stabile ilt-isotoper for Godthåbsfjorden, indsamlet i perioden 2007 til 2010, til at bestemme det relative bidrag fra de forskellige ferskvandskilder. På denne måde kan det sæsonmæssige signal af salinitet og stabile ilt-isotoper analyseres.

En boks-model bruges til at beregne ferskvandsbidraget fra gletsjerne udfra oceanografiske målinger. De kritiske parametre for at beregne mængden af glacialt smeltvand og afstrømning til fjordsystemet identificeres af modellen. Disse kritiske parametre inkluderer den stabile ilt-isotopsammensætning af gletsjeris, afstrømning og havvand, samt transporten i overfladelaget. Med øget viden om de omtalte parametre, som for eksempel hastigheden i overfladelaget og den isotopiske sammensætning af gletsjeris, kan usikkerhederne på estimerne af de forskellige ferskvandskilder kraftigt reduceres.

I følge dette studie tilføres der (11.5 ± 2.3) km³/år ferskvand til fjorden, hvoraf (7.8 ± 6.4) km³/år stammer fra gletsjer-smeltvand (eksklusive overfladesmeltning) og (3.8 ± 8.7) km³/år fra afstrømning af overfladesmeltvand. Ved at nedskalere modelresultaterne kan de individuelle bidrag fra de forskellige gletsjere vurderes. KNS bidrager med 4.8 km³/år glacialt smeltvand og 1.4 km³/år afstrømning, og dermed er det totale ferskvandsbidrag fra gletsjeren 6.2 km³/år.

Acknowledgements

This work has been carried out at the Centre for Ice and Climate (CIC) at the Niels Bohr Institute, University of Copenhagen, between September 2010 and September 2014. This period includes one year of maternity leave. My project was funded by the Niels Bohr Institute (NBI) and the Greenland Climate Research Centre (GCRC).

First and foremost, I would like to thank my advisor Dorte for having given me the opportunity to do my Ph.D. research at CIC and for her valuable help and guidance.

Next, thank you to the modeling group at CIC, who helped and inspired me during weekly meetings and in between. Many thanks go to my co-modelers at CIC, Nanna, Anne, Sebastian and Christine, and elsewhere in Copenhagen, Tolly, Ruth, Dirk and Andreas. Special thanks to Nanna and Helle for writing the *Dansk Resumé*. And thank you to everyone at CIC for creating a very pleasant and motivating work environment.

Thanks to the NEEM community, who gave me the opportunity to assist with the ice core drilling in the NEEM camp, which was a very memorable experience.

I would like to thank the PISM group, especially Andy, Ed, Daniella and Constantine, for the help to set up PISM and answering many questions. Also, I would like to thank the PISM group for hosting me for two months during my academic stay abroad. I had a great time in Fairbanks and learned a lot about PISM.

Furthermore, I want to thank my friends in my hometown Goch for always showing interest in what I do. Also, thanks to my friends from Nijmegen, Janneke, Madelon and Matthias, who also have moved on to other places in Europe.

I would like to thank my family. My parents and my brother for always supporting me. Special thanks go out to my parents, who helped taking care of Elise in the last two months so that I could finish my Thesis.

Thank you to Tim and Elise. Tim, without you I would not have moved to Copenhagen. Thank you for your unconditional support. And thank you to Elise for always making me happy, and without whom this Thesis would have been finished one year earlier.

Antje Fitzner, Copenhagen, September 2014

Contents

Abstract	i
List of Symbols	xi
Abbreviations	xiii
1 Introduction	1
1.1 Godthåbsfjorden and Kangiata Nunaata Sermia	2
1.2 Ice Sheet Models	4
1.3 Overview	5
2 From Continuum Mechanics to Ice Sheet Model	7
2.1 Rheology	8
2.2 Deformation	9
2.3 Conservation Laws	10
2.3.1 Mass Conservation	10
2.3.2 Momentum Conservation	11
2.3.3 Energy Conservation	11
2.4 Flow Law	13
2.4.1 Creep Flow	13
2.4.2 Mass Balance	15
2.4.3 Driving Stresses	18
2.4.4 Basal sliding	19
2.5 Full Stokes Model and Assumptions	20
2.5.1 Full Stokes Model	21

2.5.2	Shallow Ice Approximation	21
2.5.3	Shallow Shelf Approximation	22
2.6	Numerical Methods	23
2.7	The Parallel Ice Sheet Model	24
2.7.1	Ice Flow	24
2.7.2	Calving	26
2.8	Restrictions	26
2.A	Index Notation	27
2.B	Gauss' Divergence Theorem	28
2.C	Leibniz Integral Rule	28
3	Input Data and Initialization	29
3.1	Bed and Surface Elevation	29
3.1.1	Drainage Basin	32
3.1.2	Ice-Penetrating Radar	34
3.2	Climatic Forcing	36
3.3	Surface Velocities	39
3.4	Initialization and Spin-Up	41
3.5	Example Output	43
4	Modeling the Present and Future Behavior of KNS	45
4.1	Parameter Selection	45
4.2	Current Velocities and Fluxes	49
4.2.1	Monthly Mean 1990–2011	52
4.3	Future Predictions	57
4.4	Representative Concentration Pathway Scenarios	59
4.5	Discussion and Conclusion	60
5	Inverse Model for Bed Elevation	63
5.1	Method	64
5.2	Validation using Jakobshavn Isbræ	65
5.3	Application to KNS	68
5.4	Discussion and Conclusion	70

6	The glacial meltwater contribution to the freshwater budget	73
6.1	Data Description	74
6.2	Box Model	77
6.2.1	Downscaling	79
6.3	Salinity and $\delta^{18}\text{O}$ Estimates	79
6.4	Results	80
6.4.1	Downscaling	82
6.5	Discussion	82
6.5.1	Sensitivity	83
6.6	Conclusion	84
7	Conslusions and Outlook	87
7.1	Outlook	88
7.2	Impact	91
A	Poster EGU 2012: Modelling the outlet glaciers terminating in Godthåbsfjord.	93
B	Poster IGS 2013: Modelling the outlet glaciers terminating in Godthåbsfjord.	95
C	Poster EGU 2013: Modeling the present and future behavior of the glaciers terminating into Godthåbsfjord, West Greenland	97
D	Poster EGU 2013: Estimating the glacial meltwater contribution to the fresh water budget from salinity and $\delta^{18}\text{O}$ measurements in Godthåbsfjord	99
E	Manuscript submitted to The Cryosphere: Modeling Present and Future Behavior of the Tidewater Glacier Kangiata Nunaata Ser-mia, West Greenland	101
F	Manuscript submitted to Journal of Geophysical Research Earth Surface: Estimating the glacial meltwater contribution to the fresh-water budget from salinity and $\delta^{18}\text{O}$ measurements in Godthåbs-fjord	115

List of Symbols

A rate factor [dimensionless]	g gravitational constant [m/s ²]
$\mathbf{a}_{a/b}^\perp$ volume flux through surface/base [m ³ /s]	h surface elevation [m]
α factor controlling the pore water pressure [dimensionless] or angle [°]	H ice thickness [m]
B base [m ²]	\mathbf{H}_w water depth at the terminus [m]
b bed elevation [m]	I unit matrix [dimensionless]
β Clausius-Clapeyron constant [7.42 · 10 ⁸ to 9.8 · 10 ⁸ K/Pa] or angle [°]	\mathbf{k}_c calving coefficient [dimensionless]
β^2 drag factor [Pa yr/m]	\mathbf{k}_T thermal conductivity [6.62 · 10 ⁻⁷ J/m/K/yr for ice]
\dot{c} calving flux [kg/s]	L length of the inner fjord section [m]
c specific heat capacity [J/kg/K]	M mass [kg]
C constant in the bed elevation adjustment [m]	\mathbf{M}_T total mass balance [km ³ /yr]
D surface layer thickness [m]	μ positive friction coefficient [dimensionless] or viscosity [Pa s]
e enhancement factor [dimensionless]	n normal vector [dimensionless] or exponent in the flow law [dimensionless]
\dot{E} energy rate [J/s]	N effective pressure [Pa]
\mathbf{E}_a activation energy [J]	$\mathbf{N}_{s/b}$ normal gradient at surface/base [dimensionless]
ϵ strain [dimensionless]	p pressure [Pa]
$\dot{\epsilon}$ strain rate [s ⁻¹]	\mathbf{p}_w pore water pressure [Pa]
G geothermal heat flux [W/m ²]	ϕ till friction angle [°]

q volume flux [m^3/s] or exponent of the pseudo-plastic basal resistance model [dimensionless]	τ_d driving stress [Pa]
R general gas constant [8.31 J/mol/K]	τ_c yield stress [Pa]
ρ density [917 kg/ m^3 for ice]	τ_b basal drag or basal shear stress [Pa]
S surface [m^2] or salinity [psu]	u velocity [m/s]
σ stress [Pa]	u_b sliding velocity [m/s]
σ_M normal stress [Pa]	u_{thr} velocity threshold in the pseudo- plastic basal resistance model [m/s]
T temperature [K]	V volume [m^3]
T_{pmp} pressure melting point [K]	W width of the fjord [m]
τ deviatoric stress [Pa]	w basal water thickness [m] or the velocity of a surface [m/s]

Abbreviations

AS Akullerssuup Sermia	GCRC Greenland Climate Research Centre (http://www.natur.gl/en/climate-research-centre/)
AWS Automatic Weather Stations	
BMB Basal Mass Balance	
BP Before Present	GEUS Geological Survey of Greenland and Denmark (http://www.geus.dk/DK/Sider/default.aspx)
CIC Centre for Ice and Climate (http://www.iceandclimate.nbi.ku.dk/)	
CMIP5 Coupled Model Intercomparison Project Phase 5	GPS Global Positioning System
CRISIS Center for Remote Sensing of Ice Sheets (https://www.cresis.ku.edu)	HIRHAM <i>HIRLAM</i> and <i>ECHAM</i>
CTD conductivity-temperature-depth	HIRLAM High Resolution Limited Area Model
DEM Digital Elevation Model	ICESat Ice, Cloud, and land Elevation Satellite
DMI Danish Meteorological Institute (http://www.dmi.dk/)	InSAR Interferometric Synthetic Aperture Radar
ECHAM ECMWF (European Centre for Medium-Range Weather Forecasts) and HAMBURG	IPCC Intergovernmental Panel on Climate Change (http://www.ipcc.ch/)
FDM Finite Difference Method	ISM Ice Sheet Model
FEM Finite Element Method	ISSM Ice Sheet System Model (https://issm.jpl.nasa.gov/)
FS Full Stokes	KNS Kangiata Nunaata Sermia
GCM Global Circulation Model	KS Kangilinnguata Sermia

LT Lake Tasersuaq	RMS Root-Mean-Square
MAR Modele Atmosphérique Regional	SeaRISE Sea-level Response to Ice Sheet Evolution (http://websrv.cs.umt.edu/isis/index.php/SeaRISE_Assessment)
MM Monthly Mean	
NS Narsap Sermia	
PISM Parallel Ice Sheet Model (http://www.pism-docs.org/wiki/doku.php)	SIA Shallow Ice Approximation
QS Qamanaarssuup Sermia	SMB Surface Mass Balance
RACMO Regional Atmospheric Climate Model	SSA Shallow Shelf Approximation
RCM Regional Climate Model	UAF University of Alaska Fairbanks (http://glaciers.gi.alaska.edu/)
RCP Representative Concentration Pathway [Meinshausen et al., 2011]	w.e. water equivalent
	YM Yearly Mean

1 | Introduction

An ice sheet is a large piece of ice that spreads under its own weight. Typically, it has a diameter of thousands of kilometers, and a thickness of three kilometers at its center. There are two large ice sheets on Earth, the Greenland and the Antarctic ice sheet, which together form the world's largest freshwater storage. Both ice sheets have been losing mass in the recent decades [IPCC, 2013]. This thesis focuses on the outlet glaciers of the Greenland ice sheet terminating in Godthåbsfjord, near Nuuk in West Greenland.

The total mass of the Greenland ice sheet is estimated to be $2.93 \cdot 10^6$ Gt [Bamber et al., 2001]. Its mass loss increased from 34 Gt/yr or 0.09 mm/yr sea level rise (during 1992–2001) to 215 Gt/yr or 0.59 mm/yr (during 2002–2011) [IPCC, 2013, Chapter 4.4]. A mass loss of 375 Gt/yr during 2011–2013 was measured [Helm et al., 2014]. The whole Greenland ice sheet would hypothetically correspond to a sea level rise of 7 m [Holland et al., 2008].

Ice loss through the numerous outlet glaciers accounts for about half of the total mass loss of the Greenland ice sheet [van den Broeke et al., 2009]. The other half is run-off of surface melt. However, this distribution differs for different areas in Greenland. In the South-West, where the outlet glaciers terminating in Godthåbsfjord are located, the surface mass balance changes dominate [IPCC, 2013, Chapter 4.4]. Most outlet glaciers are accelerating, which leads to the assumption that the overall climate is responsible for the continued mass loss [Luckman et al., 2006]. However, there are more mechanisms one needs to take into account when considering mass loss, namely deformation and the movement of the ice sheet by sliding over the glacier bed. Zwally et al. [2002] show that water from the surface penetrates through the ice sheet at the margins. As a consequence, the velocity increases. High velocities give rise to frictional heating at the bed that can result in basal melt. Generally, basal melt accounts for a small amount of the total mass balance, but larger contributions of 5% have been reported for e.g. Columbia glacier in Alaska [Alexander et al.,

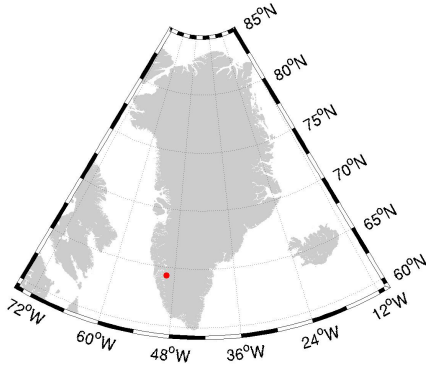


Figure 1.1: The island of Greenland, with the location of KNS indicated in red.

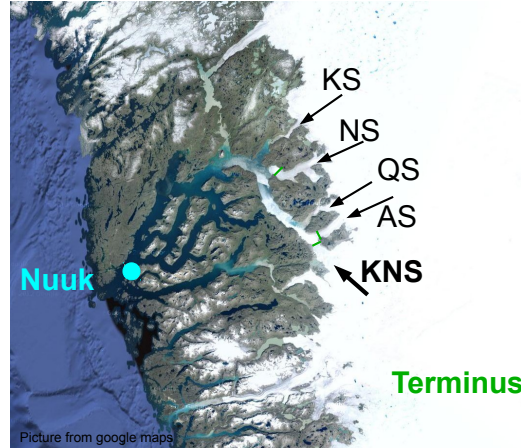


Figure 1.2: Godthåbsfjord in West Greenland with the city of Nuuk at the fjord entrance. At the inner part of the fjord, there are three tidewater glaciers, namely Kangiata Nunaata Sermia (KNS), Akullerssuup Sermia (AS) and Narsap Sermia (NS), and two land-terminating glaciers, namely Qamanaarssuup Sermia (QS) and Kangilinnuata Sermia (KS).

2013]. Also, submarine melting can be a significant part of mass loss [Motyka et al., 2003, e.g.]. Holland et al. [2008] suggest that the speed-up of outlet glaciers at the Greenlandic West coast around 1997 are a result of ocean warming. Calving of icebergs accounts for another important part of mass loss. Calving laws often rely on empirical relationships, especially when implemented in ice sheet models [IPCC, 2013, Chapter 4.4].

1.1 Godthåbsfjorden and Kangiata Nunaata Sermia

As mentioned above, this thesis focuses on the outlet glacier Kangiata Nunaata Sermia (KNS) in West Greenland, terminating in Godthåbsfjord. Its location is shown in Figure 1.1. The terminus width is ~ 4.5 km and the terminus height is estimated to be 250 m. Godthåbsfjord is a 190 km long and complex fjord system with several tidewater and land-terminating glaciers. At the inner part of the fjord, there are three tidewater glaciers, namely KNS, Akullerssuup Sermia (AS) and Narsap Sermia (NS), and two land-terminating glaciers, namely Qamanaarssuup Sermia (QS) and Kangilinnuata Sermia (KS), as shown in Figure 1.2.

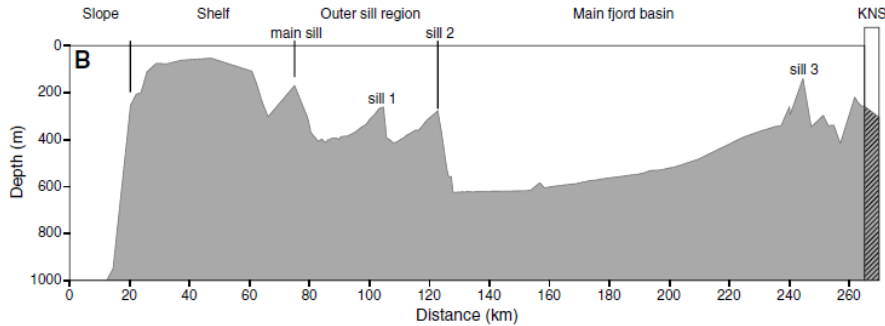


Figure 1.3: The depth profile of the fjord. Nuuk is on the left, near sill 1, and KNS is on the right end. Figure taken from Mortensen et al. [2013, Figure 1b].

The depth profile of the fjord is shown in Figure 1.3. At the fjord entrance, the main sill has a depth of 170 m, whereas the continental shelf is only 50 m deep. Inside the fjord, there are more sills, and the sill closest to KNS is ~ 160 m deep and located 21 km away from KNS [Mortensen et al., 2013, 2011]. These sills are likely to be former stable pinning points for the glaciers [Fischer, 1998]. The deepest part of the fjord is about 600 m.

For Godthåbsfjord, many oceanographic measurements were done from 2006 and onwards. From the conductivity-temperature-depth (CTD) measurements, the circulation inside the fjord is analyzed [Mortensen et al., 2013, 2011].

Several total mass loss estimates for the region are available based on different methods. The total discharge of KNS, excluding subglacial discharge, obtained from frontal velocities and fjord bathymetry, is estimated to be (7.6 ± 1.5) km³/yr of ice [Mortensen et al., 2013]. Mass loss of KNS measured by the Ice, Cloud, and land Elevation Satellite (ICESat, covering the period 2003–2008) for KNS is 2.49 km³/yr of ice [Sørensen et al., 2011]. This estimate is based on surface elevation changes. Discharge estimates for KNS and NS combined, based on measured surface velocities, are 8.1 km³/yr of ice in 1958, 1964 and 1996, 9.8 km³/yr of ice in 2000 and 2004, and 12.1 km³/yr of ice in 2005–2007 [Rignot et al., 2008]. KNS’s total mass loss in 2010 from surface mass balance and frontal ablation is 4.6–5.5 km³/yr of ice [van As et al., 2014]. An estimate based on surface velocities and ice thickness is (5 ± 1) km³/yr of ice (Podrasky, private communication).

For most Greenlandic outlet glaciers surface velocities have increased in the recent decades. Rignot and Kanagaratnam [2006] computed a speed-up of 6% from 1996 to 2000, and 27% from 2000 to 2005. The surface velocity of the neighboring outlet glacier NS, which terminates into the same fjord, increased by 68% and 150%

during the same periods. Rignot and Mouginot [2012] showed that the changes in Godthåbsfjord have been small compared to outlet glaciers in neighboring fjords. This may be due to the fact that there is a shallow sill at the fjord entrance that protects the fjord from inflow and hence from warmer ocean temperatures. KNS is the only glacier in the South-West that retreated by as much as 580 m during 2006–2007 [Moon and Joughin, 2008]. Thomas et al. [2009] showed that KNS thinned by several meters per year between 1993 and 1998. Between 1998 and 2001, thinning has increased to 8 m/yr.

Thomas et al. [2009] have analyzed one flight line along KNS. The successful sounding shows the bed to be above sea level, but about 40 km upstream, it slopes downwards. In 2009 and 2011, the Center for Remote Sensing of Ice Sheets (CReSIS) carried out radar missions near Nuuk to retrieve the bed elevation underneath KNS. Unfortunately, the ice close to the margin is too wet, so the bed could not be detected in the proximity of the terminus, in particular in the part where the ice is flowing fastest. There are no successful measurements until ~ 30 km from the terminus.

1.2 Ice Sheet Models

To understand the past, present and future behavior of ice sheets and glaciers, ice sheet models (ISMs) are developed. The simplest type of model is a flow-line model. Several flow-line models have been developed with the purpose of modeling local features such as ice streams and outlet glaciers, e.g., in Nick and Oerlemans [2006] and Nick et al. [2013]. These models are also applied to KNS in Lea et al. [2014a,b] for the period 1859 to present.

At the moment, several three-dimensional models are available, such as CISM (Community Ice Sheet Model, part of the Community Climate System Model, CCSM), Elmer/Ice (a full Stokes finite element model), SICOPOLUS (SIMulation COde for POLythermal Ice Sheets, also suitable for polythermal conditions), ISSM (Ice Sheet System Model, a finite element model), and PISM (Parallel Ice Sheet Model), which is used for this thesis.

ISMs are not yet coupled to climate models, but Quiquet et al. [2012] have shown that climatic forcing influences the ISM's outcome. In particular, at the coastal regions, detailed climatic forcing is needed for the ISM to perform well. Global circulation models (GCMs) have a too coarse resolution, so regional climate models (RCMs) with resolutions as low as 0.05° are widely used as input of ISMs. Lucas-

Picher et al. [2012] show that climate models on such high resolutions seem to imitate the climate properly. Validation of RCMs is difficult due to the lack of observations. In Greenland, there are a large number of automatic weather stations (AWSs), but especially in the coastal regions, the climate can differ on small scales due to significant changes in the topography. Downscaled RCMs can capture these topographic patterns [IPCC, 2013, Chapter 9.6].

Most ISMs use approximations for ice dynamics, and the cost of those with respect to future predictions is unknown [IPCC, 2007, Chapter 8.2]. This adds up to the total uncertainty of future predictions on, e.g., global sea level rise. The recent IPCC [2013] reports that not enough is known about the basal conditions, and that this fact limits the understanding of ice sheet stability [IPCC, 2013, Chapter 4.6].

1.3 Overview

The aim of this thesis is to estimate the freshwater flux into Godthåbsfjorden originating from KNS. This is done using two independent methods: the ice sheet model PISM and stable oxygen isotope analysis.

This thesis is organized as follows. Firstly, the continuum mechanics used in the ice sheet model PISM is described in **Chapter 2**. **Chapter 3** describes the input data of PISM, such as geometry and climatic forcing. Also, the initialization and spin-up of PISM are performed and an example run is shown. **Chapter 4** is an extended version of the submitted article *Modeling present and future behavior of the tidewater glacier Kangiata Nunaata Sermia, West Greenland*, in which PISM is applied to the KNS region (see Appendix E). **Chapter 5** shows an approach of using an inverse model to retrieve the missing bedrock topography under KNS. This method is tested on the well-studied outlet glacier Jakobshavn Isbræ, and it is then applied to KNS. **Chapter 6** contains the work that is described in the submitted article *Estimating the glacial meltwater contribution to the freshwater budget from salinity and $\delta^{18}O$ measurements in Godthåbsfjord* (see Appendix F). The analysis in this chapter is independent from the ice sheet model results. **Chapter 7** gives the overall conclusions and outlook.

Work that did not go into this thesis is the application of PISM to Helheim and Kangerdlugssuaq glaciers on the East coast of Greenland [Khan et al., 2014].

2 | From Continuum Mechanics to Ice Sheet Model

An ice sheet is a large piece of ice lying on land spreading under its own weight. The ice flow inside an ice sheet is called creep and is driven by gravity. Mass is added in the form of accumulation, so that layering and compaction of past accumulation occur in the inner part of the ice sheet. In the inner part, the ice moves away from the surface. At the ice sheet margins, mass is lost by ablation, through mechanisms such as surface melt and ice berg calving. Here, the ice moves towards the surface. The transition from the accumulation to ablation zone is called the equilibrium line. Figure 2.1 shows a simple depiction of an ice sheet cross section.



Figure 2.1: An ice sheet cross section, where the arrows show the movement of ice. Mass is added in the form of snow accumulation, and mass is lost through mechanisms such as surface melt and ice berg calving. This process is called ablation.

This chapter gives a brief account of the preliminary theoretical background for this thesis. The basic equations from continuum mechanics are introduced. Furthermore, specific ice sheet concepts, such as rheology and mass balance, are presented.

Finally, the ice sheet model used in this work, the Parallel Ice Sheet Model (PISM), is introduced. This chapter is, if not indicated otherwise, based on Paterson and Cuffey [2010], Greve and Blatter [2009] and Hooke [2005].

2.1 Rheology

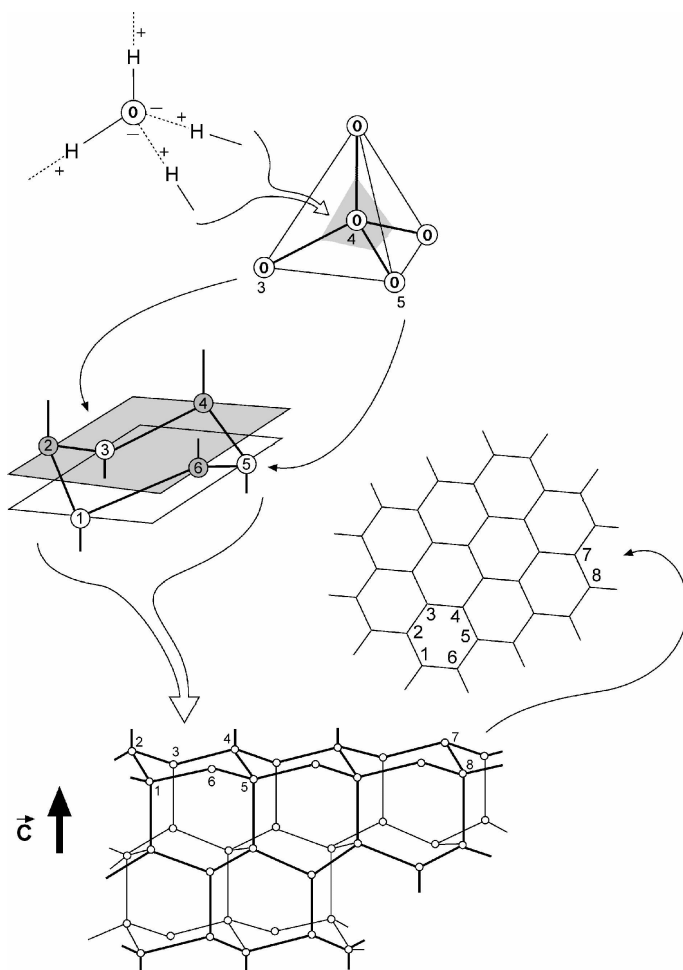


Figure 2.2: In ice, water molecules form uneven hexagonal layers. An ice crystal consists of staggered hexagonal layers, with the c -axis vector being perpendicular to these layers. Figure taken from Paterson and Cuffey [2010, Figure 3.1].

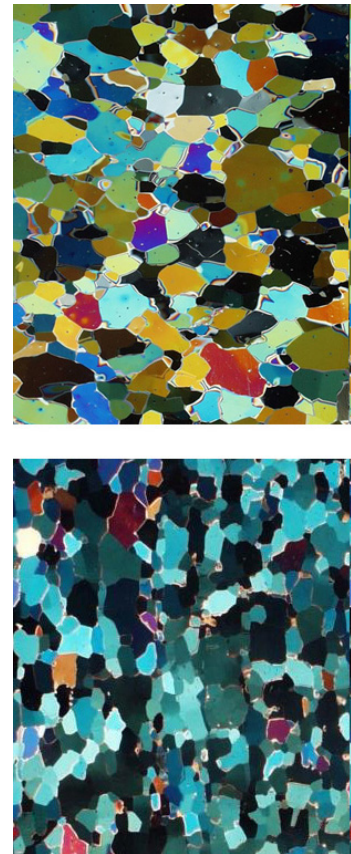


Figure 2.3: Visualisation of the ice crystal orientation by photographing thin sections using a polarization filter. Picture from the Centre for Ice and Climate.

Ice has an anisotropic crystalline structure, as shown in Figure 2.2. A water molecule consists of one oxygen and two hydrogen atoms. In ice, they form uneven hexagonal layers, the so-called basal planes. These layers are stacked. The intra-planar bonds are stronger than the interplanar bonds, which makes shearing the preferred manner of deformation. The crystal orientation is characterized by the c -axis vector,

which is perpendicular to the basal plane. A piece of ice consists of many small crystal packs that have a certain orientation. Near the surface of an ice sheet, ice is isotropic, which means that the crystal packs are oriented randomly. At larger depths, ice becomes anisotropic. However, in most ice sheet models, ice is considered to be isotropic. Figure 2.3 shows a photograph taken of a thin section of ice using a polarized filter. The color depends on the c-axis orientation of each pack.

2.2 Deformation

Continuum mechanics deals with the kinematics and deformations of continuous masses. The fact that a gaseous, liquid, or solid material, such as ice, is made of atoms, can be neglected on large length scales. Fields of physical quantities such as enthalpy, stress and velocity can be computed. In a model, a grid is imposed on the object and the field quantities are calculated at each grid point.

The strain ε describes a deformation in terms of a length change, or in three dimensions in terms of volume change. The strain rate tensor $\dot{\varepsilon} = \frac{d\varepsilon}{dt}$ is the strain change over time coming from the change in velocity $\mathbf{u} = (u_x, u_y, u_z)$. In terms of the velocity, the strain rate in index notation (see Appendix 2.A) reads

$$\dot{\varepsilon}_{ij} = \frac{1}{2} \left(\frac{\partial u_i}{\partial x_j} + \frac{\partial u_j}{\partial x_i} \right). \quad (2.1)$$

The diagonal components $\dot{\varepsilon}_{ii}$ describe parallel stretching and compression, and the sum of the three diagonal components gives the fractional rate of volume change. Ice, however, is considered to be incompressible (see Section 2.3.1), and hence the fractional rate of volume change is zero:

$$\boxed{\dot{\varepsilon}_{xx} + \dot{\varepsilon}_{yy} + \dot{\varepsilon}_{zz} = 0.} \quad (2.2)$$

For an incompressible material, the deformation depends on the full stress tensor σ and on the deviations of the stress from isotropy, which is called the deviatoric stress τ . The normal stress is $\sigma_M = \frac{1}{3}(\sigma_{xx} + \sigma_{yy} + \sigma_{zz})$, which equals the opposite of the hydrostatic pressure p . Thus, the components of the deviatoric stresses are

given by

$$\tau_{ij} = \sigma_{ij} - \sigma_M \delta_{ij} = \sigma_{ij} + p \delta_{ij}. \quad (2.3)$$

The relation between strain and stress is discussed in the flow law, as explained in Section 2.4.

2.3 Conservation Laws

Now the basic conservation laws of physics, namely mass, momentum and energy conservation, are formulated in the setting of continuum mechanics.

2.3.1 Mass Conservation

For a fixed volume V , the change in mass $\frac{dM}{dt}$ over time is the sum of the mass gain rate in the volume and the mass flux through the surface S :

$$\frac{dM}{dt} = \frac{d}{dt} \int_V \rho dV + \oint_S \rho \mathbf{u} d\mathbf{S} = 0, \quad (2.4)$$

where ρ is the density. In a closed system, mass cannot be lost or created, which means that the mass change equals zero. Using Gauss' Divergence Theorem (see Appendix 2.B), Equation (2.4) reads

$$\begin{aligned} \frac{dM}{dt} &= \frac{d}{dt} \int_V \rho dV + \int_V \nabla \cdot (\rho \mathbf{u}) dV \\ &= \int_V \left(\frac{d\rho}{dt} + \nabla \cdot (\rho \mathbf{u}) \right) dV = 0. \end{aligned} \quad (2.5)$$

From this, the continuity equation

$$\boxed{\frac{d\rho}{dt} + \nabla \cdot (\rho \mathbf{u}) = 0} \quad (2.6)$$

follows. An incompressible material, such as ice, has constant density, which reduces Equation (2.6) to

$$\boxed{\nabla \cdot \mathbf{u} = 0}, \quad (2.7)$$

which is called the condition of incompressibility.

2.3.2 Momentum Conservation

The Navier-Stokes equation describing the motion of a Newtonian fluid [Cohen and Kundu, 2004, Equation 4.44] is given by

$$\rho \frac{Du_i}{Dt} = -\frac{\partial p}{\partial x_i} + \rho g_i + \frac{\partial}{\partial x_j} \left(2\mu \dot{\epsilon}_{ij} - \frac{2}{3}\mu(\nabla \cdot \mathbf{u})\delta_{ij} \right), \quad (2.8)$$

where $\frac{D\mathbf{u}}{Dt} = \frac{\partial \mathbf{u}}{\partial t} + \mathbf{u} \cdot \nabla \mathbf{u}$ is the material derivative, p is the pressure, \mathbf{g} is the gravitational acceleration, and μ is the viscosity. In the case of ice, the acceleration and the convective force in the material derivative can be neglected, since the viscous forces dominate. From incompressibility, it follows that the last term of the Navier-Stokes equation vanishes. The following equation remains:

$$\boxed{0 = -\nabla p + \rho \mathbf{g} + 2\nabla \cdot (\mu \dot{\epsilon})}. \quad (2.9)$$

This is called the Full-Stokes (FS) equation.

2.3.3 Energy Conservation

The conservation of energy includes three components: advection, conduction and strain heating.

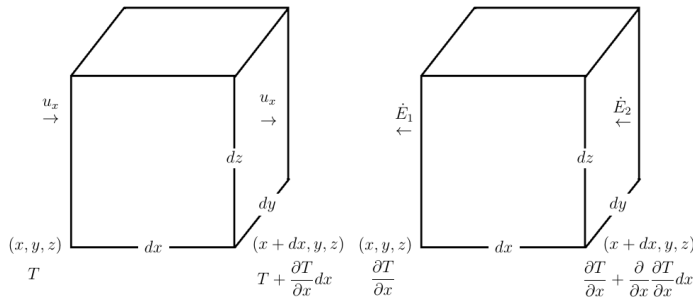


Figure 2.4: Advection is the energy rate through an infinitesimal volume $dx dy dz$ as a function of temperature gradient in a volume. Figure based on Hooke [2005, Figure 6.1].

Figure 2.5: Conduction is the energy transfer coming from a temperature gradient in a volume. Figure based on Hooke [2005, Figure 6.2].

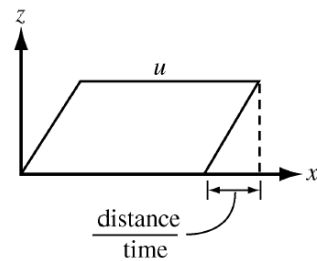


Figure 2.6: Strain heating is the generation of heat in a volume due to deformation. Figure taken from Hooke [2005, Figure 6.3].

Advection describes the energy rate through an infinitesimal volume $dx dy dz$ as a function of the temperature T , see Figure 2.4. The ingoing energy rate \dot{E}_{in} along the x-axis is given by

$$\dot{E}_{in} = u_x dy dz \rho c T, \quad (2.10)$$

where u_x is the velocity in the x-direction and c is the specific heat capacity of ice. The outgoing energy rate \dot{E}_{out} is given by

$$\dot{E}_{out} = u_x dy dz \rho c \left(T + \frac{\partial T}{\partial x} dx \right). \quad (2.11)$$

Hence, the change of the energy rate \dot{E} along the x-axis is

$$\dot{E} = \dot{E}_{out} - \dot{E}_{in} = -u_x dx dy dz \rho c \frac{\partial T}{\partial x}. \quad (2.12)$$

Converted to the change of temperature $\dot{T}_{\text{advection}}$, it becomes

$$\dot{T}_{\text{advection}} = \frac{\dot{E}}{\rho c dx dy dz} = -u_x \frac{\partial T}{\partial x}. \quad (2.13)$$

The equations for the y- and z-direction are analogous.

Conduction is the energy transfer due to a temperature gradient in a volume, see Figure 2.5. The energy rate on the $dy dz$ face of an infinitesimal volume $dx dy dz$ is, for the two sides of the volume, given by

$$\dot{E}_{x1} = -k_T \frac{\partial T}{\partial x} dy dz \quad (2.14)$$

and

$$\dot{E}_{x2} = -\left(k_T \frac{\partial T}{\partial x} + \frac{\partial}{\partial x} \left(k_T \frac{\partial T}{\partial x} \right) dx \right) dy dz, \quad (2.15)$$

where k_T is the thermal conductivity of ice. The change of energy becomes

$$\dot{E} = \dot{E}_{x2} - \dot{E}_{x1} = \frac{\partial}{\partial x} \left(k_T \frac{\partial T}{\partial x} \right) dx dy dz = \left(k_T \frac{\partial^2 T}{\partial x^2} + \frac{\partial k_T}{\partial x} \frac{\partial T}{\partial x} \right) dx dy dz. \quad (2.16)$$

In terms of temperature, it becomes

$$\dot{T}_{\text{conduction}} = \frac{k_T}{\rho c} \frac{\partial^2 T}{\partial x^2} + \frac{1}{\rho c} \frac{\partial k_T}{\partial x} \frac{\partial T}{\partial x}. \quad (2.17)$$

Again, the y- and z-direction are analogous.

Strain heating is the generation of heat in a volume due to deformation, see Figure 2.6. This term depends on the stress and strain rate:

$$\dot{T}_{\text{strain heating}} = \frac{\sigma_{zx}\dot{\epsilon}_{zx}}{\rho c} = \frac{E}{\rho c}, \quad (2.18)$$

where E is the heat produced in the volume.

The total conservation of energy combines the three above contributions in all directions:

$$\begin{aligned} \dot{T}_{\text{total}} &= \dot{T}_{\text{advection}} + \dot{T}_{\text{conduction}} + \dot{T}_{\text{strain heating}} \\ &= \left\{ -u_x \frac{\partial T}{\partial x} - u_y \frac{\partial T}{\partial y} - u_z \frac{\partial T}{\partial z} \right\} \\ &+ \left\{ \frac{k_T}{\rho c} \frac{\partial^2 T}{\partial x^2} + \frac{k_T}{\rho c} \frac{\partial^2 T}{\partial y^2} + \frac{k_T}{\rho c} \frac{\partial^2 T}{\partial z^2} + \frac{1}{\rho c} \frac{\partial k_T}{\partial x} \frac{\partial T}{\partial x} + \frac{1}{\rho c} \frac{\partial k_T}{\partial y} \frac{\partial T}{\partial y} + \frac{1}{\rho c} \frac{\partial k_T}{\partial z} \frac{\partial T}{\partial z} \right\} \\ &+ \left\{ \frac{E}{\rho c} \right\}. \end{aligned}$$

This yields

$$\boxed{\dot{T}_{\text{total}} = -\mathbf{u} \cdot \nabla T + \frac{k_T}{\rho c} \nabla^2 T + \frac{1}{\rho c} \nabla k_T \cdot \nabla T + \frac{E}{\rho c}.} \quad (2.19)$$

2.4 Flow Law

Ice is a viscous fluid that deforms under stress. This deformation is called creep flow. The empirically determined creep relation is the rate of deformation as function of the applied stress.

2.4.1 Creep Flow

For a Newtonian fluid, the applied stress is proportional to the deformation rate. In the case of perfect plasticity, no deformation occurs below a certain critical stress value, the so-called yield stress. The behavior of ice lies between these two.

Plotting the strain rate as a function of strain for a constant stress gives the so-called creep curve, as shown in Figure 2.7. There are three phases of creep: the primary, secondary and tertiary creep. Firstly, the strain rate decreases for increasing strain, called primary creep, until a minimal strain rate $\dot{\epsilon}_{\text{min}}$ is reached, the secondary

creep. Then the strain rate increases until a steady value is reached. This is called the tertiary creep.

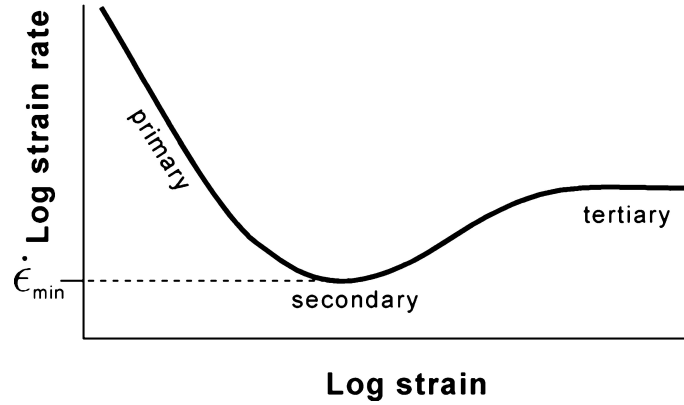


Figure 2.7: The creep curve showing the strain rate as function of strain and the three phases of creep: the primary, secondary and tertiary creep. Figure taken from [Paterson and Cuffey, 2010, Figure 3.11].

Laboratory experiments show that ice behaves as secondary creep with the minimal stresses in glacier flow to be 50–150 kPa. Glen [1955] formulated the first flow law for ice. Nye [1957] generalized this law to ice being an incompressible and isotropic material. This is referred to as the Nye-Glen Isotropic Law, and reads

$$\dot{\epsilon}_{ij} = A \tau_E^{n-1} \tau_{ij}, \quad (2.20)$$

where A is the creep or rate factor, $\tau_E^2 = \frac{\tau_{ij}\tau_{ij}}{2}$ is the second invariant of the deviatoric stress and n is a constant exponent. The generally accepted choice for the exponent is $n = 3$. The rate factor A depends on several parameters such as the water content, density of the ice, grain size and impurities, but mainly on pressure and temperature. Often only a dependence on the latter two is stated in the form of an Arrhenius equation:

$$A = A_0 \exp\left(-\frac{E_a}{R(T - T_{pmp})}\right), \quad (2.21)$$

where A_0 is a constant rate factor, E_a is the activation energy, R is the general gas constant and T_{pmp} is the pressure melting point. The pressure melting point depends on the pressure p , through $T_{pmp} = T_0 - \beta p$, where β is the Clausius-Clapeyron constant. Values of β range from $7.42 \cdot 10^8$ K/Pa for ice to $9.8 \cdot 10^8$ K/Pa for air saturated ice. In general, it reduces the melting point by 0.87 K per kilometer

overlying ice.

Because ice is actually anisotropic and can have impurities or non-random crystal orientations, it is common to add an enhancement factor e to the rate factor through $A \rightarrow eA$. The enhancement factor is larger than 1, and in general, values between 1 and 10 are accepted. The exact value of the enhancement factor e is often varied to tune ice sheet models. Holocene ice has an enhancement factor of 2.5 [Paterson and Cuffey, 2010], impure ice at Dye-3 indicates a value of 4 [Dahl-Jensen and Gundestrup, 1987], and for ice at Antarctic shear margins even values of 12 have been estimated [Echelmeyer and Mitchell, 1994].

2.4.2 Mass Balance

The total mass balance of an ice sheet is the net mass change in a certain period. All mechanisms adding or removing mass, called accumulation and ablation, are taken into account.

The surface mass balance (SMB) is the sum of precipitation, melt, deposition, refreezing and sublimation. Generally, the first two are dominating.

The basal mass balance (BMB) is the sum of basal melt and basal refreezing. It has a minor contribution to the total mass balance of a grounded ice sheet. However, the BMB is connected to basal velocities. High basal velocities lead to increased ice loss at the margins, which can be substantial. The net energy at the base is given by

$$E_b = G + u_b \tau_b + k_T \frac{\partial T}{\partial z}, \quad (2.22)$$

where G is the geothermal heat flux, τ_b is the basal drag, u_b is basal sliding velocity and $\frac{\partial T}{\partial z}$ is the temperature gradient. The basal drag and velocity are explained in Section 2.4.3. If $E_b < 0$, there is a basal accumulation of ice or freeze-on in case water is available. Also, there can be freeze-on if the temperature drops below the pressure melting point. If $E_b > 0$, there is basal melt. In the special case of fast flowing ice streams, enough frictional heating occurs to generate basal melt, which increases the basal velocity even more.

Another important mechanism is mass loss through calving. Calving occurs at the margins of an ice sheet when the glacier ejects ice bergs into the water. Currently, mostly empirical calving laws are used in ice sheet models. A very simple calving

law is presented in Brown et al. [1982]. The calving flux \dot{c} is given by

$$\dot{c} = k_c H_w, \quad (2.23)$$

where H_w is the water depth at the terminus and k_c is a constant calving coefficient. More advanced and physical calving laws are under development and are implemented into flow line models. The use of advanced calving laws in three-dimensional models is still a challenge.

Boundary conditions can be derived for the surface S of an ice sheet and its ice base B . Let $h(x, y, t)$ be the z-coordinate of the surface. In this way, the surface S is given by

$$S = z - h = 0. \quad (2.24)$$

The normal vector is given by

$$\mathbf{n} = \frac{1}{N_S} \left(-\frac{\partial h}{\partial x}, -\frac{\partial h}{\partial y}, 1 \right), \quad (2.25)$$

where N_S is a normalized constant. The directional derivative $\frac{d_w S}{dt}$ of the surface along the velocity \mathbf{w} of the surface satisfies

$$\frac{d_w S}{dt} = \frac{\partial S}{\partial t} + \mathbf{w} \cdot \nabla S = 0. \quad (2.26)$$

The volume flux a_S^\perp through the surface is the difference between the ice velocity \mathbf{u} through the surface and the velocity of the surface itself \mathbf{w} :

$$a_S^\perp = (\mathbf{w} - \mathbf{u}) \cdot \mathbf{n}. \quad (2.27)$$

This is the surface mass balance, where accumulation is defined to be positive. Combining Equations (2.25), (2.26) and (2.27), the kinematic boundary condition at the surface is given by

$$a_S^\perp N_S = \frac{\partial h}{\partial t} + u_x \frac{\partial h}{\partial x} + u_y \frac{\partial h}{\partial y} - u_z. \quad (2.28)$$

Let $b(x, y, t)$ be the z-coordinate of the base. The base B is given by

$$B = b - z = 0. \quad (2.29)$$

An analogous approach is used for the basal mass balance a_B^\perp :

$$a_B^\perp = (\mathbf{u} - \mathbf{w}) \cdot \mathbf{n}, \quad (2.30)$$

where basal ablation is defined to be negative. The normal vector is given by

$$\mathbf{n} = \frac{1}{N_B} \left(\frac{\partial b}{\partial x}, \frac{\partial b}{\partial y}, -1 \right). \quad (2.31)$$

The directional derivative $\frac{d_w B}{dt}$ of the base along \mathbf{w} satisfies

$$\frac{d_w B}{dt} = \frac{\partial B}{\partial t} + \mathbf{w} \cdot \nabla B = 0. \quad (2.32)$$

The final result reads

$$a_B^\perp N_B = \frac{\partial b}{\partial t} + u_x \frac{\partial b}{\partial x} + u_y \frac{\partial b}{\partial y} - u_z. \quad (2.33)$$

The ice thickness evolution is derived from the incompressibility condition. To this end, Equation (2.7) is vertically integrated from the base b to the surface h :

$$\int_b^h (\nabla \cdot \mathbf{u}) dz = \int_b^h \frac{\partial u_x}{\partial x} dz + \int_b^h \frac{\partial u_y}{\partial y} dz + \int_b^h \frac{\partial u_z}{\partial z} dz = 0. \quad (2.34)$$

Here, the Leibniz integral rule (see Appendix 2.C) is used for the first two terms. It follows that

$$\begin{aligned} \frac{\partial}{\partial x} \int_b^h u_x dz - u_x|_{z=h} \frac{\partial h}{\partial x} + u_x|_{z=b} \frac{\partial b}{\partial x} + \frac{\partial}{\partial x} \int_b^h u_y dz - u_y|_{z=h} \frac{\partial h}{\partial x} + u_y|_{z=b} \frac{\partial b}{\partial x} \\ + u_z|_{z=h} - u_z|_{z=b} = 0. \end{aligned} \quad (2.35)$$

Inserting the mass balances from Equation (2.28) and (2.33) and defining the vertically integrated velocities as volume fluxes q , one obtains

$$\frac{dq_x}{dx} + \frac{dq_y}{dy} + \frac{\partial h}{\partial t} - N_S a_S^\perp - \frac{\partial b}{\partial t} + N_B a_B^\perp = 0. \quad (2.36)$$

The ice thickness is given by $H = h - b$, and hence

$$\frac{dq_x}{dx} + \frac{dq_y}{dy} + \frac{\partial H}{\partial t} - N_S a_S^\perp + N_B a_B^\perp = 0. \quad (2.37)$$

In vector notation, the so-called ice thickness equation reads

$$\boxed{\frac{\partial H}{\partial t} = -\nabla \cdot \mathbf{q} + N_S a_S^\perp - N_B a_B^\perp.} \quad (2.38)$$

2.4.3 Driving Stresses

An ice sheet deforms due to its gravitational weight. The driving stress depends on the weight, the surface slope and the slope of the underlying bed topography. There are two mechanisms describing this deformation.

Firstly, consider a piece of ice with constant thickness H on a sloped bed with

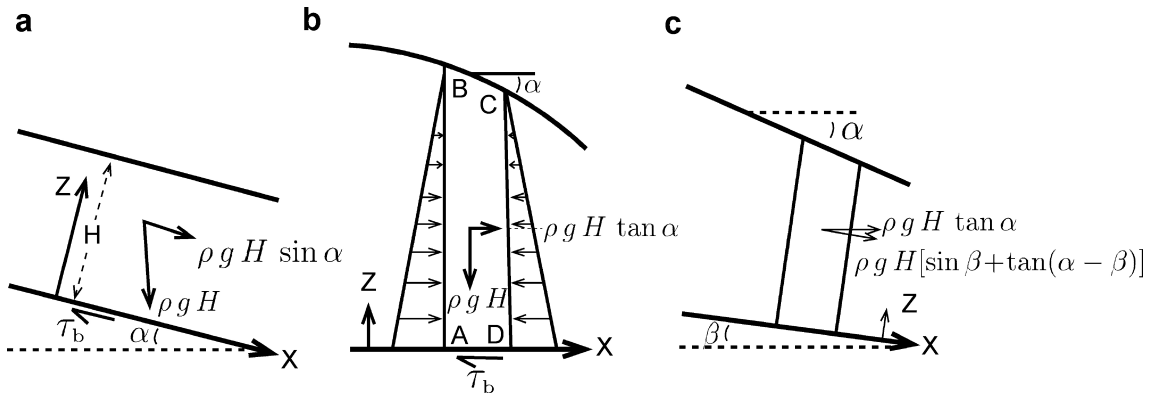


Figure 2.8: The driving stress depends on the surface slope (a) and the slope of the underlying bed topography (b). (c) shows a combination of both mechanisms for a surface slope and slope at the bed. Figure taken from Paterson and Cuffey [2010, Figure 8.5].

angle α , see Figure 2.8 a. The driving stress τ_d is given by the weight $\rho g H$ of the overlying ice column parallel to the plane:

$$\tau_d = \rho g H \sin(\alpha). \quad (2.39)$$

The second mechanism is pressure driven flow, see Figure 2.8 b. The driving stress is a function of the difference $\frac{dH}{dx}$ in ice thickness at the boundaries of an ice column. The driving stress is given by

$$\tau_d = -\rho g H \frac{dH}{dx} = \rho g H \tan(\alpha), \quad (2.40)$$

where α is the surface slope angle.

Nye [1952] proposed the combination of both mechanisms, see Figure 2.8 c. The driving stress, for surface slope α and bed slope β , reads

$$\tau_d = \rho g H \sin(\beta) + \rho g H \tan(\alpha - \beta). \quad (2.41)$$

For small slopes, $\tan(\alpha) \approx \sin(\alpha) \approx \alpha$ applies, so that

$$\tau_d = \rho g H \alpha. \quad (2.42)$$

The driving stress depends on the surface slope only. Basal drag τ_b can be described as a function of the driving stress by

$$\tau_b = f \tau_d, \quad (2.43)$$

where f is a dimensionless function. The total driving stress is the sum of the basal drag, the longitudinal stresses and lateral drag, as shown in Figure 2.9. The total driving stress is

$$\tau_d = \tau_b + \tau_{\text{lat}} + \tau_{\text{lon}}, \quad (2.44)$$

where τ_{lon} is the gradient $2\frac{\partial H \tau_{xx}}{\partial x}$. Combining Equations (2.43) and (2.44), it follows that

$$f = 1 - \frac{\tau_{\text{lat}} + \tau_{\text{lon}}}{\tau_d} < 1. \quad (2.45)$$

In case the driving stress exceeds the basal drag, sliding occurs.

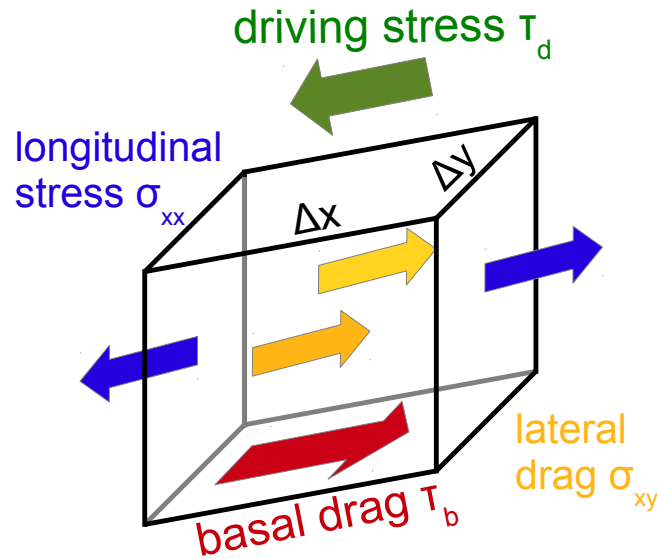


Figure 2.9: Conceptual figure of the stresses applied to a ice volume. Here, only the stresses in x-direction are shown.

2.4.4 Basal sliding

In addition to movement caused by deformation, as derived in Section 2.2, sliding occurs. If the basal temperature is at the pressure melting point, liquid water is

present, and the ice sheet can move without deformation. From surface velocity measurements, one cannot conclude definitively whether sliding is present or not. There are only few places where local direct observations are possible. One of them is the Svartisen Subglacial Laboratory in Norway. Sliding velocities can be as high as hundreds of meters per day.

Following Macayeal et al. [1995], the basal shear stress τ_b as function of the basal sliding velocity u_b is given by

$$\tau_b = -\beta^2 u_b, \quad (2.46)$$

where $-\beta^2$ is the drag factor. Pinpointing values for the drag factor is challenging, and values differ between individual glaciers and ice sheet locations. In theory, there are two types of sliding, one on a hard bed and one on a sedimentary soft bed.

In case there is a direct ice-rock interface, it is referred to as a hard bed. Here, a combination of regelation and creep take place [Weertman, 1957]. Regelation implies that at the upstream side of a small obstacle, the ice melts due to local high pressure and flows to the downstream side. There it refreezes again due to a lower pressure. The released heat is then transported through the obstacle to the upstream side. Creep flow describes the fact that ice deforms when passing a larger obstacle. It causes an increase of stress, so that the ice can deform easier to pass the obstacle. More common are soft beds, where sediments are present between ice and bedrock. Such sediments are called till. The till is often water-saturated, and the strength of the till layer determines the amount of sliding. A wet soft bed is weaker and more sliding occurs.

2.5 Full Stokes Model and Assumptions

The mechanics and thermodynamics of an ice mass are described by the FS equation, i.e., Equation (2.9). The evolution of an ice sheet includes the ice thickness changes due to the flow of ice and applied mass balance changes. Due to computational limitations, approximations have to be made. These should be chosen carefully.

First efforts in ice sheet modeling were made in the late 1970's by Fowler and Larson [1978, 1980a,b], who made a first scaling analysis for a plane isothermal ice sheet and computed the isothermal glacier flow analytically. Followed by that, Hutter [1981, 1983] developed the Shallow Ice Approximation (SIA) for a planar ice sheet in 1981 and in three dimensions in 1983. Morland et al. [1984] developed the first

empirical linear sliding law [Hutter et al., 1986].

Since then, the computational capabilities have been improved significantly. However, it is still not feasible to solve the Full Stokes equations for large ice sheets, such as the Greenlandic or Antarctic Ice Sheet.

2.5.1 Full Stokes Model

The FS model includes the complete set of FS equations. The strain rates are related to velocity gradients following Equation (2.1). Equation (2.9) becomes

$$\begin{aligned} \frac{\partial}{\partial x} \left(2\mu \frac{\partial u_x}{\partial x} \right) + \frac{\partial}{\partial y} \left(\mu \frac{\partial u_x}{\partial y} + \mu \frac{\partial u_y}{\partial x} \right) + \frac{\partial}{\partial z} \left(\mu \frac{\partial u_x}{\partial z} + \mu \frac{\partial u_z}{\partial x} \right) - \frac{\partial p}{\partial x} &= 0, \\ \frac{\partial}{\partial x} \left(\mu \frac{\partial u_x}{\partial y} + \mu \frac{\partial u_y}{\partial x} \right) + \frac{\partial}{\partial y} \left(2\mu \frac{\partial u_y}{\partial y} \right) + \frac{\partial}{\partial z} \left(\mu \frac{\partial u_y}{\partial z} + \mu \frac{\partial u_z}{\partial y} \right) - \frac{\partial p}{\partial y} &= 0, \\ \frac{\partial}{\partial x} \left(\mu \frac{\partial u_x}{\partial z} + \mu \frac{\partial u_z}{\partial x} \right) + \frac{\partial}{\partial y} \left(\mu \frac{\partial u_y}{\partial z} + \mu \frac{\partial u_z}{\partial y} \right) + \frac{\partial}{\partial z} \left(2\mu \frac{\partial u_z}{\partial z} \right) - \frac{\partial p}{\partial z} - \rho g &= 0. \end{aligned} \quad (2.47)$$

The Full-Stokes equations all take stresses into account. In practice, however, some stresses can be neglected for large scale ice sheets. In the following, this is explained in more detail.

2.5.2 Shallow Ice Approximation

As mentioned earlier, one of the first approximations developed was the *Shallow Ice Approximation* (SIA) [Hutter, 1983]. It performs well for very flat ice sheets with small slopes and is used in many ice sheet models because it is computationally cheap.

In the SIA, longitudinal and transverse stresses are neglected, which leaves the driving stress and basal drag as the only important forces. This is valid for ice sheets with a small depth-to-width ratio, where the internal shear deformation parallel to the base dominates the flow of the ice sheet. There is no shearing at the surface, and all the vertical shearing takes place near the bedrock. There is strong contact between bedrock and ice, and only a minimum of sliding takes place. The SIA is a good approximation for a large scale model, but it is not valid close to the margins and at the ice divide of an ice sheet.

The incompressibility equation and the FS equations become

$$\begin{aligned}
 \frac{\partial}{\partial x} \left(2\mu \frac{\partial u_x}{\partial x} \right) + \frac{\partial}{\partial y} \left(\mu \frac{\partial u_x}{\partial y} + \mu \frac{\partial u_y}{\partial x} \right) + \frac{\partial}{\partial z} \left(\mu \frac{\partial u_x}{\partial z} + \mu \frac{\partial u_z}{\partial x} \right) - \frac{\partial p}{\partial x} &= 0, \\
 \frac{\partial}{\partial x} \left(\mu \frac{\partial u_x}{\partial y} + \mu \frac{\partial u_y}{\partial x} \right) + \frac{\partial}{\partial y} \left(2\mu \frac{\partial u_y}{\partial y} \right) + \frac{\partial}{\partial z} \left(\mu \frac{\partial u_y}{\partial z} + \mu \frac{\partial u_z}{\partial y} \right) - \frac{\partial p}{\partial y} &= 0, \\
 \frac{\partial}{\partial x} \left(\mu \frac{\partial u_x}{\partial z} + \mu \frac{\partial u_z}{\partial x} \right) + \frac{\partial}{\partial y} \left(\mu \frac{\partial u_y}{\partial z} + \mu \frac{\partial u_z}{\partial y} \right) + \frac{\partial}{\partial z} \left(2\mu \frac{\partial u_z}{\partial z} \right) - \frac{\partial p}{\partial z} - \rho g &= 0, \\
 \frac{\partial u_x}{\partial x} + \frac{\partial u_y}{\partial y} + \frac{\partial u_z}{\partial z} &= 0.
 \end{aligned} \tag{2.48}$$

The equations left to solve are

$$\begin{aligned}
 \frac{\partial}{\partial z} \left(\mu \frac{\partial u_x}{\partial z} \right) - \frac{\partial p}{\partial x} &= 0, \\
 \frac{\partial}{\partial z} \left(\mu \frac{\partial u_y}{\partial z} \right) - \frac{\partial p}{\partial y} &= 0, \\
 \frac{\partial p}{\partial z} + \rho g &= 0.
 \end{aligned} \tag{2.49}$$

Integrating the latter equation yields

$$p = \rho g(h - z), \tag{2.50}$$

which is the hydrostatic pressure distribution. For the horizontal pressure gradient, it follows that

$$\frac{\partial p}{\partial x} = \rho g \frac{\partial h}{\partial x} \quad \text{and} \quad \frac{\partial p}{\partial y} = \rho g \frac{\partial h}{\partial y}. \tag{2.51}$$

Note that the stresses are determined by the geometry of the ice sheet only.

2.5.3 Shallow Shelf Approximation

MacAyeal [1989b], Morland et al. [1984] and MacAyeal [1989a] developed the *Shallow Shelf Approximation* (SSA). Ice shelves have a width-to-thickness ratio comparable to the one of ice sheets, but they are smaller, thinner and they flow faster. The main difference is at the base, where the ice shelf has an ice-to-sea boundary without basal drag, i.e., $\tau_b = \tau_{sea} \approx 0$. This results in a velocity that does not depend on the depth. The SSA assumes that the horizontal gradients of the vertical velocity are negligible compared to the vertical gradients. Also, the vertical shear stress is negligible: $\dot{\epsilon}_{xz} = \dot{\epsilon}_{yz} = 0$. This simplification results in a two-dimensional model with a membrane-type flow because u_x and u_y are depth-independent.

The FS equations become

$$\begin{aligned}
\frac{\partial}{\partial x} \left(2\mu \frac{\partial u_x}{\partial x} \right) + \frac{\partial}{\partial y} \left(\mu \frac{\partial u_x}{\partial y} + \mu \frac{\partial u_y}{\partial x} \right) + \frac{\partial}{\partial z} \left(\mu \frac{\partial u_x}{\partial z} + \mu \frac{\partial u_z}{\partial x} \right) - \frac{\partial p}{\partial x} &= 0, \\
\frac{\partial}{\partial x} \left(\mu \frac{\partial u_x}{\partial y} + \mu \frac{\partial u_y}{\partial x} \right) + \frac{\partial}{\partial y} \left(2\mu \frac{\partial u_y}{\partial y} \right) + \frac{\partial}{\partial z} \left(\mu \frac{\partial u_y}{\partial z} + \mu \frac{\partial u_z}{\partial y} \right) - \frac{\partial p}{\partial y} &= 0, \quad (2.52) \\
\frac{\partial}{\partial x} \left(\mu \frac{\partial u_x}{\partial z} + \mu \frac{\partial u_z}{\partial x} \right) + \frac{\partial}{\partial y} \left(\mu \frac{\partial u_y}{\partial z} + \mu \frac{\partial u_z}{\partial y} \right) + \frac{\partial}{\partial z} \left(2\mu \frac{\partial u_z}{\partial z} \right) - \frac{\partial p}{\partial z} - \rho g &= 0,
\end{aligned}$$

which simplifies to

$$\begin{aligned}
\frac{\partial}{\partial x} \left(2\mu \frac{\partial u_x}{\partial x} \right) + \frac{\partial}{\partial y} \left(\mu \frac{\partial u_x}{\partial y} + \mu \frac{\partial u_y}{\partial x} \right) + \frac{\partial}{\partial z} \left(\mu \frac{\partial u_z}{\partial x} \right) - \frac{\partial p}{\partial x} &= 0, \\
\frac{\partial}{\partial x} \left(\mu \frac{\partial u_x}{\partial y} + \mu \frac{\partial u_y}{\partial x} \right) + \frac{\partial}{\partial y} \left(2\mu \frac{\partial u_y}{\partial y} \right) + \frac{\partial}{\partial z} \left(\mu \frac{\partial u_z}{\partial y} \right) - \frac{\partial p}{\partial y} &= 0, \quad (2.53) \\
\frac{\partial}{\partial x} \left(\mu \frac{\partial u_z}{\partial x} \right) + \frac{\partial}{\partial y} \left(\mu \frac{\partial u_z}{\partial y} \right) + \frac{\partial}{\partial z} \left(2\mu \frac{\partial u_z}{\partial z} \right) - \frac{\partial p}{\partial z} - \rho g &= 0,
\end{aligned}$$

Ice streams can be considered as barely-grounded ice shelves due to the large amount of sliding taking place at the base. The basal drag is proportional to the velocity.

2.6 Numerical Methods

The governing equations can only be solved analytically in simple cases. In three dimensions, equations for, e.g., velocity and temperature fields have to be solved using numerical methods. Computationally this means that the whole domain is split up into smaller elements and each grid cell contains the average physical information of that cell. The size of these grid cells should be as small as possible, but it still needs to take into account computational capabilities.

There are two main methods used in ice sheet models: the *finite difference method* (FDM) and the *finite element model* (FEM).

FDM, which is used by PISM, has a rectangular grid, in which all grid cells have the same size. The differentials are approximated by differences of the field variables between the neighboring grid cells using, e.g., the backward scheme

$$\frac{d\phi}{dx} \approx \frac{\phi_i - \phi_{i-1}}{\Delta x}.$$

FEM has grid cells of different sizes and the differential equations are approximated using the sum of integrals. For the field variable ϕ , one would use

$$\frac{d\phi}{dx} = f(x) \rightarrow \phi = \int_0^x f(x)dx \rightarrow \phi \approx \sum_{i=1}^n f(x_i)\Delta x.$$

More information on this method can be found in e.g. Reddy [2005].

2.7 The Parallel Ice Sheet Model

PISM [PISM-authors, 2010] is an open source c++ three-dimensional ice sheet model developed at the University of Alaska Fairbanks. It is a three-dimensional model that uses two shallow approximations: the non-sliding SIA and the SSA, which are applied in parallel. For the special case of ice stream flow, both approximations are combined in such a way that the SSA is representing sliding and ‘added’ to the SIA velocities [Bueler and Brown, 2009]. This is referred to as a hybrid run, which is used in this thesis. Velocities are computed at each time step from the geometry, temperature and basal strength using the stress momentum equations.

PISM has been part of the Marine Ice Sheet Model Intercomparison Project [Patyn et al., 2012]. Regional modeling capabilities of PISM have been demonstrated for Jakobshavn Isbræ [DellaGiustina, 2011]. This regional approach is used in this thesis.

The used version is PISM development 2313605.

2.7.1 Ice Flow

PISM uses an enthalpy formulation of polythermal conditions, as described in Aschwanden et al. [2012b]. This approach allows a better description of temperate ice than achieved when using a temperature formulation. It uses the Glen-Paterson-Budd-Lliboutry-Duval flow law [Glen, 1955, Lliboutry and Duval, 1985, Paterson and Budd, 1982, PISM-authors, 2010] that includes softening of the ice when reaching the pressure melting point and when water is present. The flow law depends on the temperature, liquid water fraction, pressure and grain size.

The generalized form of Glen's flow law, i.e. Equation (2.20), is used when the exponent is $n = 3$. The driving stress τ_d is given by

$$\tau_d = -\rho g H \frac{dh}{dx}. \quad (2.54)$$

The SSA is applied to floating ice or grounded ice sliding over a weak bed such as ice streams, as proposed in Schoof [2006a,b]. The advantage of using this method is the fact that the location of ice streams is not prescribed on beforehand.

The basal shear stress is given by Equation (2.46). PISM uses a parameterization of the drag factor $-\beta^2$. The basal shear stress τ_b used in PISM is given by

$$\tau_b = \tau_c \frac{|\mathbf{u}_b|^{q-1}}{u_{\text{thr}}^q} \mathbf{u}_b, \quad (2.55)$$

where \mathbf{u}_b is the modeled sliding velocity, q is the exponent of the pseudo-plastic basal resistance model, u_{thr} is the velocity threshold in the pseudo-plastic basal resistance model and τ_c is the till yield stress. The till yield stress is given by the Mohr-Coulomb criterion [Paterson and Cuffey, 2010], which describes the strength of the material, a mixture of water, ice and till, at the base. Sliding is present when the basal shear stress exceeds the basal yield stress. The basal shear stress is [Schoof, 2006a,b]

$$\tau_c = \tan(\phi)N, \quad (2.56)$$

where ϕ is the till friction angle. The effective pressure is

$$N = \rho g H - p_w, \quad (2.57)$$

where p_w is the pore water pressure defined as

$$p_w = \alpha w \rho g H, \quad (2.58)$$

where w is the basal water thickness, and α is a factor controlling the pore water pressure that determines how the effective thickness of basal water affects the pore water pressure. Thus, α gives the fraction of the overburden pressure that is the pore water pressure. The basal water thickness depends on the temperature that determines the softness of the ice. Also, dissipation heating and frictional heating at the base are taken into account. However, in the PISM version used here, there is no transport of the basal water between grid cells. The till friction angle describes the local strength of the material and depends on the composition of the till (e.g., grain size and water content). In general, the till friction angle is unknown or only

known very locally from bore hole measurements. PISM uses a constant or elevation dependent parametrization for the till friction angle. It is assumed that a deep bed has a marine history, and, hence, is softer. The till friction angle ϕ is a function of the bed elevation as follows

$$\phi = \begin{cases} \phi_{min} & \text{for } b \leq b_{min}, \\ \phi_{min} + (b(x, y) - b_{min}) \frac{\phi_{max} - \phi_{min}}{b_{max} - b_{min}} & \text{for } b_{min} < b < b_{max}, \\ \phi_{max} & \text{for } b \geq b_{max}, \end{cases} \quad (2.59)$$

where b_{min} , b_{max} , ϕ_{min} and ϕ_{max} are constant values.

2.7.2 Calving

PISM has two simple calving options available: `float_kill` and `ocean_kill`. In `ocean_kill`, all ice in an ocean grid cell is calved off. More realistic is the `float_kill` option, in which all floating ice is calved off. Ice shelves are not allowed. This option works good for most Greenlandic glaciers without a floating tongue.

For Antarctic ice shelves, PISM has been improved with a physical two-dimensional calving parametrization based on horizontal strain rates $\dot{\epsilon}_{\pm}$, called eigen-calving, in PISM-PIK [Levermann et al., 2012, Winkelmann et al., 2011]. The calving rate \dot{c} is given by

$$\dot{c} = K \dot{\epsilon}_{+} \dot{\epsilon}_{-} \quad \text{when} \quad \dot{\epsilon}_{\pm} > 0, \quad (2.60)$$

where K is a constant. Ice bergs are calved off whenever both strain rates are positive. This method has been tested on Antarctica and succeeds in modeling the big ice shelves. However, Greenlandic fjords are very narrow, and the horizontal stresses across the fjord are negative most of the time. Hence, using eigen calving, the ice sheet can grow into the fjord without calving.

2.8 Restrictions

Models do not reflect reality. When using an ice sheet model, one must keep in mind that it is only a model. They are tuned to imitate the past, present and future behavior. However, validation is difficult for past, present and certainly future

performance. There are limited observations describing the state of ice sheets. As mentioned earlier, basal conditions are generally unknown. Inverse models are used to learn about the base, but the validation is difficult since there is no access to the glacier bed.

Ice sheet models require gridded input fields for geometry and climate. Ice penetrating radars are used to retrieve ice thickness and bedrock elevation. Measurements are interpolated towards a continuous grid to use for models. For the majority of Greenland, flight lines are sparse, see Figure for the flight lines used for the commonly used ice sheet geometry by Bamber et al. [2001, 2013]. At the inner part of the ice sheet, a coarser grid works well, but at the coastal regions, more detailed measurements are essential [Durand et al., 2011].

Models assume that the ice sheet is in equilibrium, which is not true, since the total mass balance is unequal to zero. Climate models are ran separately and often on a coarser grid. Solgaard and Langen [2012] have shown that climate patterns change with an evolving ice sheet. An ice sheet will evolve differently when using an adapted climate pattern. However, a coupled ice sheet and climate model is computationally expensive.

All those restrictions must be kept in mind when interpreting ice sheet model output and when making predictions.

2.A Index Notation

A short way of denoting vectors and tensors is in index notation. A vector

$$\mathbf{a} = (a_1, a_2, a_3)$$

is then written as

$$\mathbf{a} = a_1\mathbf{e}_1 + a_2\mathbf{e}_2 + a_3\mathbf{e}_3 = \sum_{i=1}^3 a_i\mathbf{e}_i.$$

In addition, Einstein's summation convention states that double indices have to be summed, which makes the notation even shorter

$$\mathbf{a} = a_i\mathbf{e}_i.$$

Thus, the dot product becomes

$$\mathbf{a} \cdot \mathbf{b} = a_i b_i.$$

The Kronecker delta is given by

$$\delta_{ij} = \begin{cases} 1 & \text{for } i = j \\ 0 & \text{for } i \neq j \end{cases}.$$

2.B Gauss' Divergence Theorem

Gauss' Divergence Theorem for a vector field \mathbf{a} in a fixed volume V is as follows

$$\oint_S \mathbf{a} \cdot d\mathbf{S} = \int_V \nabla \cdot \mathbf{a} dV, \quad (2.61)$$

where S is the boundary of V .

2.C Leibniz Integral Rule

The Leibniz integral rule is as follows:

$$\frac{\partial}{\partial x} \left(\int_{a(x)}^{b(x)} f(x, z) dz \right) = \int_{a(x)}^{b(x)} \frac{\partial f(x, z)}{\partial x} dz + f(x, b(x)) \frac{\partial b(x)}{\partial x} - f(x, a(x)) \frac{\partial a(x)}{\partial x} \quad (2.62)$$

where f is a spatial varying function.

3 | Input Data and Initialization

This chapter describes the geometry of the Nuuk region and the climate model output, which are used as an input for PISM. Also, observed surface velocities, used for model validation, are discussed. After that, PISM is set up and finally, the model output for an example is shown.

3.1 Bed and Surface Elevation

Bed and surface elevation data have been collected from several sources: the data set by Bamber et al. [2001], the high resolution DEM for the margins and the high resolution bathymetry.

The data set by Bamber et al. [2001] and Bamber et al. [2013] on a grid with 5 km spacing is shown in Figure 3.1. The ice-penetrating radar missions are shown in Figure 3.2. These are interpolated to the smooth bed map. KNS's 4 km narrow fjord is not resolved in this data set, which makes this data alone useless for modeling KNS, since KNS would be land-terminating. Considering the aim and computing costs, a 2 km grid is used in the following modeling efforts.

In addition, a high resolution digital elevation model (DEM), as shown in Figure 3.3, is added to the existing data set. The Natural History Museum of Denmark has reanalysed a 1985 Greenland photo survey and produced a DEM of the marginal land regions (Natural History Museum of Denmark, private communication). The original grid spacing of this data set is 25 m. This DEM is remapped, using simple bilinear interpolation, to the same 2 km grid.

The Greenland Climate Research Center (GCRC) has provided a high resolution map of the fjord bathymetry (Rysgaard, private communication), which is shown in Figure 3.4. The original resolution is 100 m, and it is remapped onto the same 2 km grid using bilinear interpolation.

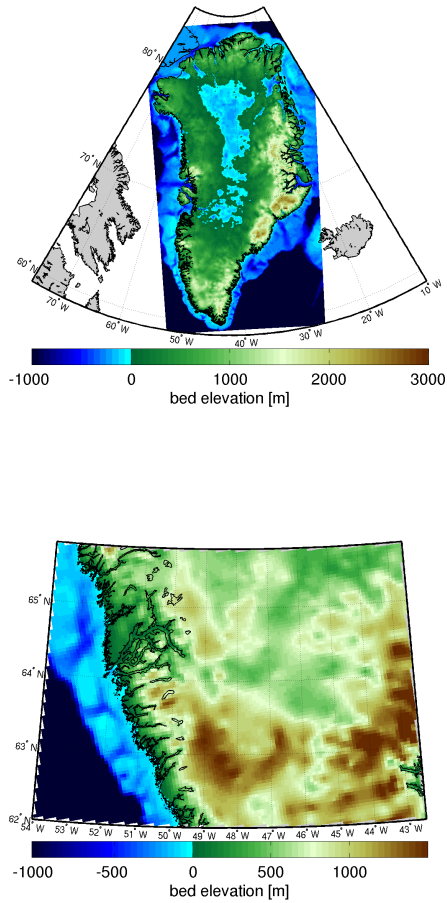


Figure 3.1: The bed elevation for the Greenland ice sheet, and the KNS region on a 5 km grid by Bamber et al. [2001].

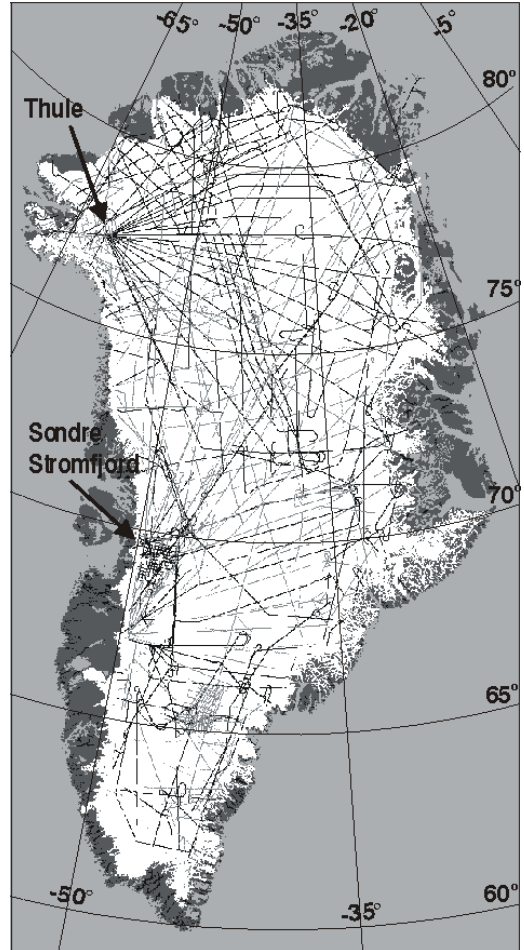


Figure 3.2: Flight lines used for the 5 km resolution bed map in Figure 3.1. Figure taken from [Bamber et al., 2001].

Finally, the geometry data sets are merged as follows. The Bamber et al. [2001] map is the basis because it does not have any data gaps. Then the DEM data is used to replace the old data wherever there is data available. Regions below sea level are filled in using the bathymetry. A visual check is performed to make sure that there are no strange transitions.

More recently, a 1 km data set for Greenland has become available [Bamber et al., 2013], as shown in Figure 3.6. This map is much more detailed, especially at the ice sheet margins. The flight lines, on which the gridded bed map is based, is shown in Figure 3.5. Large ice streams, such as Jakobshavn Isbræ are surveyed frequently. Also in the KNS region, new flight lines are added, but not in the

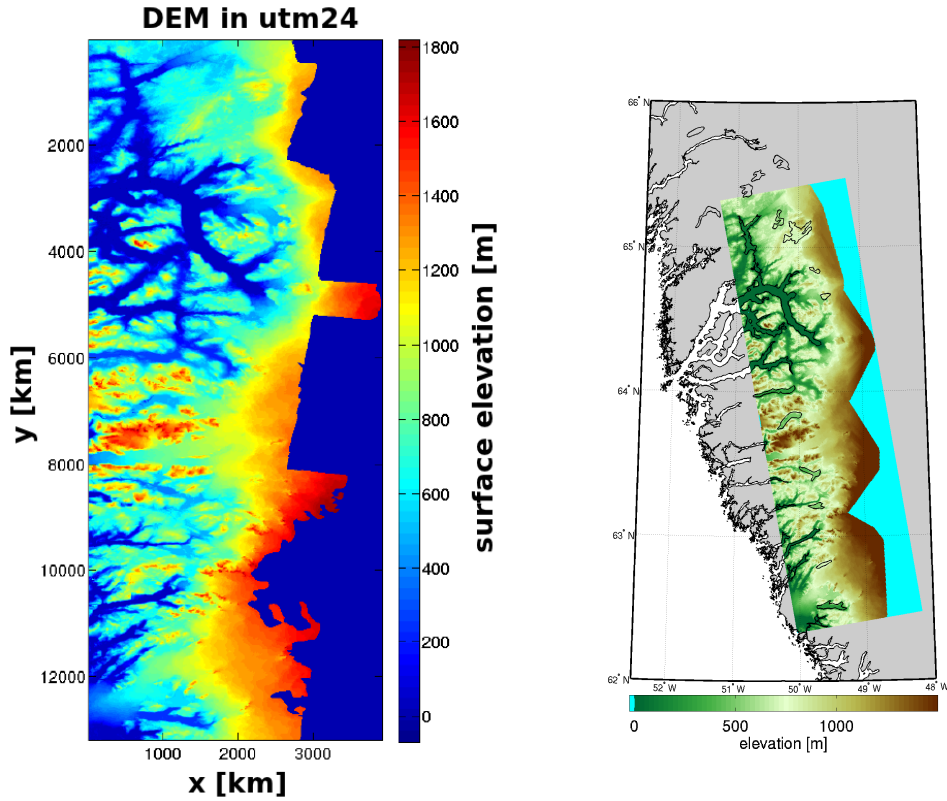


Figure 3.3: The high resolution DEM of the marginal land region by the Natural History Museum of Denmark and remapped onto a 2 km grid (right).

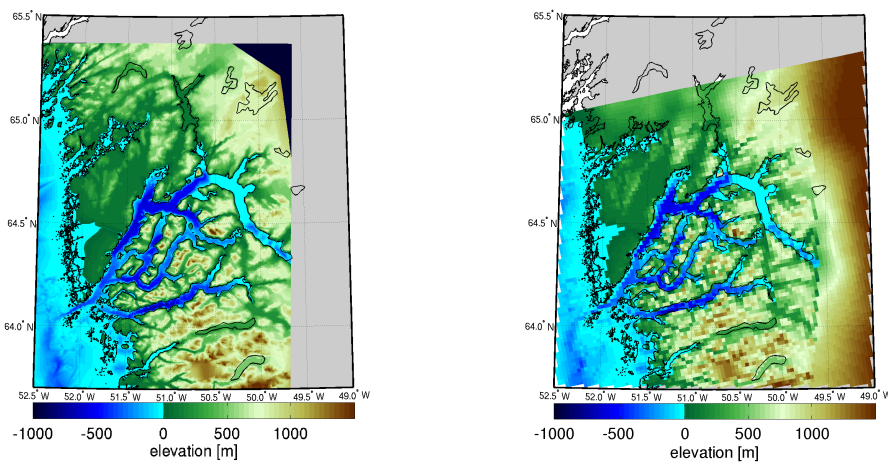


Figure 3.4: The high resolution bathymetry of Godthåbsfjord (left), and remapped onto the 2 km grid (right).

immediate proximity of the terminus. The same procedure has been applied to this map as described above. The model runs have been performed using both bed

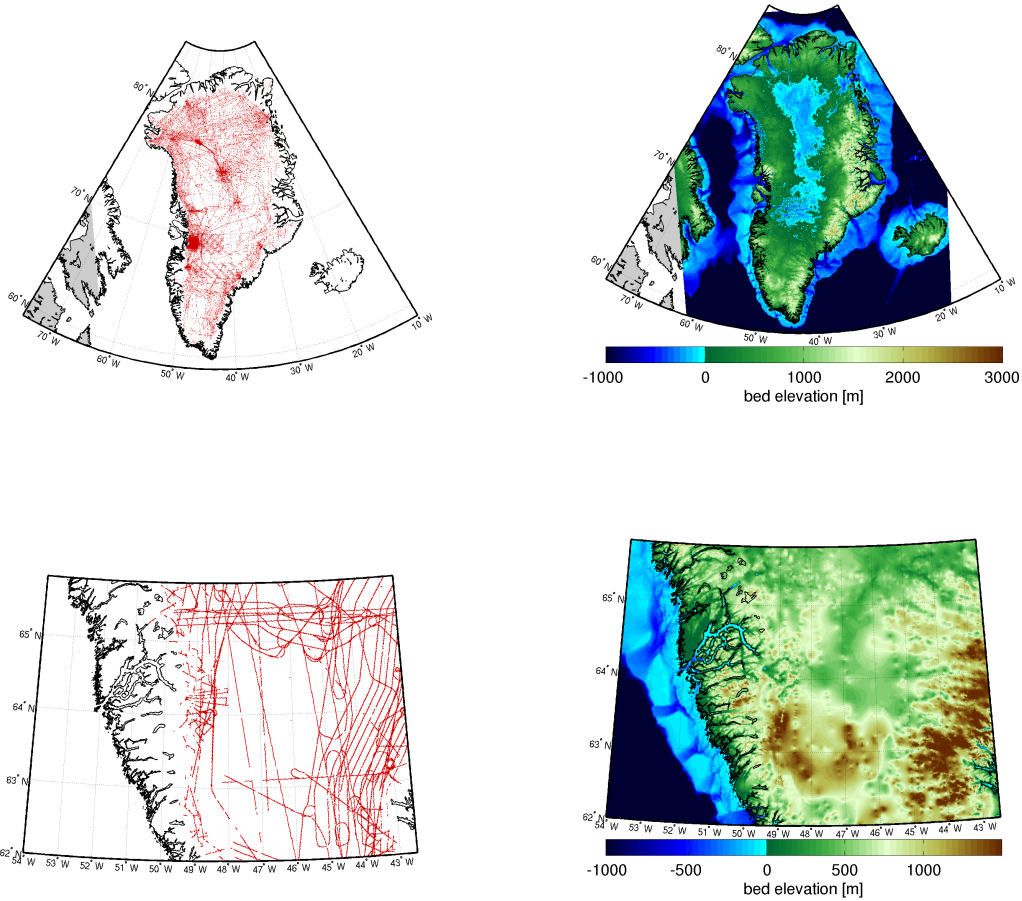


Figure 3.5: Flight lines that are used for the new 1 km resolution bed map [Bamber et al., 2001].

Figure 3.6: The bed elevation for the Greenland ice sheet and the KNS region on the 1 km grid by Bamber et al. [2013].

elevation and ice thickness maps.

The final bed maps used in this study is shown in Figure 3.7 on a 2 km grid based on both the Bamber et al. [2001] and Bamber et al. [2013] maps. Also, the difference in the bed elevation of both maps is shown. There are differences of several hundreds of meters at some points.

3.1.1 Drainage Basin

Hardy et al. [2000] have established drainage basins for the Greenland ice sheet.

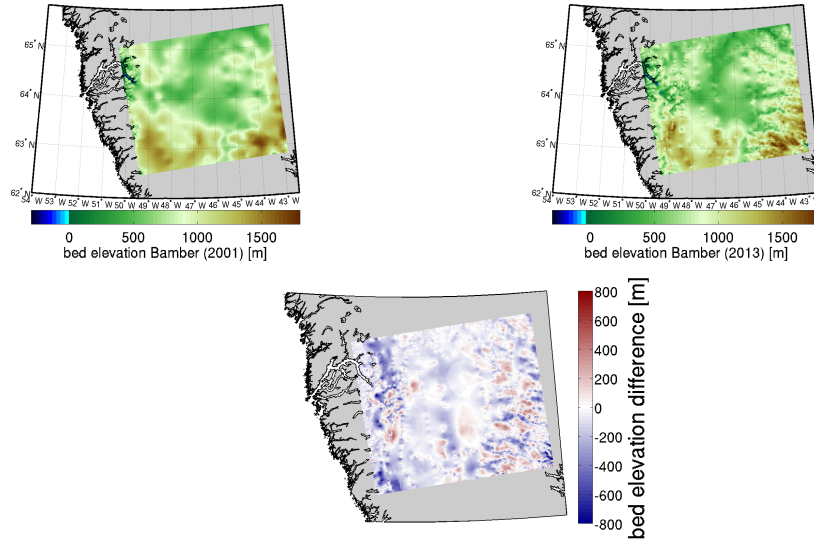


Figure 3.7: Bed elevation used as input for PISM based on the Bamber et al. [2001] (left) and the Bamber et al. [2013] (right) bed elevation map. The bottom figure shows the difference of both, where blue means that the new bed elevation is lower compared to the older map.

They describe these basins as individual units that do not have any flow crossing the boundaries. Hence, drainage basins can be handled individually. PISM’s regional mode, `pismo`, is developed to model such a drainage basin, and high resolution runs are possible for individual outlet glaciers. The basin is generated using PISM’s drainage basin generator. All streamlines following the surface gradient [Budd and Warner, 1996] that end in a terminus rectangle chosen by hand are part of the drainage basin. A depiction of the drainage basin is shown in Figure 3.8. Around the basin, a larger rectangular box is taken as the modeled region, where the physical quantities are prescribed as boundary conditions. PISM uses periodic boundary conditions. In case one would model the whole island of Greenland, there would be ocean grid cells at the boundary, so that there would be no ice flux through the edges. In the case of PISM’s regional mode, there is ice at the boundaries and hence the *no model strip* is introduced. This strip is one grid cell wide with constant prescribed values for the geometry, enthalpy, basal melt, and sliding velocities. These quantities are set after performing the spin-up covering the whole Greenland ice sheet (see Section 3.4). In the area between the no model strip and the drainage basin, the present geometry is held near the prescribed present day value, where the so-called *force-to-thickness* mechanism is applied. In order to keep the present-day geometry, the surface and basal mass balance are altered. The geometry in the drainage basin can evolve freely.

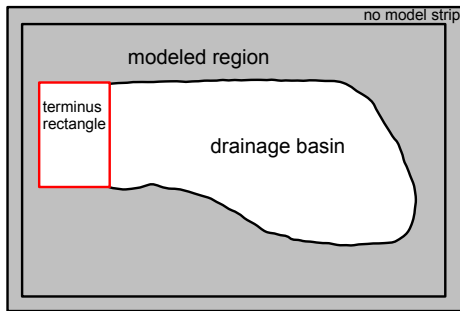


Figure 3.8: Depiction of the drainage basin, terminus region, modeled region and the no model strip, as used in PISM.

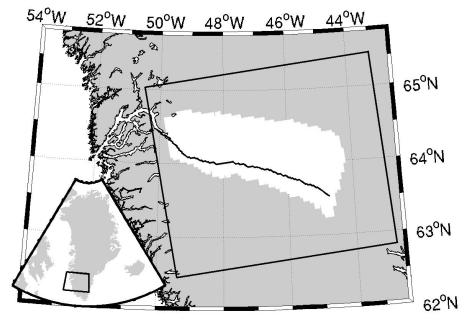


Figure 3.9: The KNS drainage basin and modeled region in white. A center line, following the surface gradients, is shown in black.

An alternative way to compute the drainage basin would be to use observed surface velocity data to define the drainage basin. However, the velocity data available here is not smooth enough to define the outlines in a good way.

The modeled region and the drainage basin for KNS are shown in Figure 3.9. The KNS drainage basin has an area of 27448 km^2 , and the complete modeled region covers 74624 km^2 .

A center line is used to visualize the variations of parameters, such as velocity, across the drainage basin. The center line starts at a point on the ice divide and follows the surface gradient towards the terminus, as shown in Figure 3.9. This center line follows the southern fast flowing arm of KNS.

3.1.2 Ice-Penetrating Radar

In general, bed elevation and ice thickness are unknown. To retrieve the bed elevation underneath an ice sheet, ice-penetrating radars are used. Such a radar operates at different radio or microwave frequencies depending on the aim of the study. The radar itself is usually operated from a vehicle driving over the ice surface or from an air plane. A depiction and an example radargram are shown in Figure 3.10. Part of the transmitted radiation is reflected at any change of density, and is then

recorded. The travel time is converted into depth, making assumptions for the density changes in the ice sheet based on ice core records. The strongest reflection is from the surface. At the inner part of the ice sheet, there are internal layers, the so-called isochrones, which give rise to weaker reflections. Finally, the ice-bed interface is the last signal received. Certain conditions, such as impurities or liquid water embedded in the ice, influence the measurements. Water absorbs the radiation so that the area underneath cannot be sounded.

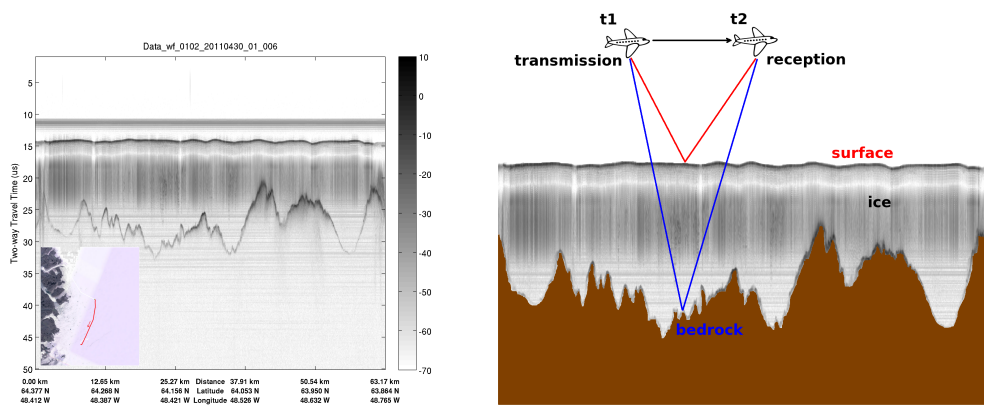


Figure 3.10: Radargram of the KNS region (left) and depiction of the operation of ice-penetrating radar (right).

As shown in Figures 3.2 and 3.5, there is a substantial number of flight lines in Greenland. However, the measurements give very local information on bed elevation, and interpolation is necessary. In this process, small scale features might be missed or enhanced. At the inner part of the ice sheet, an interpolated grid works well for ice sheet models. At the margins, however, more detailed measurements are essential [Durand et al., 2011].

In 2009 and 2011, the Center for Remote Sensing of Ice Sheets (CReSIS) has carried out radar missions near Nuuk to retrieve the bed underneath KNS. Figure 3.11 shows the successful bed elevation measurements for both years. Unfortunately, the ice close to the margin is very wet and the bed could not be detected in the proximity of the terminus. Especially where the ice is flowing fastest, there are no successful measurements until 30 km to the terminus. Figure 3.11 also shows the ice thickness measurements on top of the used ice thickness map on a 2 km grid. At some locations, there are differences of hundreds of meters.

Initially, CReSIS planned to sound the terminus area again in 2012 or 2013, using a temperate radar. Unfortunately, this could not be realized.

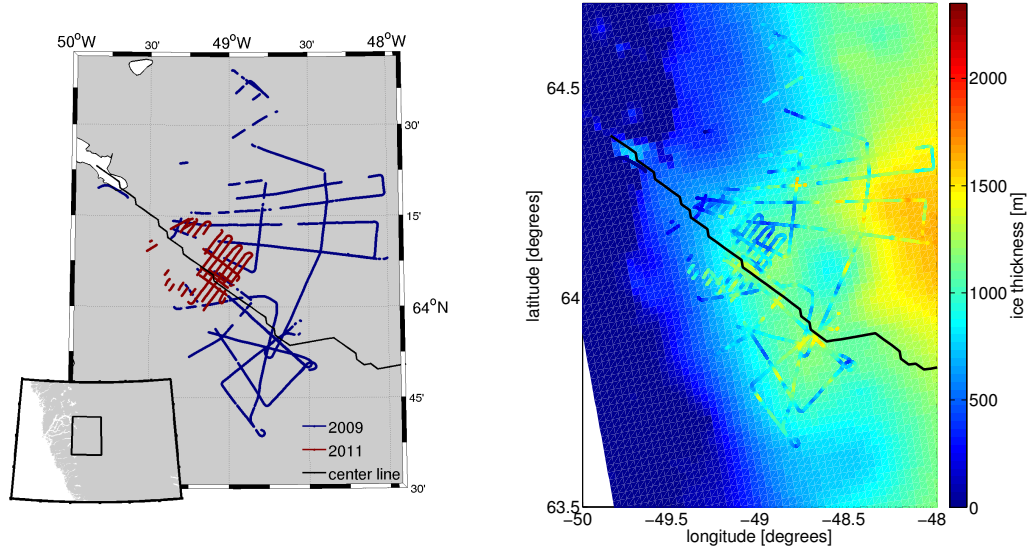


Figure 3.11: The flight lines for the Nuuk region carried out by CReSIS in 2009 and 2011 on the left. The black line is a center line following the the southern fast flowing arm of KNS. On the right, bed elevation measurements are shown on top of the used ice thickness map on a 2 km grid.

3.2 Climatic Forcing

Climatic forcing fields required by PISM are surface mass balance (SMB) and surface temperature. Here, HIRHAM5 and RACMO2 climate model output data are used. The temperature is the near surface air temperature, and the SMB is the sum of accumulation, evaporation, surface melt and refreezing.

HIRHAM5 is a regional climate model developed at the Danish Meteorological Institute (DMI). It is based on HIRLAM (High Resolution Limited Area Model, [Eerola, 2006]) and ECHAM5 [Roeckner et al., 2003]. HIRLAM provides the atmospheric dynamics, and the global ECHAM5 provides the physics. HIRHAM5 is validated through ice cores and automatic weather stations [Box and Rinke, 2003, Dethloff et al., 2002, Kiilsholm et al., 2003, Lucas-Picher et al., 2012, Mottram et al., 2012, Stendel et al., 2008]. Here, monthly mean model output for the 1990–2011 period is used, which is originally on a 0.05° resolution. This is remapped using conservative remapping onto a 5 km rectangular grid.

RACMO2 (Regional Atmospheric Climate Model) is developed at the Institute for Marine and Atmospheric Research Utrecht (IMAU) in the Netherlands [Eetema

et al., 2009] and is widely used, e.g., in the SeaRISE experiment. The climatic forcing for the 1958–2007 average has been remapped to the PISM 5 km grid by the PISM group. The original resolution is about 11 km.

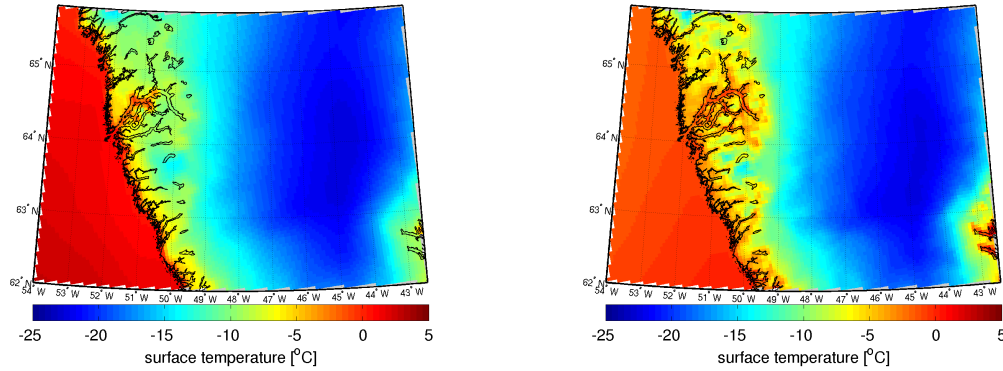
Comparison. Recent comparison studies show that HIRHAM5 is generally warmer than RACMO2 probably due to a lower albedo. Also, the SMB is more negative compared to other discussed models including RACMO2, as shown in Rae et al. [2012].

The spin-up, as discussed in Section 3.4, uses the yearly mean of 1990, HIRHAM5's first model year, and the 1958–2007 average from RACMO2. A direct comparison of these two model outputs is shown in Figure 3.12 for the SMB and surface temperature. There are differences arising from the fact that the model output resolutions differ. The surface temperatures show differences in the fjords, where HIRHAM5 is warmer. The SMB at the inner part of the ice sheet is more positive for RACMO2. The SMB from HIRHAM5 has been interpolated in the ice free regions (by Andy Aschwanden) in order to allow the ice margin to advance during the model runs. However, in the short prognostic runs performed in this thesis, this interpolation is not necessary.

Figure 3.13 shows the SMB and surface temperature along the center line. The surface temperature show that HIRHAM5 is about 3°C colder at the inner part of the ice sheet, but almost 8°C warmer in the fjord, where HIRHAM5 reaches +0.63°C. The SMB within 50 km of the terminus is very similar, at the inner part, however, RACMO2 is more positive. Also, the position of the equilibrium line, where the SMB turns negative, differs by about 40 km.

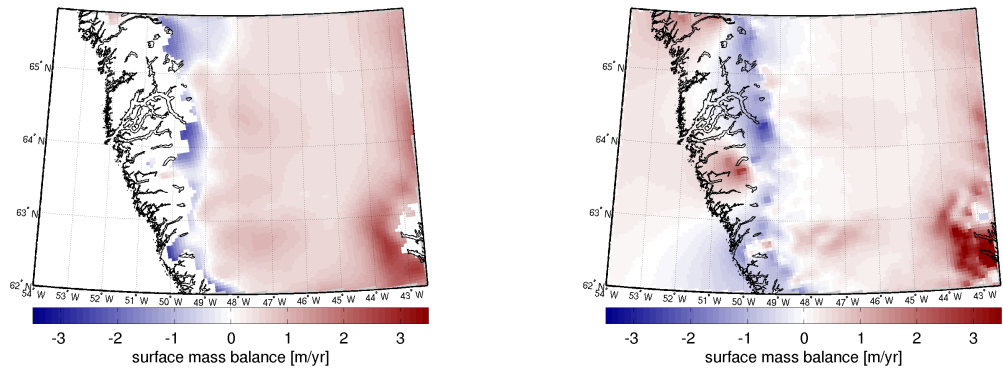
Figure 3.14 shows the seasonal variations and yearly mean values in the drainage basin for the 1990–2011 period. The surface temperature ranges from -33.77°C in the winter to -3.11°C, and it has a total mean of -16.66°C over the whole period. The SMB has a minimum of -53.33 km³/yr and +37.21 km³/yr with a total mean of 3.00 km³/yr. The RACMO2 1958–2007 average is plotted as well at 11.10 km³/yr for the SMB and -18.26°C for the surface temperature.

HIRHAM5 is warmer, especially after 1995. The last model year, 2011, is warmest. There is an overall lower SMB for HIRHAM5, which is even negative compared to RACMO2 for the years 2007, 2008 and 2011. From this, one expects an ice sheet with a larger mass loss due to the lower SMB, when forced with HIRHAM5.



(a) The surface temperature for RACMO2 regional climate model output (average over 1958–2007).

(b) The surface temperature for HIRHAM5 regional climate model output (yearly mean 1990).



(c) The SMB for RACMO2 regional climate model output (average over 1958–2007).

(d) The SMB for HIRHAM5 regional climate model output (yearly mean 1990).

Figure 3.12: Comparison of the surface temperature and surface mass balance pattern for RACMO2 und HIRHAM5 model output.

Paleo climate. One of the spin-up options described below uses past temperature and sea-level records. Figure 3.15 shows both as anomaly from present day for the past 125000 years. The temperature anomaly is derived from the GRIP stable isotope record [Dansgaard et al., 1993, 1989, GRIP-Members, 1993, Grootes et al., 1993, Johnson et al., 1997], and the sea level anomaly is taken from [Imbrie, 2006].

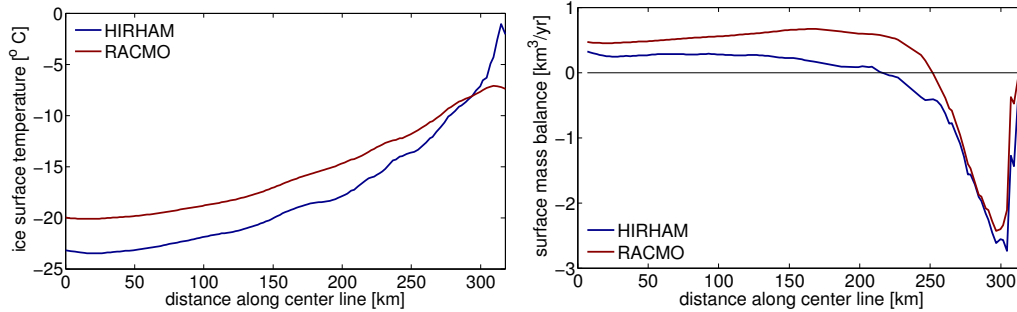


Figure 3.13: The SMB and surface temperature along a center line for HIRHAM5 (yearly mean 1990) and RACMO2 (average over 1958–2007).

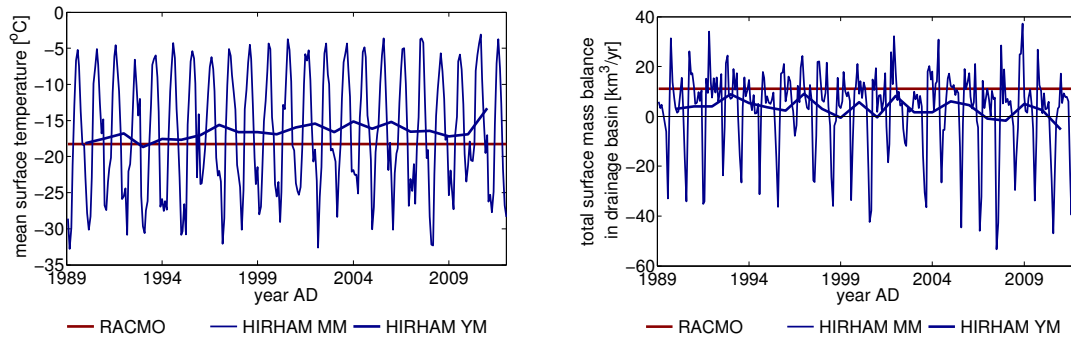


Figure 3.14: The SMB and surface temperature monthly means for HIRHAM5 regional climate model output and average for the 1958–2007 RACMO2 period.

3.3 Surface Velocities

For validation of the model output, observed surface velocities from RADARSAT interferometric synthetic aperture radar (InSAR, Joughin et al. [2010, 2012], Moon et al. [2012]) are used, as shown in Figure 3.16. These velocities are winter velocities averaged over the period 2007–2010. The maximum surface velocity at the KNS terminus is 7.61 km/yr. KNS has three fast flowing arms, where the Southern arm is the largest. In the used bed elevation map there are no features explaining this velocity pattern (see Figure 3.1). In the newer map, however, there are some features further inland that could be the onset to this pattern (see Figure 3.6).

The Geological Survey of Greenland and Denmark (GEUS) has measured surface velocities close to the terminus using three Global Positioning Systems (GPSs) [Ahlstrøm et al., 2013]. Figure 3.18 shows the position of these GPSs that are positioned about 19 km, 22 km and 29 km away from the KNS calving front. The measured mean

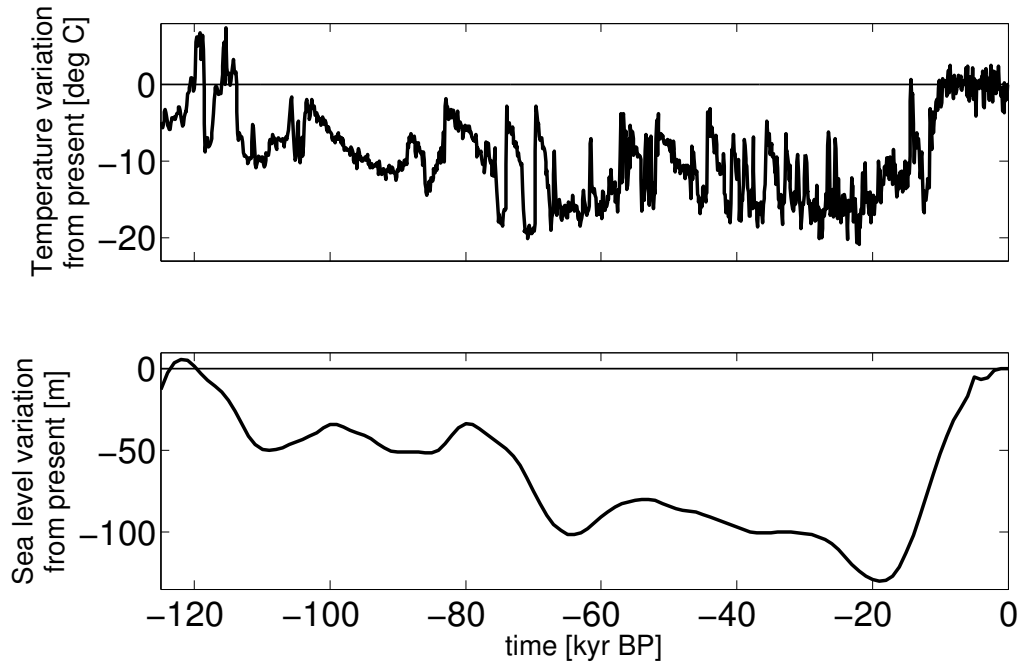


Figure 3.15: The temperature and sea level anomaly with respect to present day conditions.

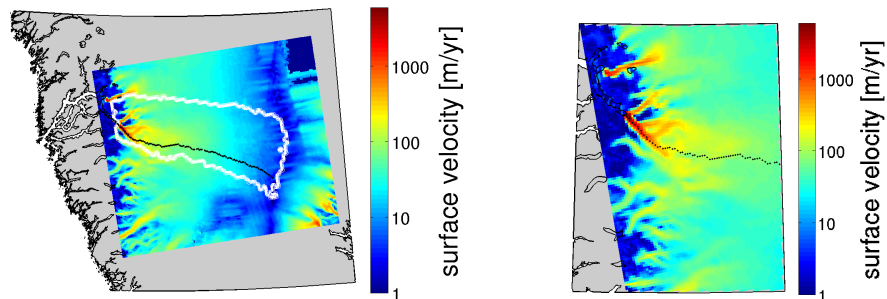


Figure 3.16: Observed surface velocities from InSAR. The drainage basin outlines are shown in white, and the center line used for the one-dimensional plots is depicted in black.

velocities are 1312 m/yr, 1202 m/yr and 586 m/yr respectively. The agreement between InSAR velocities and the GPSs are good. Figure 3.17 shows the whole two year long record with seasonal variations. Here, a summer speed-up of about 30% with respect to the minimum velocity in the winter is recorded.

In addition, the summer velocity at the calving front is estimated to be 30 m/day, which correspondes to 10.96 km/yr (Podrasky, Truffer and Fahnenstock, private communication).

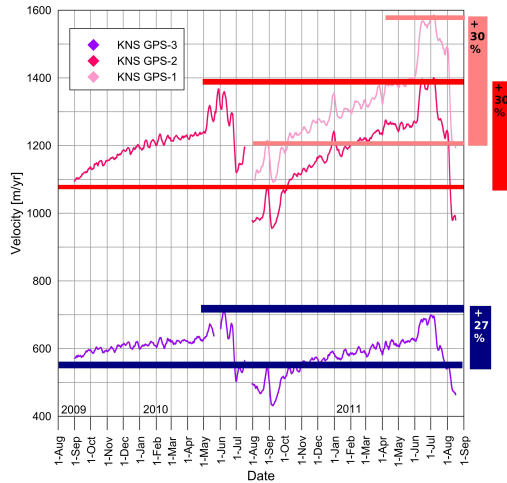


Figure 3.17: KNS surface velocities measured by three GPSs deployed at KNS. Figure taken from Ahlstrøm et al. [2013].

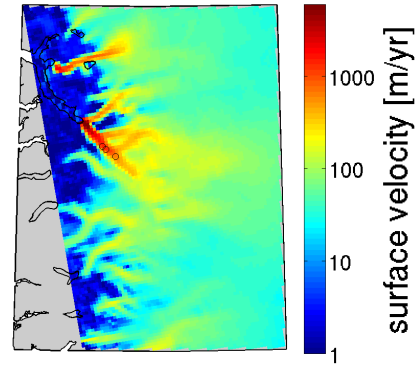


Figure 3.18: Black circles show the GPS positions deployed at KNS [Ahlstrøm et al., 2013].

3.4 Initialization and Spin-Up

The spin-up of an ice sheet plays an important role for its initial state ice sheet [Aschwanden et al., 2012a]. Here, both regional climate model outputs, RACMO2 and HIRHAM5, are used, and two different spin-up scenarios are performed: a constant spin-up and a paleo-climatic spin-up. An overview of both is shown in Figures 3.19 and 3.20.

The constant spin-up uses the present day climate patterns without any variation during the whole spin-up, as shown in Figure 3.19. SMB and surface temperature are held constant until the modeled ice sheet is in equilibrium. Here, a 50000 yr long run using the SIA only is performed, followed by a 50000 yr hybrid run. Both are carried out on a 5 km grid. This spin-up is performed using HIRHAM5 model output for the first model year, i.e., 1990.

The paleo-climatic spin-up, as shown in Figure 3.20, covers one glacial cycle, i.e., 125000 years. The past surface temperature and SMB are estimated using ice core records and global sea level. This spin-up, on a 5 km grid, has been done by the PISM group for the whole Greenland ice sheet. It is followed by a regional run for the period 3000 BP to 1000 BP on the same grid with a constant climate. This

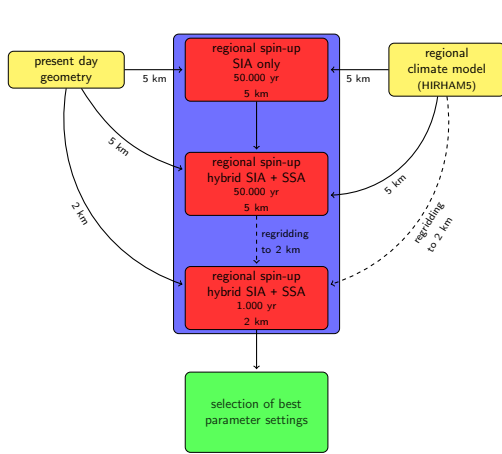


Figure 3.19: The constant spin-up. Present day climate patterns without any variation are used during the whole spin-up.

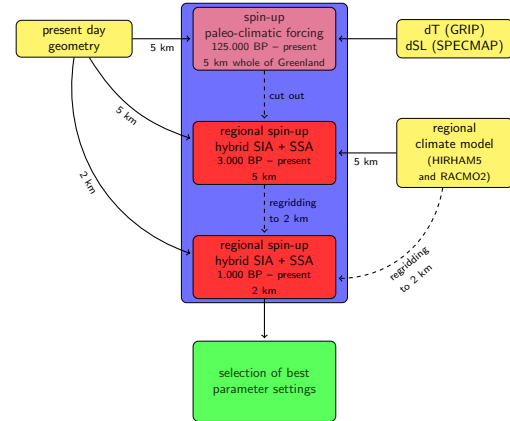


Figure 3.20: The paleo-climatic spin-up covers one glacial cycle, i.e., 125,000 years. The past surface temperature and surface mass balance are estimated using ice core records (dT) and global sea level (dSL).

last part of the spin-up is carried out using HIRHAM5 (first model year, 1990) and RACMO2 (1958–2007 average).

The regional run is performed after both spin-ups. The spinned-up end state is regrided to the 2 km grid. It is continued by a regional run for the past 1000 years. In this stage, several parameters have been changed, as described in Chapter 4.

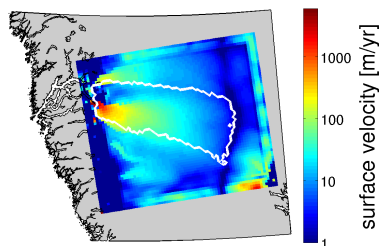


Figure 3.21: Modeled surface velocity using the default parameter setting and HIRHAM5 climate model output.

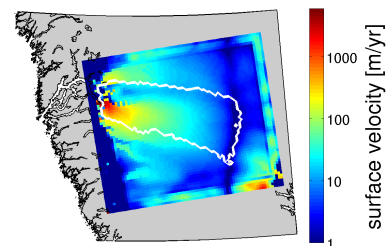


Figure 3.22: Modeled surface velocity using the default parameter setting and RACMO2 climate model output.

Modeled surface velocity patterns using both HIRHAM5 and RACMO2, the same default parameter settings and a paleo-climatic spin-up, are shown in Figures 3.21 and 3.22 respectively. Both succeed in having a clear velocity increase towards the terminus. The maximal velocity is similar for both: 18.25 km/yr for HIRHAM5 and 19.65 km/yr for RACMO2. Both are more than double the observed InSAR velocity of 7.6 km/yr. The observed velocity pattern with distinct fast flowing arms,

as shown in Figure 3.16, is not captured by the model. RACMO2 results in a wider fast flowing area towards the South and an ice divide farther to the West. From this, HIRHAM5 shows better results in capturing the overall surface velocity.

3.5 Example Output

In this section, the PISM output is discussed for one of the best parameter settings selected in the next chapter. This run has a paleo-climatic spin-up and uses HIRHAM5 climate model output and is based on the Bamber et al. [2001] bed elevation map. The factor α controlling the pore water pressure, see Equation (2.58), is 0.97, and the threshold velocity u_{thr} , see Equation (2.55), is 10 m/yr. The till friction angle ϕ , see Equation (2.59), is ranging from 0° to 15° , and the SIA enhancement factor e , see Section 2.4, is 1. Figure 3.23 shows the modeled pattern for basal melt, basal shear stress τ_b , basal yield stress τ_c , and driving stress τ_d , after the regional run is performed. Note that only the values in the drainage basin are considered.

In about one third of the drainage basin, basal melt of less than a few centimeters ice per year is present. At the terminus, the basal melt increases to 0.64 m/yr. The basal shear stress and yield stress is small in the largest part of the basin. At the ice divide, the basal shear stress reaches 233 kPa and the yield stress has a maximum of 4864 kPa. The driving stress runs from nearly zero at the ice divide up to 120 kPa at the terminus.

Figure 3.24 shows the variation of bed elevation, surface elevation, stresses τ , basal water thickness w , velocities, basal melt and till friction angle ϕ along the center line. The modeled surface velocity on a linear scale shows that the velocity rapidly increases in the last 70 km until reaching its maximum of 7.43 km/yr at the calving front. There, sliding dominates the surface velocity over deformation. In the case there is sliding, basal melt is present, with a maximum of 0.68 m/yr. The basal water thickness increases towards the terminus until a maximum of 2 m is reached, which is the maximum allowed in PISM. Additional water is just lost in the PISM version used here. Then, the basal, driving and yield stresses are shown. The driving stress increases slowly towards the terminus, meaning that the velocity due to deformation is increasing. The yield stress decreases towards the terminus, and the basal shear stress increases. At the last 70 km, the basal shear stress exceeds the yield stress, which means there is basal sliding. The rapid decrease in the basal yield stress τ_c , and hence the basal shear stress τ_b , arises from the fact that the basal water thickness

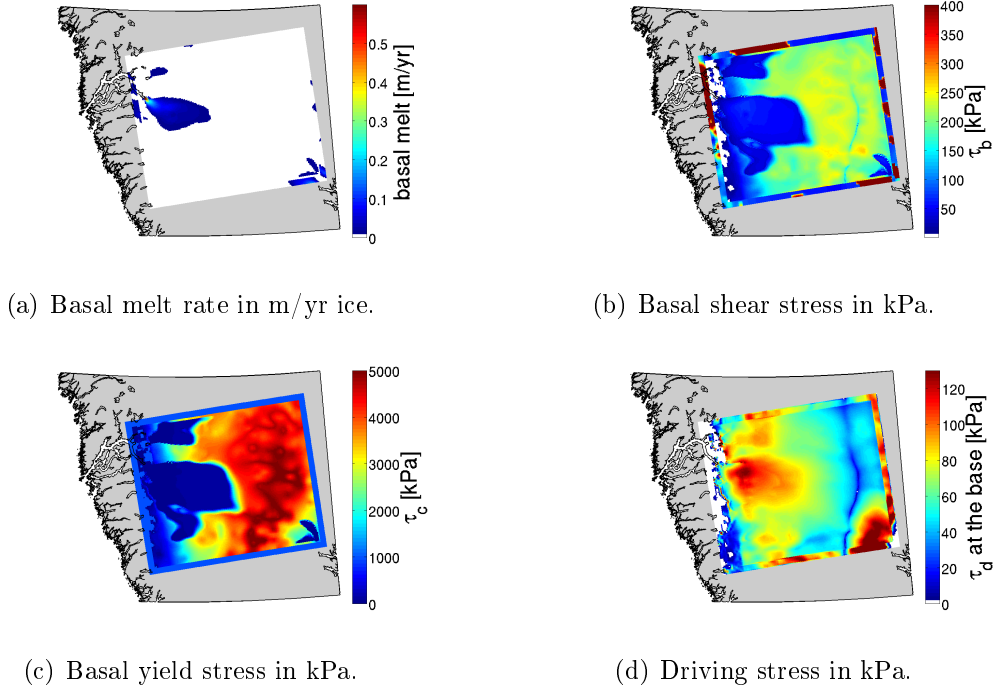


Figure 3.23: Modeled pattern after the regional run is performed. Note that only the values in the drainage basin are considered.

increases. Finally, the bed elevation dependent till friction angle ϕ is shown.

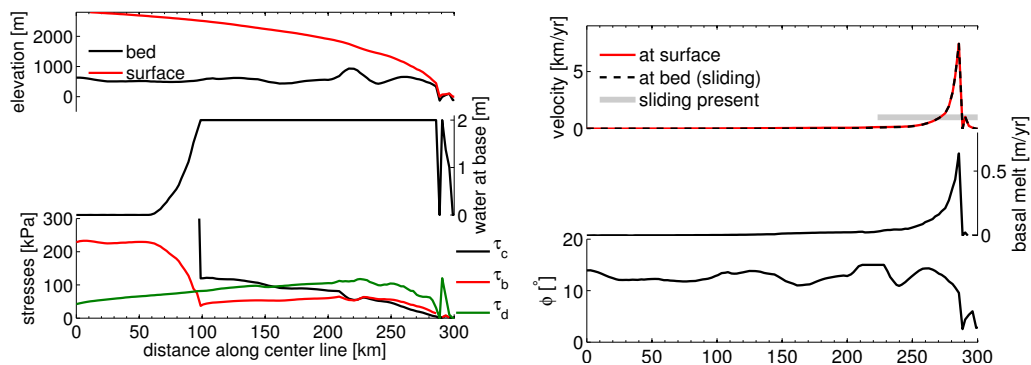


Figure 3.24: Properties modeled by PISM along a center line.

The total basal melt for 1990 in the KNS drainage basin is $0.18 \text{ km}^3/\text{yr}$ and the total SMB is $0.43 \text{ km}^3/\text{yr}$. The total calving flux is $-4.57 \text{ km}^3/\text{yr}$, which clearly dominates the mass loss here. The total mass balance is the sum of these three: $M_T = -4.32 \text{ km}^3/\text{yr}$.

4 | Modeling the Present and Future Behavior of KNS

This chapter is an extended version of the paper submitted to The Cryosphere. The aim is to describe the present and future behavior of KNS. In total, around 90000 CPU hours were performed for PISM model runs in this study. Here, regional model runs following the spin-ups are, as shown in the previous chapter, are performed. Finally, the whole HIRHAM monthly mean climate model output is applied to a subset of model runs, whose selection criteria are described in the following section. This study is performed using the older Bamber et al. [2001] and the newer Bamber et al. [2013] ice thickness, separately.

4.1 Parameter Selection

The parameters altered in the parameter study are climatic forcing and initialization, flow enhancement factor e , pore water pressure fraction α , till friction angle (ϕ_{min}, ϕ_{max}) and threshold velocity u_{thr} , as shown in Table 4.1.

All combinations of possible parameter settings, a total of 108 combinations, are performed for three different climatic forcing and initialization scenarios using the Bamber et al. [2001] ice thickness: HIRHAM5 forcing with paleo-climatic spin-up (Hp), HIRHAM5 forcing with constant present day spin-up (Hc), and RACMO2 forcing with paleo-climatic spin-up (Rp). In addition, the model runs using the Bamber et al. [2013] ice thickness are performed for HIRHAM5 and RACMO2 forcing and a paleo-climatic spin-up. This makes a total of 540 model runs with a computing time of about 90000 CPU hours.

Table 4.1: Parameter space of the runs. Altered parameters are flow enhancement factor e , pore water pressure fraction α , till friction angle (ϕ_{min}, ϕ_{max}) , and threshold velocity u_{thr} . Two different climatic forcings (H: HIRHAM5, R: RACMO2) and two initializations (p: paleo climatic spin-up, c: constant spin-up) are tested. Bold numbers are the default values chosen by the PISM group for the regional mode based on Jakobshavn Isbræ.

e []	Equation (2.20)	1	3	5
α []	Equation (2.58)	0.97	0.98	0.99
u_{thr} [m/yr]	Equation (2.55)	10	100	1000
(ϕ_{min}, ϕ_{max}) [degrees]	Equation (2.59)	(0,15)	(0,20)	(5,30) (20,45)
forcing	Section 3.2	H	R	
initialization	Section 3.4	p	c	

The end state of all runs is compared to observed ice thickness and surface velocities. The surface velocity is not an input field for the model; ice thickness, however, is. The individual best run, selected using the following six criteria (M1 – M6), is then selected for each method and for the combined best run.

M1 Root-mean-square (RMS) of the modeled and observed surface velocity per grid cell. Best parameter setting:

$$\mathbf{M1}: e=1 - \alpha=0.97 - u_{thr}=100 \text{ m/yr} - (\phi_{min}, \phi_{max})=(5,30) - \text{Hc},$$

$$\mathbf{M1*}: e=1 - \alpha=0.97 - u_{thr}=10 \text{ m/yr} - (\phi_{min}, \phi_{max})=(20,45) - \text{Hp}.$$

M2 Difference in the mean of the modeled and observed surface velocity. Best parameter setting:

$$\mathbf{M2}: e=1 - \alpha=0.97 - u_{thr}=10 \text{ m/yr} - (\phi_{min}, \phi_{max})=(0,15) - \text{Hp},$$

$$\mathbf{M2*}: e=1 - \alpha=0.97 - u_{thr}=100 \text{ m/yr} - (\phi_{min}, \phi_{max})=(5,30) - \text{Hp}.$$

M3 RMS of the modeled and observed ice thickness per grid cell. Best parameter setting:

$$\mathbf{M3}: e=3 - \alpha=0.98 - u_{thr}=10 \text{ m/yr} - (\phi_{min}, \phi_{max})=(20,45) - \text{Hp},$$

$$\mathbf{M3*}: e=3 - \alpha=0.97 - u_{thr}=1000 \text{ m/yr} - (\phi_{min}, \phi_{max})=(20,45) - \text{Hp}.$$

M4 Difference in the mean of the modeled and observed ice thickness. Best parameter setting:

$$\mathbf{M4}: e=1 - \alpha=0.97 - u_{thr}=1000 \text{ m/yr} - (\phi_{min}, \phi_{max})=(5,30) - \text{Hp},$$

$$\mathbf{M4*}: e=3 - \alpha=0.97 - u_{thr}=10 \text{ m/yr} - (\phi_{min}, \phi_{max})=(20,45) - \text{Hp}.$$

M5 RMS of the modeled velocity and observed velocity along a center line following the southern fast flowing arm of KNS. Best parameter setting:

M5: $e=5 - \alpha=0.97 - u_{thr}=10$ m/yr - $(\phi_{min}, \phi_{max})=(5,30)$ - Hc,

M5*: $e=3 - \alpha=0.98 - u_{thr}=10$ m/yr - $(\phi_{min}, \phi_{max})=(20,45)$ - Hp.

M6 The combined ranking of the first five methods. Best parameter setting:

M6: $e=1 - \alpha=0.99 - u_{thr}=100$ m/yr - $(\phi_{min}, \phi_{max})=(20,45)$ - Hp,

M6*: $e=3 - \alpha=0.97 - u_{thr}=10$ m/yr - $(\phi_{min}, \phi_{max})=(5,30)$ - Hp.

Following these criteria, only runs using the HIRHAM5 climatic forcing got selected. The distribution of selected parameters is shown in Figure 4.1. There is a tendency towards a smaller pore water fraction α (see Figure 4.1 a and e) and a smaller threshold velocity u_{thr} for both ice thickness maps (see Figure 4.1 b and f). The till friction angle ϕ is smaller than default for the Bamber et al. [2001] and larger for the Bamber et al. [2013] ice thickness (see Figure 4.1 c and g). The enhancement factor e that matches the observations best, equals 1 for the 2001 and 3 for the 2013 map (see Figure 4.1 d and h).

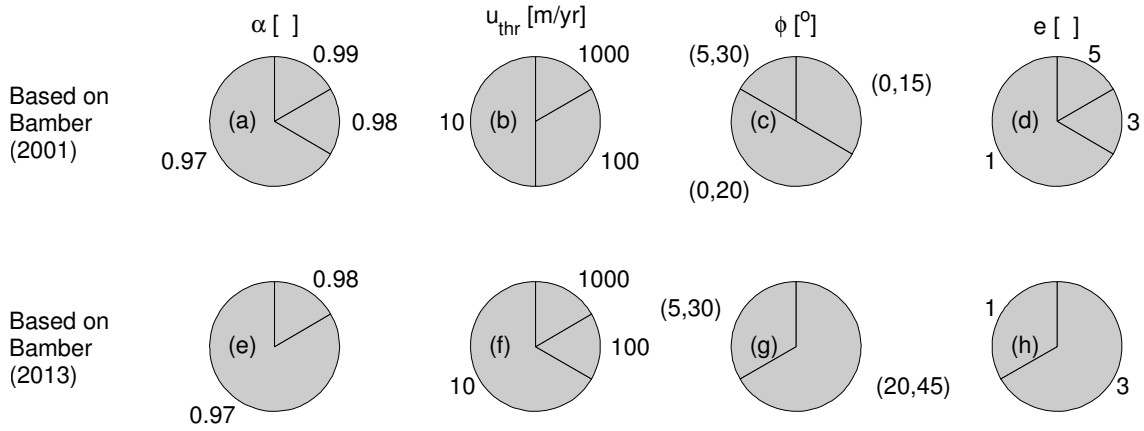


Figure 4.1: Distribution of parameters (i.e., the pore water fraction α (a,e), the threshold velocity u_{thr} (b,f), the till friction angle ϕ , (c,g) and the enhancement factor e (d,g)) of the selected settings whose model runs match the observations best.

The volume of the drainage basin for all 540 runs is shown in Figure 4.2, in which the selected runs are highlighted. These remain close to the observed volume. Except for a few outliers, the volume of the drainage basin remains constant after about 500 years. This means that the basin can be considered to be in equilibrium and the regional run of 1000 years is long enough in order to adapt to the changed parameters. Figure 4.3 shows the distribution of the final volume of the drainage basin for all 540 model runs. The black line indicates the observed volume. 99.07% of the model runs have a volume that lies within 1σ of the observed volume¹. 80.19%

¹ 1σ is 68.3% confidence level, 2σ is 95.4% confidence level, and 3σ is 99.7% confidence level.

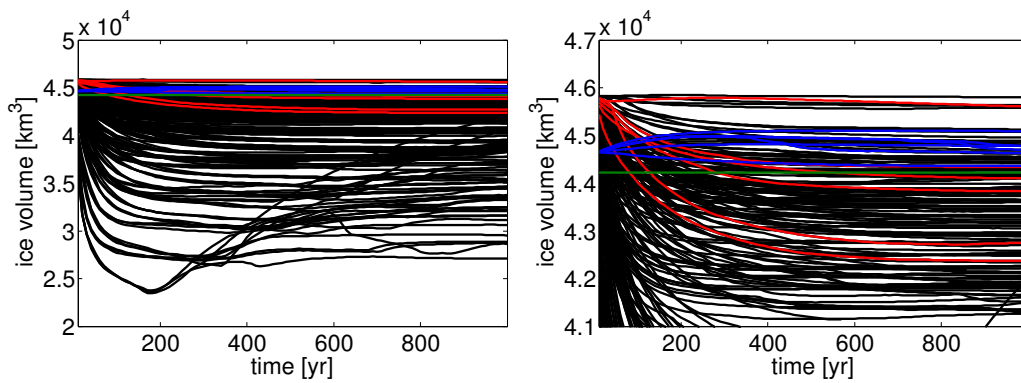


Figure 4.2: The volume of the drainage basin for all 540 model runs, in which the selected runs highlighted in red [Bamber et al., 2001] and blue [Bamber et al., 2013]. These remain close to the observed volume, which is shown in green. Except for a few outliers, the volume of the drainage basin remains constant after about 500 years.

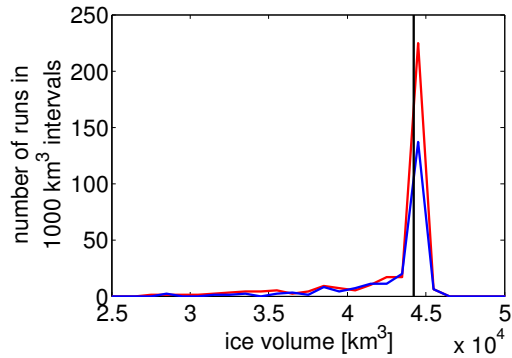


Figure 4.3: The distribution of the final volume of the drainage basin for all 540 model runs in red [Bamber et al., 2001] and blue [Bamber et al., 2013]. The black line indicates the observed volume.

lie within 2σ , and 3.15% within 3σ .

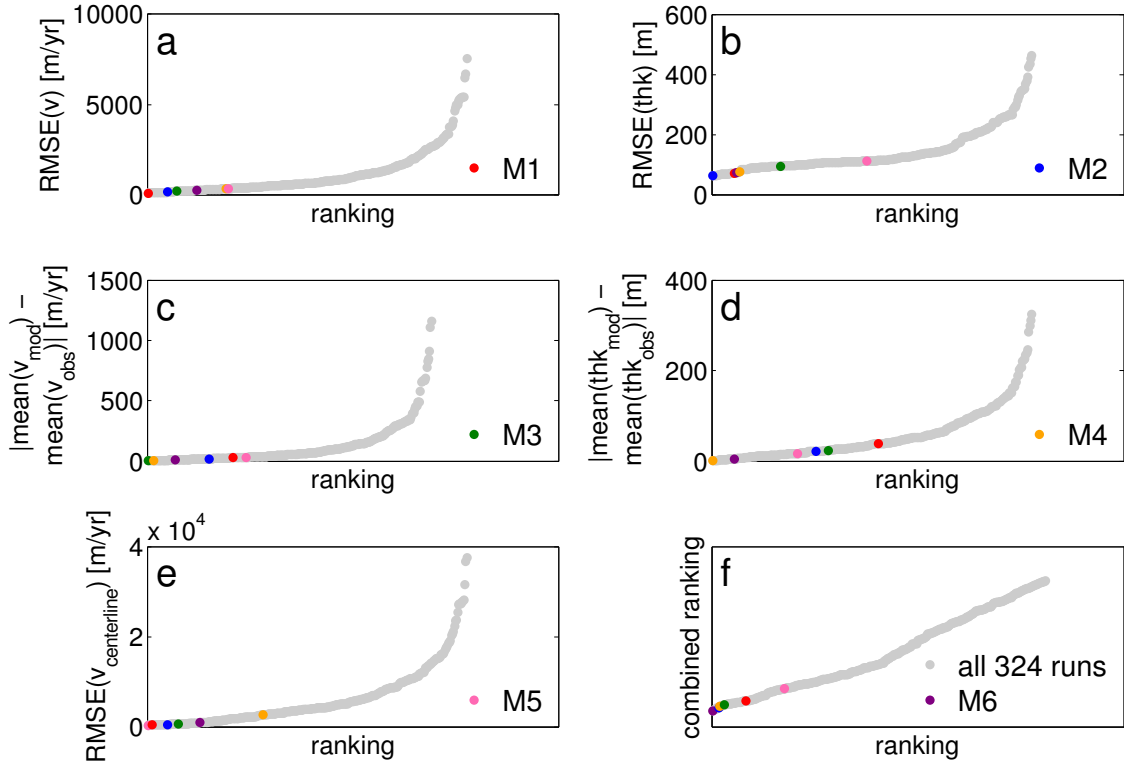


Figure 4.4: Ranking of the selected runs for all six criteria using the Bamber et al. [2001] ice thickness.

Figures 4.4 and 4.5 show how the selected runs rank for each criterion. None of the selected parameter settings is ranking badly for one of the other criteria. However, M1 and M5 rank worst for the other criteria and the combined ranking.

4.2 Current Velocities and Fluxes

Figures 4.6 and 4.7 show the pattern of observed and modeled surface velocities in the modeled region. The outlines of the KNS drainage basin are shown in white. Note that the pattern of fast flowing arms is not captured by any of the model runs. For M1, the ice stream is small and narrow compared to, e.g., M4 and M6. The position of the ice divide, i.e., where the surface velocity is smallest, is moved to the East for M3 and M5. The model runs using the Bamber et al. [2013] ice thickness are generally more narrow compared to the Bamber et al. [2001] map. Also, for M3* to M6*, some features are emerging in the modeled surface velocity, but not as detailed as it is observed. However, it could be the onset that could emerge further

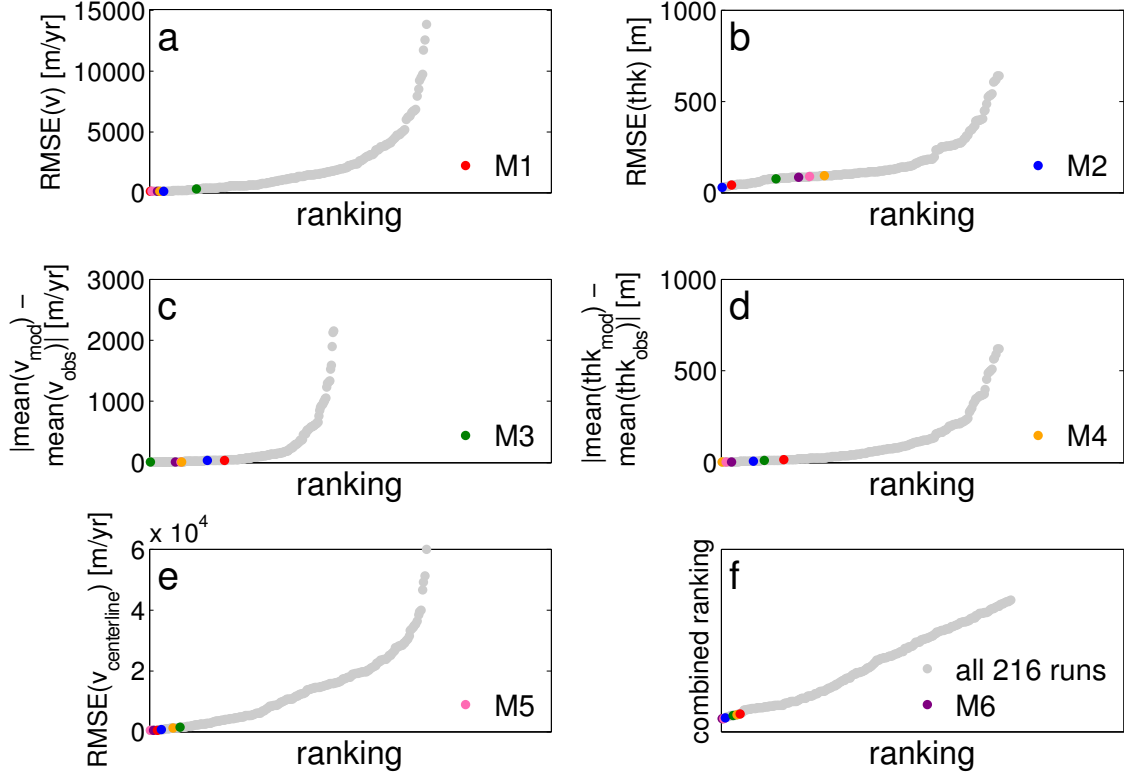


Figure 4.5: Ranking of the selected runs for all six criteria using the Bamber et al. [2013] ice thickness.

in the model once there is a realistic bed map.

The modeled surface velocities and ice thickness along a center line following the southern fast flowing arm of KNS is shown in Figure 4.8. The selected modeled surface velocities at the terminus range from 0.1 km/yr to 25.9 km/yr. Note that in the model runs using the new ice thickness and bed map, KNS has retreated about 10 km. This is due to the fact that the bed elevation is below sea level farther inland compared to the map from 2001. Observed surface velocities from InSAR [Joughin et al., 2010, Moon et al., 2012] indicate that M2 captures the InSAR observations at the terminus best. M2, M5, M4* and M5* show a better match to the velocities measured by GEUS’s GPSs, and M6 matches the estimated summer velocity at the calving front of 30 m/day (Podrasky (UAF), private communication). The modeled ice thickness along the center line is captured best by M2 and M2*. For the Bamber et al. [2001] ice thickness, the modeled ice stream appears to be too thick when modeled surface velocities are too small, i.e., M1, M3 and M5. For the new Bamber et al. [2013] ice thickness, all modeled ice streams are thicker than observed close to the terminus.

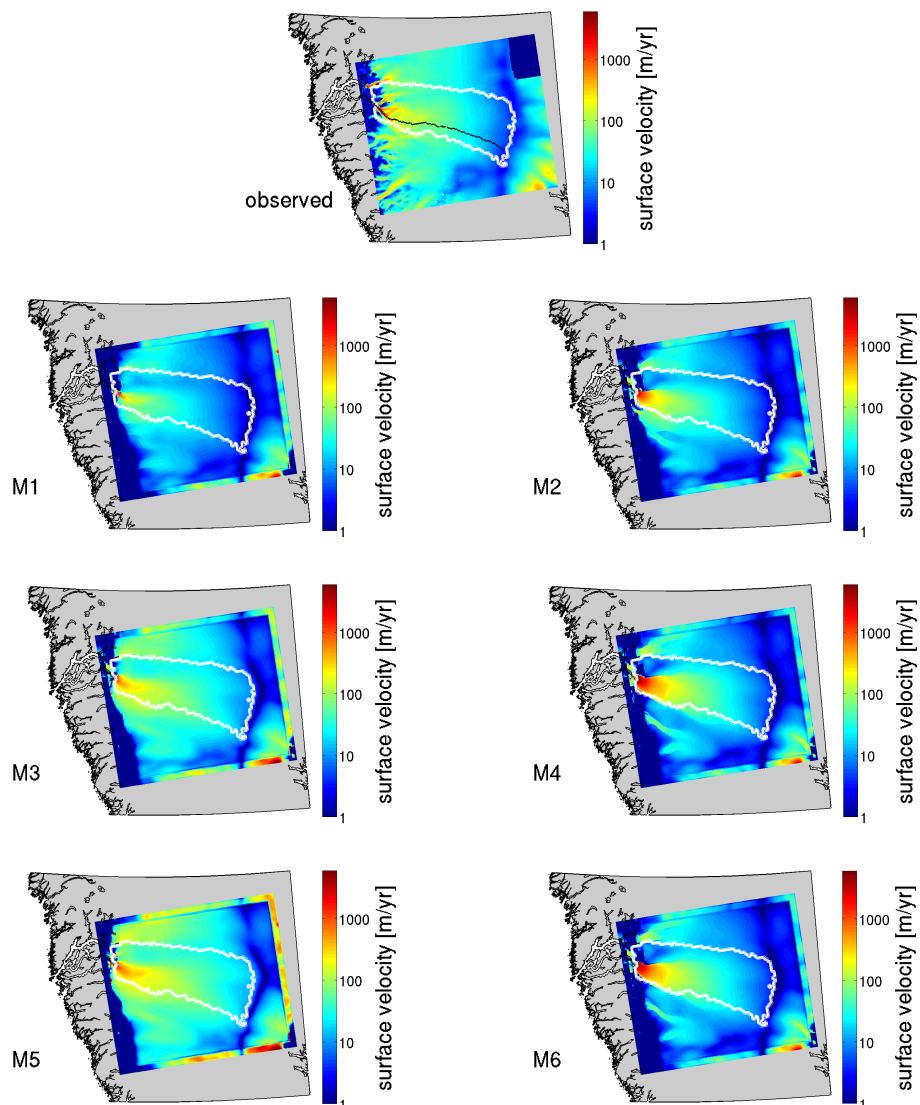


Figure 4.6: Modeled surface velocities for the Bamber et al. [2001] bed elevation. Observed velocities from InSAR [Joughin et al., 2010, Moon et al., 2012]. The black line indicates a center line from the ice divide towards the terminus following the southern fast flowing arm of KNS.

Figure 4.9 shows the basal melt, and driving, basal shear and yield stresses along the center line. Basal melt at the proximity of the terminus reaches from 0.10 m/yr for M1* to 4.00 m/yr for M4*. The driving stress is below 100 kPa for the largest part of the ice stream. In the last 30 km, the driving stress increases to, e.g., 388 kPa for M1*.

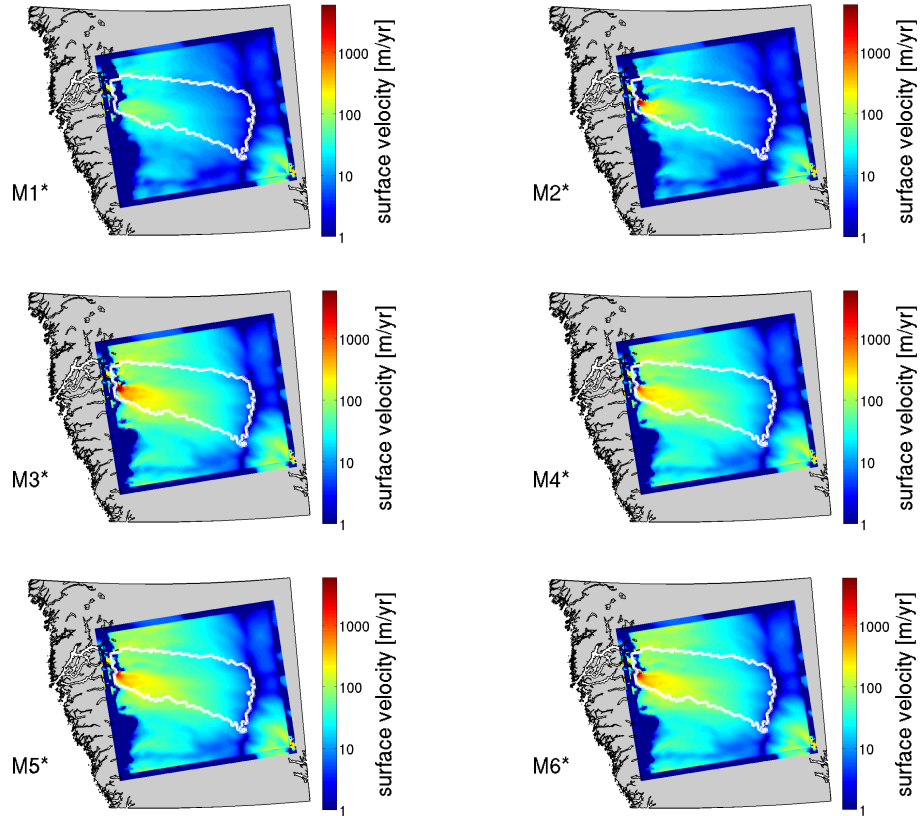


Figure 4.7: Modeled surface velocities for the Bamber et al. [2013] bed elevation. The black line indicates a center line from the ice divide towards the terminus following the southern fast flowing arm of KNS.

4.2.1 Monthly Mean 1990–2011

As described above, a monthly climatic forcing for the 1990–2011 period covered by the HIRHAM5 model output is applied. PISM is able to output seasonal variability in the modeled fluxes when monthly means of the climatic forcing are applied. The result is shown in Figure 4.10. The solid ice flux is taken from PISM, which is the amount of ice calved off, corresponding to when it becomes afloat. Modeled fluxes are between $0 \text{ km}^3/\text{yr}$ and $9.7 \text{ km}^3/\text{yr}$. An estimate based on surface velocities and ice thickness is $(5 \pm 1) \text{ km}^3/\text{yr}$ (Podrasky (UAF) private communication). Based on this estimate, M2 and M4* match the solid ice flux best, with $4.5 \text{ km}^3/\text{yr}$ and $4.6 \text{ km}^3/\text{yr}$ modeled calving loss, respectively.

Basal melt in the drainage basin is calculated from model output. The modeled basal melt has to be considered with care, since the PISM version used here does not have a sophisticated basal transport model implemented. Modeled basal melt values range from $0.1 \text{ km}^3/\text{yr}$ to $0.6 \text{ km}^3/\text{yr}$. There are no estimates for basal melt

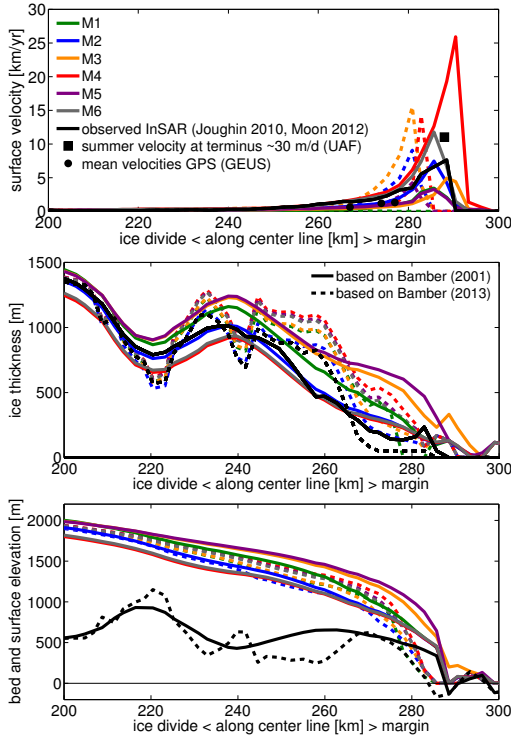


Figure 4.8: Modeled surface velocities (top) and ice thickness (bottom) along a center line following the southern fast flowing arm of KNS. Full lines are the model runs using the Bamber et al. [2001] ice thickness, and dashed lines use the newer ice thickness by Bamber et al. [2013]. Observed surface velocities are from InSAR [Joughin et al., 2010, Moon et al., 2012], velocities measured by GEUS’s GPSs [Ahlstrøm et al., 2013] and summer terminus velocity (Podrasky (UAF), private communication).

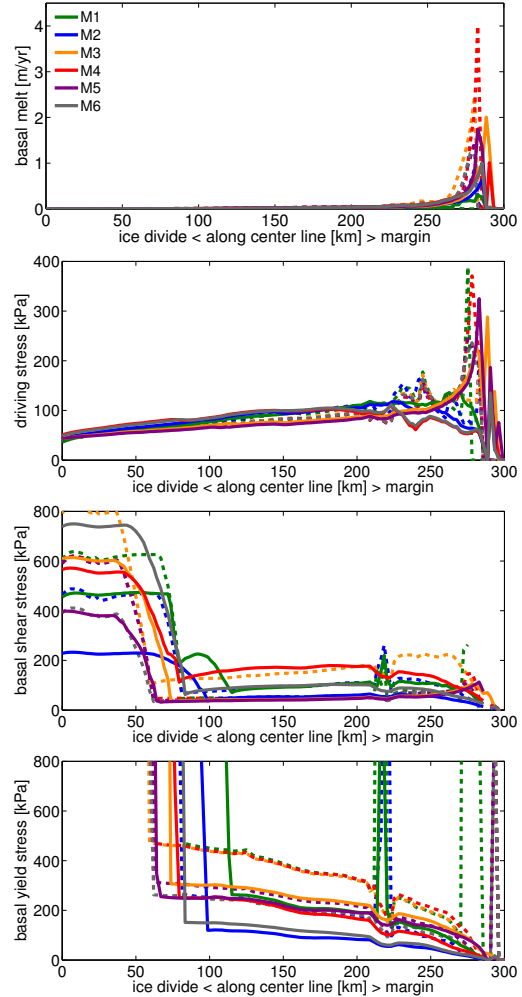


Figure 4.9: Modeled basal melt, and driving, basal shear and yield stresses along the center line following the southern fast flowing arm of KNS.

of KNS available at this point.

The total mass balance M_T , the sum of solid ice flux, basal melt and surface mass balance, is slightly positive in the 1990s and shows a negative trend after 2005. Only model run M1* is gaining mass throughout the whole period. This is due to the fact that in this scenario, KNS has retreated and has lost contact to the fjord. Hence, there is no solid ice flux and the total flux is dominated by the surface mass balance. The modeled total yearly mass balance M_T covering the IceSAT period 2003–2008 is shown in Table 4.2. Comparison with the IceSAT estimate for the drainage basin [Sørensen et al., 2011] indicates that M2 and M3 imitate the observation of

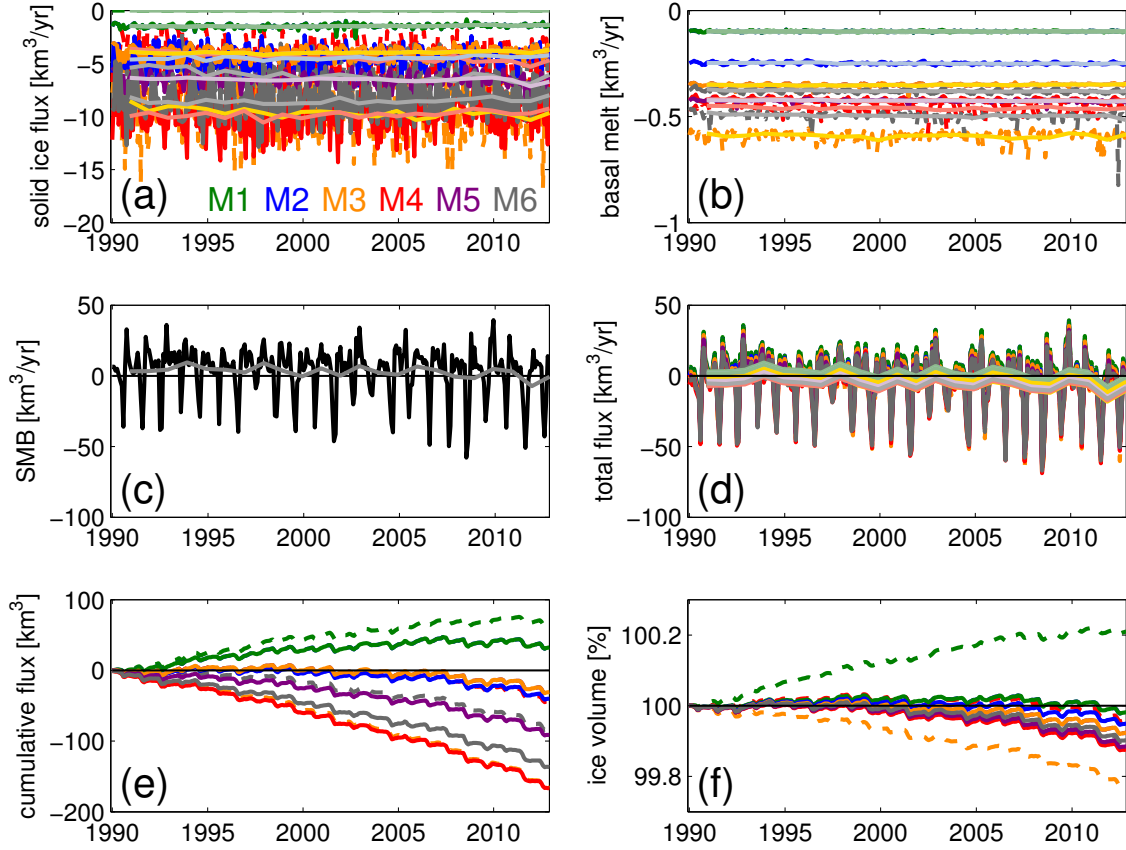


Figure 4.10: Monthly variation of solid ice flux (a), basal melt (b), surface mass balance (c), total mass balance M_T (d), cumulative flux (e) and ice volume (f) for the selected parameter settings for the period covered by the HIRHAM5 model output, 1990–2011. Colors correspond to colors used in, e.g., Figure 4.6.

-2.49 km³/yr for the KNS drainage basin best.

The cumulative flux shows that most runs have a continuous mass loss after 1990, whereas M1 has an initial mass increase, and as mentioned earlier M1* is gaining mass. Looking at the ice volume as a percentage from the starting volume, all runs with the exception of M1* show a smaller ice volume in 2011 compared to 1990.

Figure 4.11 shows the seasonal variation of the modeled surface velocity at the terminus and near one of GEUS’s GPSs. The velocity at the calving front is estimated to be 30 m/day during summer (Podrasky, Truffer and Fahnenstock, private communication), which matches model run M6 best. Modeled summer velocities speed-up for the model runs range from 17% (M5) to 37% (M2), where observed speed-up is approximately 30%.

Table 4.2: Total modeled mass balance M_T averaged over the periods 2003–2008 when using monthly HIRHAM5 forcing and 2010–2050 for using yearly mean forcing. For comparison, the IceSAT elevation change for the period 2003–2008 from Sørensen et al. [2011]. Positive values indicate mass gain, and negative values mean mass loss.

	M_T [km ³ /yr]	M_T [km ³ /yr]	M_T [km ³ /yr]
	2003–2008	2010–2050	2010–2050
		conservative	RCP scenarios
	Section 4.2.1	Section 4.3	Section 4.4
M1	+0.39	-0.30	-7.21
M2	-2.77	-3.31	-9.77
M3	-2.35	-3.04	-9.73
M4	-8.19	-8.60	-15.05
M5	-5.03	-5.58	-12.16
M6	-6.96	-7.35	-13.90
M1*	+1.84	+1.05	-6.03
M2*	-1.91	-2.64	-9.44
M3*	-8.47	-9.01	-15.81
M4*	-3.16	-4.43	-10.90
M5*	-4.46	-5.55	-11.92
M6*	-5.02	-6.05	-12.63
mean	-3.84±3.18	-4.59±3.10	-11.21±2.87
IceSAT	-2.49		

The velocity follows on average a sine with increasing velocities from April to October and decreasing during the rest of the year. The GPSs observe a steady increase of the velocity between August and May/June (see Figure 3.17). Then, there is a sudden increase in velocity, and a sudden decrease in July/August. PISM does not reproduce this behavior. The sudden increase is probably a result of bed lubrication due to melt water that penetrates to the bed and speeds up the glacier. In the PISM version used here, no water is transported from the surface to the bed through crevasses or moulins.

Near one of GEUS’s GPSs, KNS-1 (see Figure 3.17), the modeled velocity is shown in the bottom. Also for this location, M6 fits the observations best.

Based on velocity and ice loss observations, M2 simulates the current behavior of KNS best.

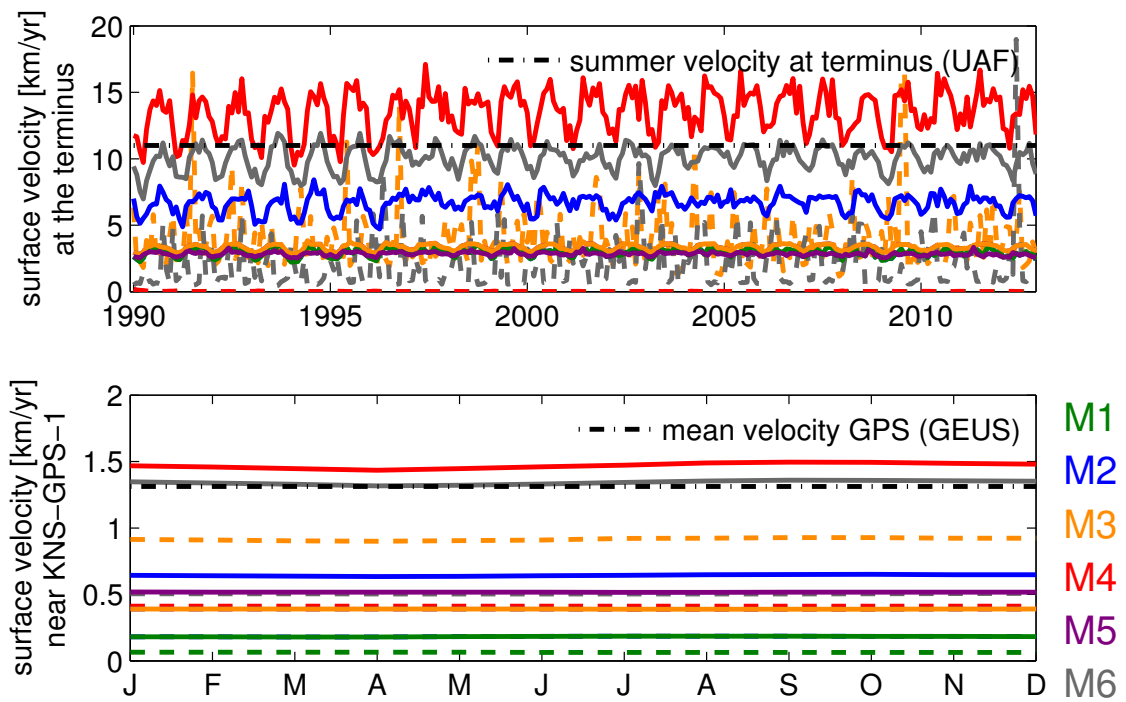


Figure 4.11: Monthly variation of the modeled surface velocity (top) and the normalized monthly average of the modeled surface velocity (bottom). Colors correspond to colors used in, e.g., Figure 4.6.

4.3 Future Predictions

To extend the climatic forcing to 2050, a conservative approach is applied. The 2002–2011 interval is extracted and is then repeated following the existing record to 2050. No additional warming is added to the forcing, which means that the future estimate shown here accounts for a minimal mass loss until 2050. Additional warming as proposed in several scenarios of the IPCC report [IPCC, 2007] would increase the mass loss due to warmer temperatures and lower surface mass balance.

The annual variation of the same quantities and parameter setting as in the previous section are shown in Figure 4.12. Solid ice flux and basal melt are decreasing slightly over time because of the reduced ice volume in the drainage basin. The surface mass balance between 2002 and 2011 is repeated until 2050. Total flux averages after 2010 are as shown in Table 4.2. The modeled mass loss after 2010 is larger than during the IceSAT period. Cumulative flux and ice volume show a steady mass loss in the extended period.

Using the run that performed best to model the current behavior, M2, the continued mass loss after the year 2010 is $3.3 \text{ km}^3/\text{yr}$, which is about 0.2% of its volume with respect to 1990. The remaining selected model runs, excluding M1 and M1*, have a mass loss ranging from $2.6 \text{ km}^3/\text{yr}$ to $9.0 \text{ km}^3/\text{yr}$, corresponding to a volume loss of 0.01% to 0.7%, respectively. The mean mass loss for all twelve runs is $(4.6 \pm 3.1) \text{ km}^3/\text{yr}$, see Table 4.2.

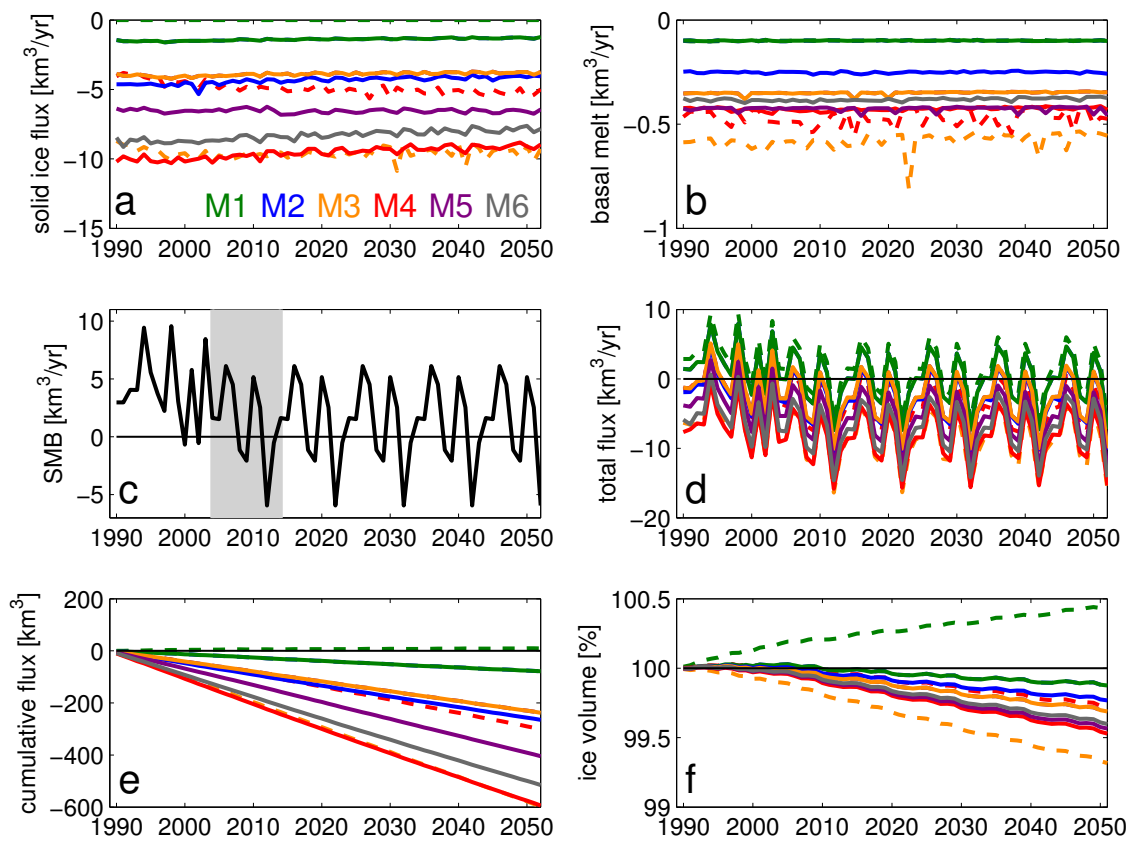


Figure 4.12: Yearly means of solid ice flux (a), basal melt (b), surface mass balance (c), total mass balance M_T (d), cumulative flux (e) and ice volume (f) for the selected parameter settings for the extended period, 1990–2050.

4.4 Representative Concentration Pathway Scenarios

Emission scenarios for Greenhouse gases, called Representative Concentration Pathways (RCPs), are available [Meinshausen et al., 2011]. They are used in the recent IPCC report [IPCC, 2013]. There are four forcing scenarios, named after their radiative forcing range in the year 2100 with respect to the pre-industrial level: RCP2.6, RCP4.5, RCP6 and RCP8.5 for 2.6, 4.5, 6.0 and 8.5 W/m^2 , respectively (see Figure 4.13). These emission scenarios are converted to a temperature change in Greenland using the Coupled Model Intercomparison Project Phase 5 (CMIP5), and the land-cells between 10° and 70° W and 60° to 85° W have been averaged [Simonsen et al., 2013].

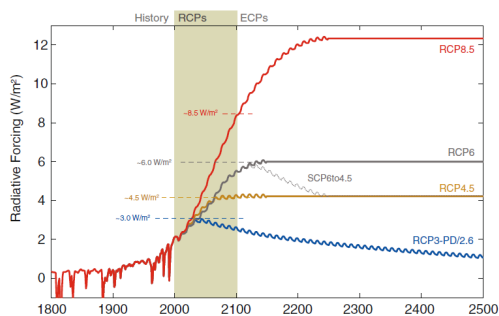


Figure 4.13: Representative Concentration Pathways (RCPs) as used in the recent IPCC report [IPCC, 2013]. There are four forcing scenarios, named after their radiative forcing range in the year 2100 with respect to the pre industrial level: RCP2.6, RCP4.5, RCP6 and RCP8.5 for 2.6, 4.5, 6.0 and 8.5 W/m^2 , respectively.

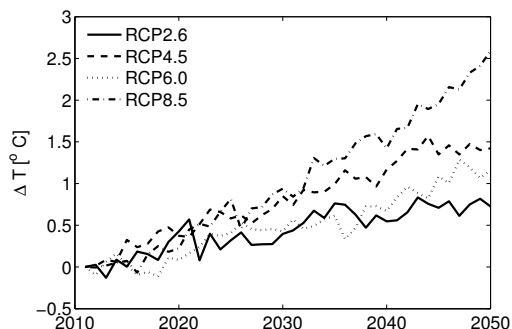


Figure 4.14: The temperature increase in 2050 relative to 2011 is 0.73°C , 1.42°C , 1.16°C and 2.59°C for RCP2.6, RCP4.5, RCP6 and RCP8.5, respectively.

In this work, the temperature anomaly is used after the year 2011. The HIRHAM5 monthly mean record for 1990 to 2011 is extended with the temperature anomaly until 2050. The surface mass balance remains constant after 2011 at its 2011 value. The temperature increase is shown in Figure 4.14 for the period 2011 to 2050. The total temperature increase in 2050 relative to 2011 is 0.73°C , 1.42°C , 1.16°C and 2.59°C for RCP2.6, RCP4.5, RCP6 and RCP8.5, respectively.

The annual variation of the same quantities and parameter setting as in the previous sections are shown in Figures 4.15 and 4.16 using the Bamber et al. [2001] and Bamber et al. [2013] bed elevation map, respectively. The difference between the individual RCP scenarios is very small. Solid ice flux and basal melt are decreasing

over time because of the reduced ice volume in the drainage basin, similar to the previous section. The surface mass balance remains at its 2011 value, which is the minimum value of the HIRHAM5 model output. The modeled total flux remains negative after 2010. The total flux averages after 2010 are shown in Table 4.2. Cumulative flux and ice volume show a steady mass loss in the extended period. The modeled mean mass loss for all four scenarios is (11.21 ± 2.87) km³/yr, and the previously determined best run, M2, suggests a total mass loss of 9.77 km³/yr.

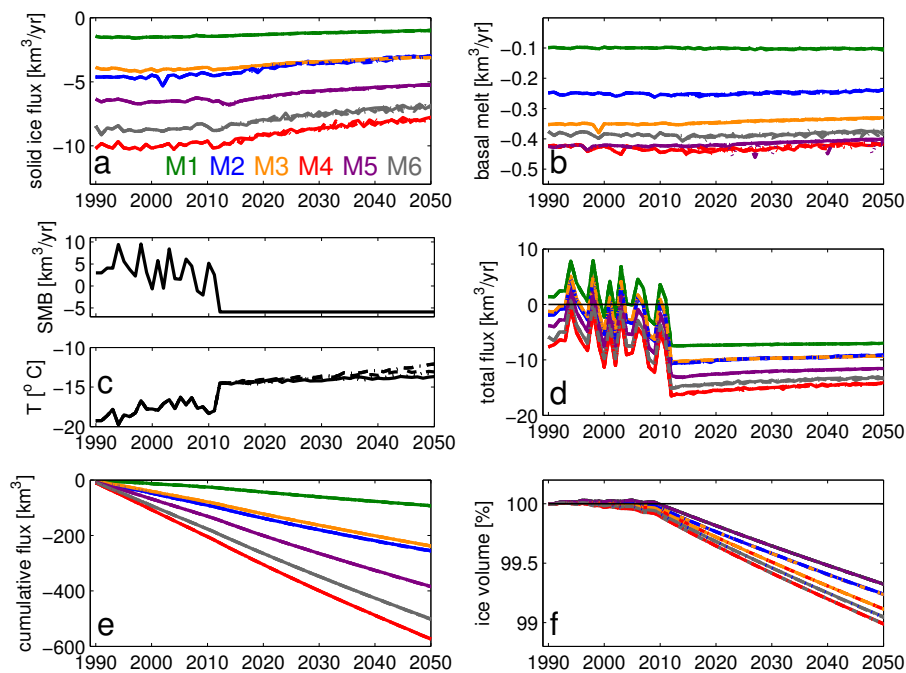


Figure 4.15: Yearly means of solid ice flux (a), basal melt (b), surface mass balance and ice surface temperature (c), total mass balance M_T (d), cumulative flux (e) and ice volume (f) for the selected parameter settings for the four RCP scenarios, using the Bamber et al. [2001] bed elevation map.

4.5 Discussion and Conclusion

PISM, in the version used here, has a very simple basal hydrology model with local basal melt, but without transport between grid cells. The basal melt estimated here is the total sum in the whole drainage basin assuming that in steady state all liquid basal melt water will exit through KNS. Modeled basal melt for KNS is small compared to estimates from other tide water glaciers in Greenland. Due to its small value, it has only a small influence on the total flux.

The calving criterion used here is the so called ‘floatkill’ option in PISM. Here, all ice is calved off when it becomes afloat at the terminus. Even though this is not a

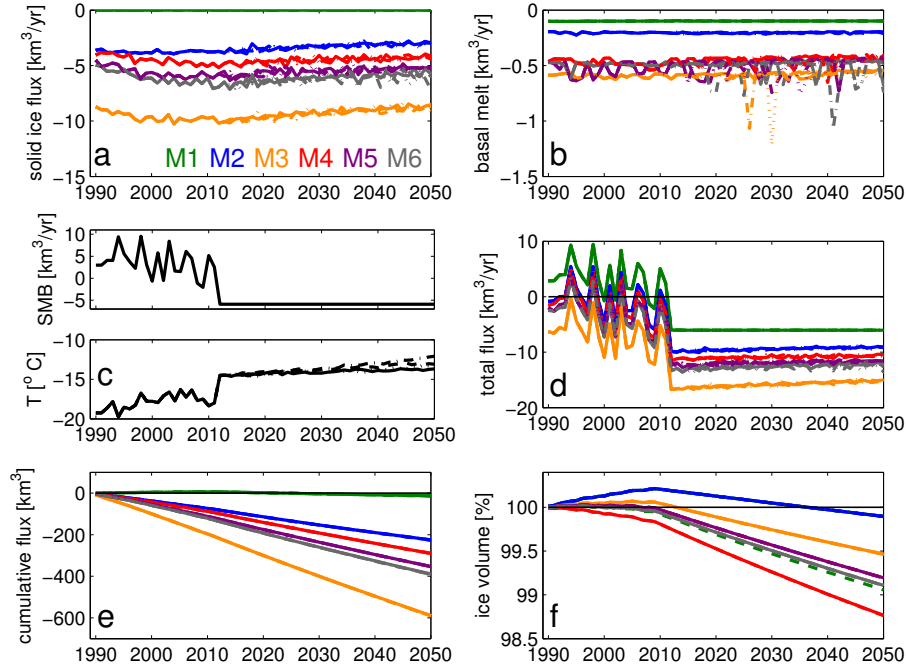


Figure 4.16: Yearly means of solid ice flux (a), basal melt (b), surface mass balance and ice surface temperature (c), total mass balance M_T (d), cumulative flux (e) and ice volume (f) for the selected parameter settings for the four RCP scenarios, using the Bamber et al. [2013] bed elevation map.

physical calving criterion, it shows good results in the narrow fjords in Greenland. In this study, the calving fluxes match the observations well.

As mentioned earlier, the pattern of fast flowing arms is not captured well by the model. This is a result of the very smooth bedrock elevation grid, especially at the terminus. There have been no successful ice thickness measurements using ice penetrating radar in the proximity of the terminus because warm and wet ice conditions absorb the radar signal. Bedrock troughs under the ice would make it possible to model the actual surface velocity pattern.

The climatic forcing applied in the prognostic runs is very conservative. Including additional emission scenarios, like the RCP, result in an even larger mass loss until 2050.

PISM reproduces the present behavior of KNS, and seasonal variations are modeled. Modeled solid ice flux, surface velocities and total mass flux agree well with observations from InSAR velocities, calving flux estimates and IceSAT elevation changes. KNS is currently losing mass and will continue to lose mass. Using present day climate without additional warming, the KNS drainage basin will likely suffer a mass loss of (4.6 ± 3.1) km³/yr. The best model run, M2, suggests a mass loss of 3.3 km³/yr until 2050. The modeled mean mass loss for all four RCP scenarios is

$(11.21 \pm 2.87) \text{ km}^3/\text{yr}$, and the previously determined best run, M2, suggests a total mass loss of $9.77 \text{ km}^3/\text{yr}$.

5 | Inverse Model for Bed Elevation

The work presented in this chapter has been started during my academic stay abroad at the University of Alaska, Fairbanks (UAF) under supervision of Ed Bueler. The aim of this chapter is to retrieve the bed elevation from easier to observed quantities such as surface velocities.

Due to the lack of successful flight lines, as shown in Section 3.1.2, the bed topography underneath KNS is basically unknown. The connection between the bathymetry and the Bamber et al. [2001] bed map shows a height difference of more than 500 m. In addition, all radar measurements are point measurements and the bed maps that are produced are a result of interpolation, called kriging, which introduces uncertainties, since local features in the ice sheet bed can be enhanced or missed. Within the ISSM group, there have been efforts to not use kriging as interpolation method for the bed, but to use the surface mass balance and surface velocities instead. This method uses only the known flight line values for ice thickness [Morlighem et al., 2011].

Inverse models are used to obtain unknown physical information from observations. For example, they are used to estimate basal properties of ice sheets from easier observed quantities, such as surface elevation and surface velocity [e.g., Habermann et al., 2012]. Also, the bed elevation has been obtained using inverse models [e.g., McNabb et al., 2012, van Pelt et al., 2013].

Here, a simple method, to adjust the bedrock map using observed surface velocities is presented. As forward model, PISM is used on a 2 km grid with HIRHAM5 as climatic forcing, and the modeled surface velocity is compared to the observed surface velocity in each grid cell. In case the observed velocity is larger than the modeled one, the bed elevation is lowered by a certain amount. The surface elevation

is held constant, so the ice thickness will increase. This in turn will increase the modeled surface elevation when using the forward model. The opposite is done in case the observed velocity is smaller than the modeled one. A lift of the bed elevation results in a smaller ice thickness and lower modeled surface velocities. This is done iteratively, until the bed elevation changes become small. A schematic view is shown in Figure 5.1.

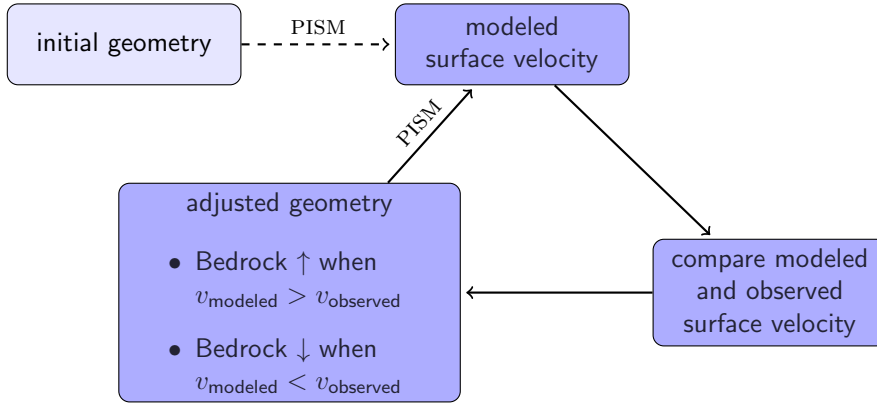


Figure 5.1: Schematic view of the method.

5.1 Method

In each grid cell, the fraction of modeled and observed surface velocity $\frac{u_{\text{observed}}}{u_{\text{modeled}}}$ is computed. Where the fraction exceeds 1 the bed is lowered, and where the fraction is smaller than 1 the bed is lifted. A cost function for the bed elevation change Δb is

$$\Delta b = -C \cdot \log \left(\frac{|u_{\text{observed}}|}{|u_{\text{modeled}}|} \right), \quad (5.1)$$

where C is a constant that varies spatially, but remains constant for all iterations. The constant is derived as follows. The surface velocity in the SIA, following Greve and Blatter [2009, Equation (5.84)], is

$$\mathbf{u}_{\text{surface}} = \mathbf{u}_{\text{base}} - \frac{2eA(\rho g)^n}{n+1} H^{n+1} |\nabla h|^{n-1} \nabla h, \quad (5.2)$$

where e is the enhancement factor, A is the rate factor, ρ is the density of ice, g is the acceleration of gravity, n is the exponent in the flow law, H is the ice thickness, and

h is the surface elevation. Neglecting sliding, i.e., setting $\mathbf{u}_{\text{base}} = 0$, and choosing $n = 3$, the magnitude of the surface velocity is

$$|\mathbf{u}_{\text{surface}}| = \frac{1}{2}eA(\rho g|\nabla h|)^3 H^4. \quad (5.3)$$

Using $H = h - b$, the bed elevation b becomes

$$b = h - \left(\frac{2|\mathbf{u}_{\text{surface}}|}{eA(\rho g|\nabla h|)^3} \right)^{1/4}. \quad (5.4)$$

Substituting $U = \log |\mathbf{u}_{\text{surface}}|$, the derivative of the bed elevation becomes

$$\frac{db}{dU} = -\frac{1}{4} \left(\frac{2 \exp(U)}{eA(\rho g|\nabla h|)^3} \right)^{1/4}. \quad (5.5)$$

Using $dU = d(\log |\mathbf{u}_{\text{surface}}|) = \log |\mathbf{u}_{\text{observed}}| - \log |\mathbf{u}_{\text{modeled}}|$, the change Δb in the bed elevation is

$$\Delta b = -\frac{1}{4} \left(\frac{2|\mathbf{u}_{\text{observed}}|}{eA(\rho g|\nabla h|)^3} \right)^{1/4} \log \left(\frac{|\mathbf{u}_{\text{observed}}|}{|\mathbf{u}_{\text{modeled}}|} \right). \quad (5.6)$$

Hence, the constant C is given by

$$C = \frac{1}{4} \left(\frac{2|\mathbf{u}_{\text{observed}}|}{eA(\rho g|\nabla h|)^3} \right)^{1/4}. \quad (5.7)$$

The bed elevation change can be improved by scaling with a constant factor taking into account that the adjustment should be smaller where the observed velocities are small as well. Also, the sign of C is chosen in such a way that the bed gets depressed or lifted in the proper way. In this way, the bed elevation change becomes

$$\Delta b = C \cdot \log \left(\frac{|\mathbf{u}_{\text{observed}}|}{|\mathbf{u}_{\text{modeled}}|} \right) \cdot \frac{|\mathbf{u}_{\text{observed}}|}{|\mathbf{u}_{\text{observed, max}}|}. \quad (5.8)$$

In the following, the above method is tested on Greenland's largest outlet, glacier Jakobshavn Isbræ.

5.2 Validation using Jakobshavn Isbræ

Jakobshavn Isbræ is a well-studied glacier, and there is a very detailed bed topography available on the CReSIS website. The bed elevation map on a 2 km grid is

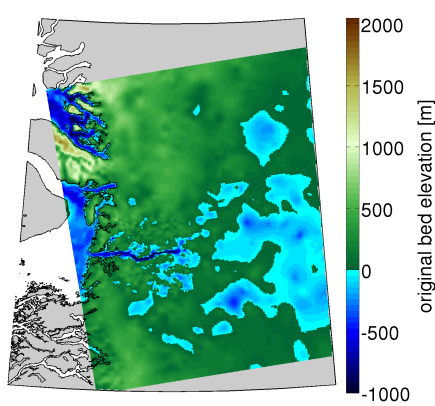


Figure 5.2: Original bed elevation map for Jakobshavn Isbræ on a 2 km grid.

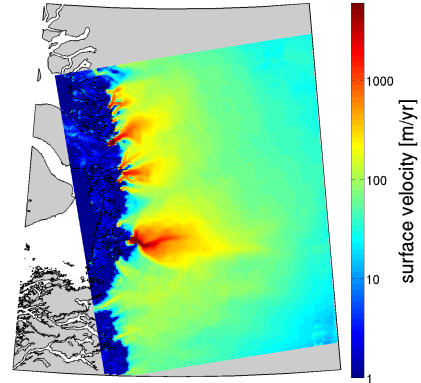


Figure 5.3: Observed InSAR surface velocity [Joughin et al., 2010, 2012, Moon et al., 2012] for Jakobshavn Isbræ on a 2 km grid.

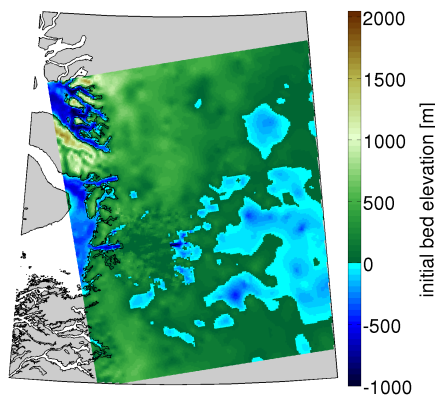


Figure 5.4: Jakobshavn Isbræ without the deep trough used as starting point.

shown in Figure 5.2. The surface velocity pattern, as shown in Figure 5.3, reflects the underlying bed topography, which has an S-shaped deep trough at the terminus. This location is used to validate the described method. To this end, the deep trough is removed and set to sea level, as shown in Figure 5.4.

Twenty iterations are performed, where after each iteration the modeled surface velocity is compared to the observed surface velocity. The bed elevation is adjusted according to Equation (5.8). The bed elevation after 1, 4, 8, 16 and 20 iterations is shown in Figure 5.5. Already after the very first iteration, the trough starts to emerge. After more iterations, the trough is deepening, and after 20 iterations the trough is as deep as observed close to the terminus. However, the deep trough does not penetrate as deep inland as is observed.

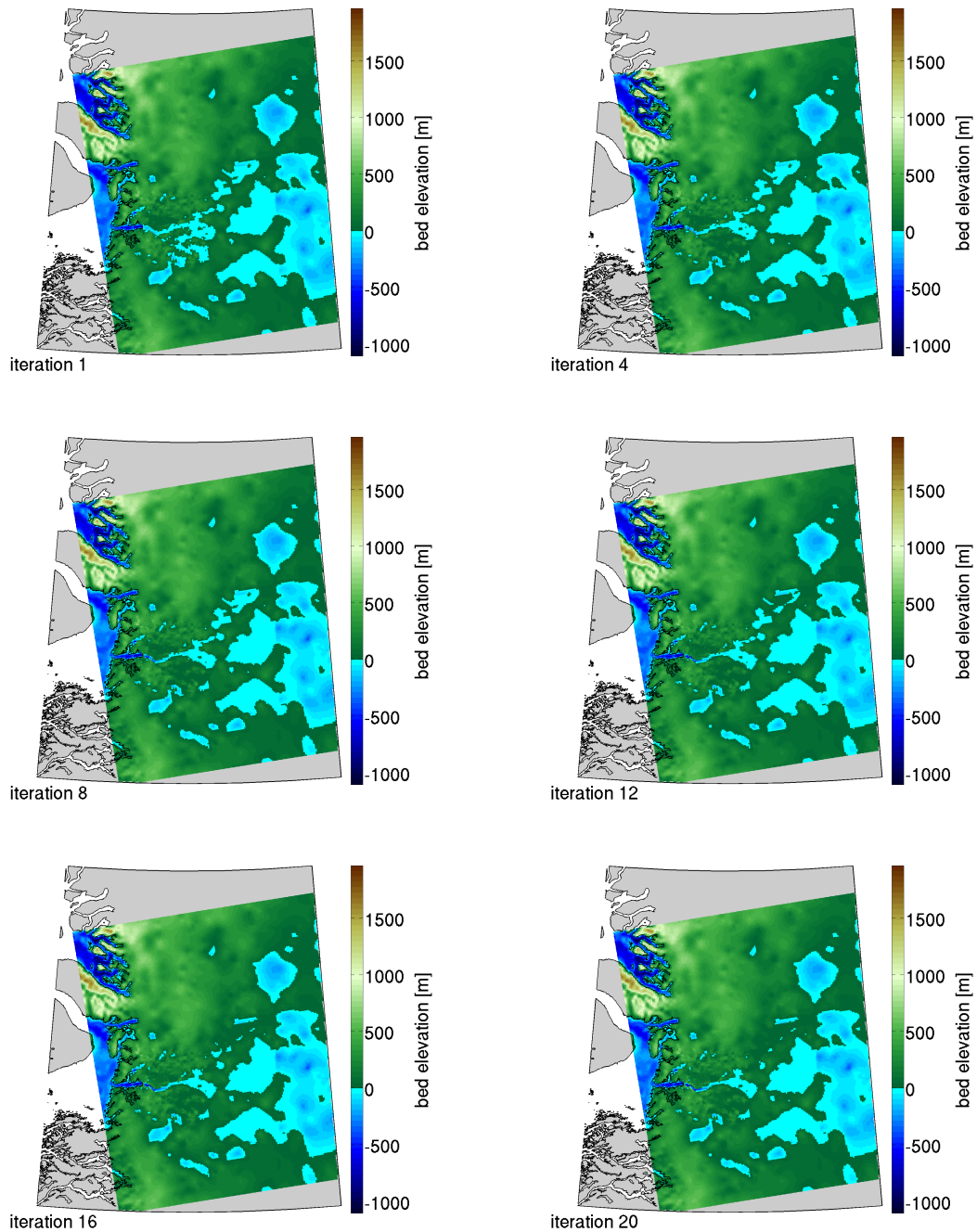


Figure 5.5: Bed elevation after 1, 4, 8, 12, 16 and 20 iterations for Jakobshavn Isbræ.

The bed elevation and surface velocity along a cross section through the drainage basin is shown in Figure 5.6 for all iterations and observed values. This cross section is passing the deep trough three times. The velocity is modeled well after 20 iterations. In the observed surface velocity, there is a velocity decrease at the terminus,

when entering the fjord. The modeled surface velocities adapt to this pattern, which results in a lifting of the bed elevation near the calving front.

The bed elevation shows that the trough becomes as deep as observed after 20 iterations, but the bed adjustments are significant until 50 km upstream. Further inland, the surface velocity is decreasing rapidly and hence the applied bed elevation changes Δb are small.

Figure 5.7 shows the mean elevation change in the drainage basin for each iteration. Initially, the adaptations are large, but after seven iterations, the changes remain constant, although they are not approaching zero.

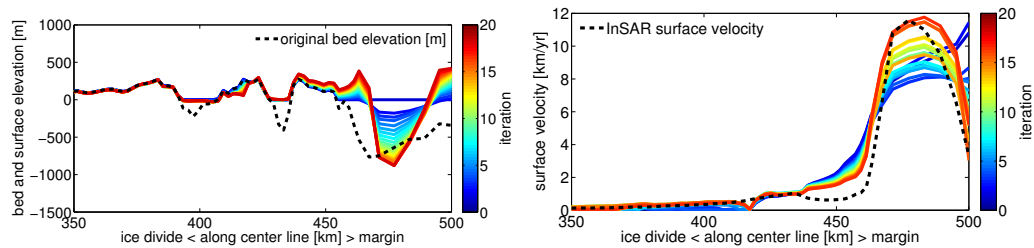


Figure 5.6: The bed elevation and surface velocity along a cross section through the drainage basin. The color represents the iteration from blue to red, and the observed values are shown in black.

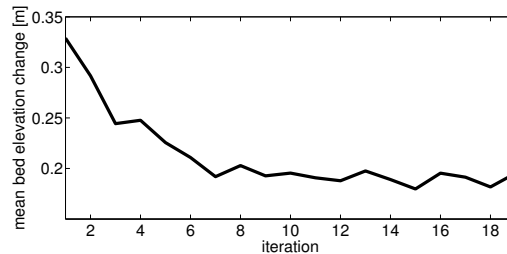


Figure 5.7: The mean elevation change in the drainage basin for each iteration.

5.3 Application to KNS

This approach is applied to KNS with the bed elevation map used earlier based on the Bamber et al. [2001] bed map. There, no trough-like features are visible. The newer map by [Bamber et al., 2013] does show a trough emerging further inland, but does not continue to the terminus due to missing bed elevation measurements. Using this method, a trough is expected to emerge where the surface velocities are high.

Figure 5.8 shows the bed elevation map at the starting point and after 4, 8, 12, 16 and 20 iterations. As expected, troughs are emerging where observed velocities are

high. Also the neighboring outlet glacier, i.e., AS, is starting to show in the bed map.

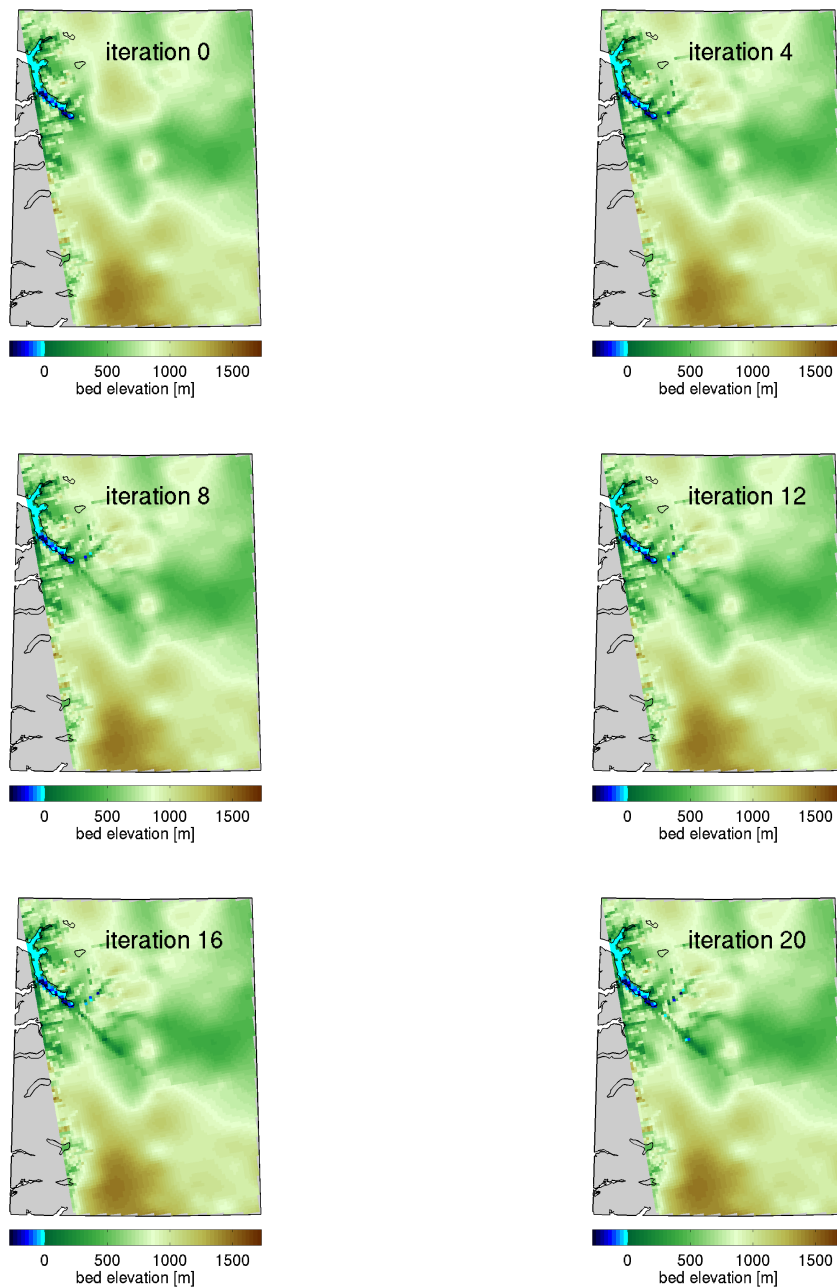


Figure 5.8: Bed elevation at the strating point and after 4, 8, 12, 16 and 20 iterations for KNS.

Figure 5.9 shows the bed elevation and surface elevation along a center line. Also, the Bamber et al. [2001] and Bamber et al. [2013] bed elevation is shown. From this, one sees that the iterative bed approaches the newer bed map at some points,

i.e., between 240–270 km. There, the bed is lowered several hundreds of meters. At about 250 km, the bed drops even below sea level. Near the calving front, the bed is lowered significantly to almost sea level; however, due to the retreat of about 5 km in the model, a bedrock bump remains near the calving front. This bump could be removed by hand. The modeled surface velocity approaches the observed one, however due to the retreat, the final 5 km with high velocities are not modeled. Figure 5.10 shows the mean bed elevation change at each iteration. Also here, the change remains constant, but there are outliers, e.g., for iteration 11.

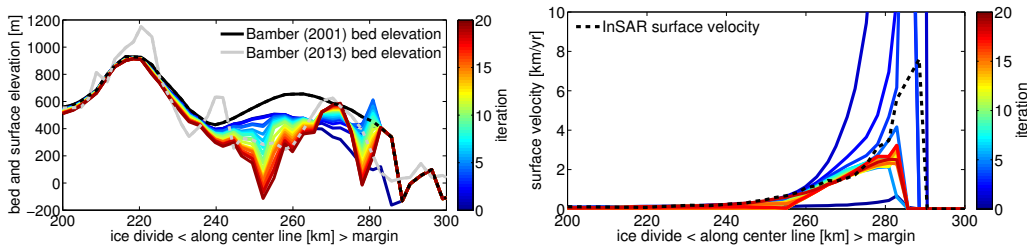


Figure 5.9: The bed elevation and surface velocity along the center line. The color represents the iteration from blue to red, and the observed value are shown in black and gray [Bamber et al., 2013].

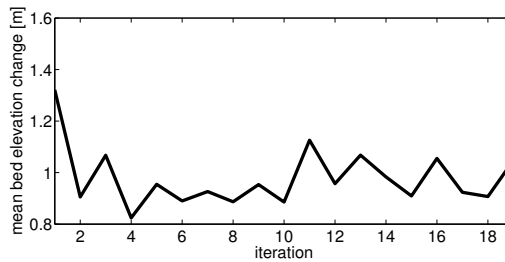


Figure 5.10: The mean elevation change in the drainage basin for each iteration.

5.4 Discussion and Conclusion

The iterative inversion for bed elevation is tested on Jakobshavn Isbræ. It is possible to retrieve the bed elevation in the proximity of about 50 km of the terminus, where surface velocity measurements are available. The immediate region of the calving front should be excluded. There, strange bed elevations can occur when the calving front in the observed velocity data and the model runs do not coincide. For the same reason, the bed inversion does not work properly when the glacier is retreating in the model runs.

This approach is applied to KNS, since there are no bed elevation measurements close to the terminus. Here, a trough in the bed is emerging. The final result for

KNS is shown in Figure 5.11.

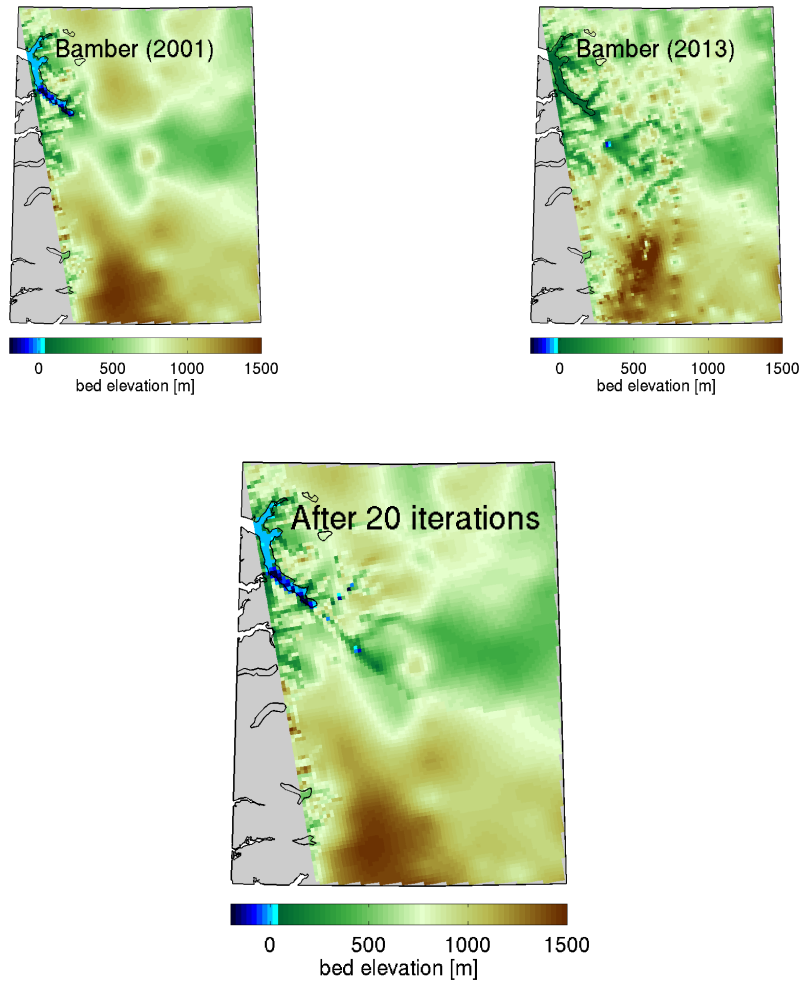


Figure 5.11: The bed elevation map for Bamber et al. [2001] and Bamber et al. [2013] (top), and the final result after 20 iterations (bottom).

6 | The glacial meltwater contribution to the freshwater budget

This chapter has been submitted with the title *Estimating the glacial meltwater contribution to the freshwater budget from salinity and $\delta^{18}O$ measurements in Godthåbsfjord* and the co-authors D. van As, J. Bendtsen, D. Dahl-Jensen, X. Fettweis and S. Rysgaard.

The mass loss of the Greenland ice sheet increases due to changes in the surface mass balance and accelerated ice discharge through numerous outlet glaciers at the margins. Calving, surface melt and basal melt contribute to the total discharge into the ocean. Observations and climate models can give estimates for calving and surface melt. Basal melt, however, cannot be observed directly for tidewater glaciers. Even though mass loss by basal melting is neglected on the global scale, it plays an important role in the regional environment. Higher ocean temperatures increase frontal melt, and warmer air temperatures increase the production of surface meltwater on the ice sheet, that runs off to the base of the ice. The resulting lubrication accelerates outlet glaciers [Holland et al., 2008, Motyka et al., 2003, Rignot et al., 2010]. All freshwater sources including precipitation regulate the freshwater budget of Godthåbsfjord, which influences the fjord ecosystem.

In the fjord, a seasonal variability is measurable in the salinity content. Based on salinity measurements, the freshwater amount can be quantified, but it is not possible to distinguish between the different freshwater sources. Here salinity and stable oxygen isotope measurements are combined to distinguish between different sources like glacial meltwater, i.e. basal melt, frontal melt, calved ice bergs and melange melt, and run-off, i.e. precipitation and surface melt.

This study focuses on Godthåbsfjord, a 190 km long and complex fjord system

with several tidewater and land-terminating glaciers. Figure 6.1 shows the fjord and the frontal location of the tidewater glaciers Kangiata Nunaata Sermia (KNS), Akullerssuup Sermia (AS), Narsap Sermia (NS), and the land-terminating glaciers Qamanaarssuup Sermia (QS) and Kangilinnuata Sermia (KS).

Extensive oceanographic measurements [Mortensen et al., 2013, 2011], studies covering the behavior of the glaciers [Ahlstrøm et al., 2013], and automatic weather station records [van As, 2011, van As et al., 2014], are available for this region.

6.1 Data Description

The studied area with its measurement locations is shown in Figure 6.1.

Water temperature and salinity were measured using a Sea-Bird Electronics SBE 19plus SEACAT Profiler CTD (conductivity, temperature and depth). The SBE 19plus was calibrated by the manufacturer every 1–2 yr, and uncertainties of the salinity after calibration were typically within the range 0.005–0.010 psu. Temperature uncertainties were near to the initial accuracy of the instrument of 0.005 °C.

For oxygen isotope analysis, water samples of 2 mL were collected from each station in gas-tight vials and analyzed on a Picarro Isotopic Water Analyzer, L2120-I (Picarro, Sunnyvale, CA, USA). Water samples were introduced into the vaporization chamber using an attached PAL autosampler (Leap Technologies, Carrboro, NC, USA). Each sample was analyzed three times (three consecutive replicate injections; $\sigma < 0.005\text{--}0.007 \text{ ‰}$) alongside a set of three laboratory reference materials, which had previously been calibrated to the VSMOW (Vienna Standard Mean Ocean Water) scale [Coplen, 1994].

The ratio of the stable oxygen isotopes in the water ^{16}O and ^{18}O , $\delta^{18}\text{O}$, is calculated.

In this study, only measurements in the surface layer with a total depth of less than 10 m and in the inner part of the fjord are used. Between 2007 and 2010, there were 72 samples.

The seasonal variation of the surface measurements of salinity and $\delta^{18}\text{O}$ in the outer fjord is shown in Figure 6.2, with an extreme in August. For the analysis of the glacial meltwater contribution, only the inner fjord measurements are considered. This means that all measurements between the first measuring point and the Lake Tasersuaq inlet (LT in Figure 6.1) – about 40 km – are taken into account, which cover April, May, August and September only.

The velocity of the surface layer, measured by drifters during summer, is less than

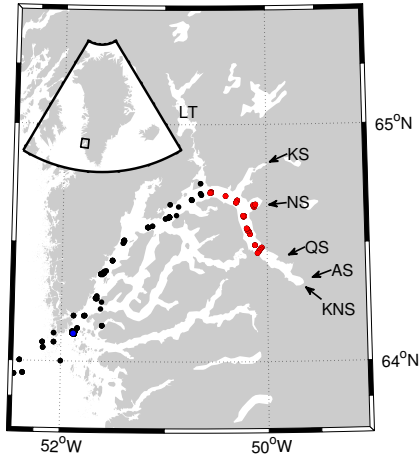


Figure 6.1: Godthåbsfjord and the location of the tidewater glaciers Kangiata Nunaata Sermia (KNS), Akullerssuup Sermia (AS), Narsap Sermia (NS) and the land-terminating glaciers Qamanaarsuup Sermia (QS) and Kangilinnuata Sermia (KS), and Lake Tasersuaq (LT).

In total, there are 510 surface measurements in Godthåbsfjord (black and red), and 72 of them in the inner part (red). The blue station is used to determine the base values for salinity and $\delta^{18}\text{O}$.

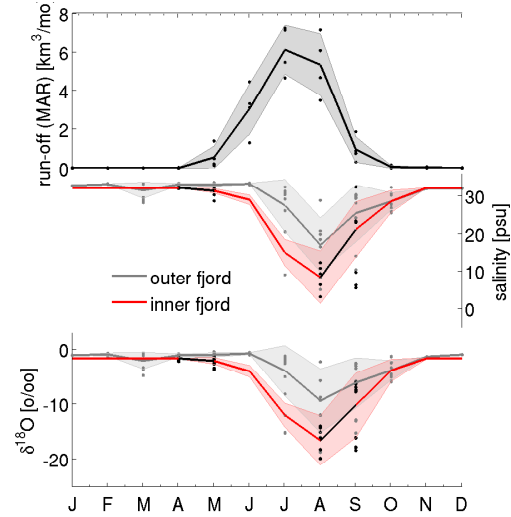


Figure 6.2: Seasonal variation of modeled MAR run-off and measured salinity and $\delta^{18}\text{O}$. The MAR run-off is shown for the 2007–2010 period (dots), and a monthly mean and standard deviation is calculated (line with shading). Salinity and $\delta^{18}\text{O}$ measurements, taken between 2007 and 2010, are shown for the whole fjord region in gray, which peak in August. The inner fjord region measurements are shown in black and cover April, May, August and September only. Missing data in the remaining month are estimated from the outer fjord variability (red).

10 cm/s [Mortensen et al., *subm.*].

The thickness of the surface layer, also shown in Mortensen et al. [2013, 2011], is 6 to 10 m during the summer and about 10 m during winter, and the considered section has typical average velocities of about 4 cm/s in the winter and 8 cm/s during the summer [Mortensen et al., *subm.*]. The sensitivity to the estimated velocity and surface layer thickness is discussed later.

The monthly means are used in this analysis and are shown in Table 6.1.

Regridded regional climate model output from MAR (Modele Atmosphérique Regional, Fettweis et al. [2011], van As et al. [2014]) for the seasonal variation of the run-off in the same period (2007–2010) is used for comparison of the here calculated run-off contribution.

Table 6.1: The monthly variation of all input parameters also indicating the origin of values: estimated, measured or modeled. Values in brackets show estimated values each month, where no data is available, as shown in Figure 6.2.

			Jan	Feb	Mar	Apr	May	Jun
velocity v	[cm/s]	est.	4	4	4	4	4	6
thickness D	[m]	est.	10	10	10	10	10	8
S_{outer}	[psu]	meas.	32.83	33.18	31.54	33.12	33.06	33.30
S_{inner}	[psu]	meas.	(32.23)	(32.23)	(32.23)	32.23	31.40	(29)
S_{sea}	[psu]	meas.	33.20	33.20	33.20	33.20	33.20	33.20
$\delta^{18}O_{outer}$	[‰]	meas.	-1.05	-0.91	-2.06	-1.08	-0.98	-0.75
$\delta^{18}O_{inner}$	[‰]	meas.	(-1.64)	(-1.64)	(-1.64)	-1.64	-2.09	(-4)
$\delta^{18}O_{sea}$	[‰]	meas.	-0.80	-0.80	-0.80	-0.80	-0.80	-1.50
$\delta^{18}O_{run-off}$	[‰]	mod.	-25.62	-25.58	-22.52	-18.57	-15.38	-13.13
run-off $_{MAR}$	[km ³ /mo]	mod.	0.03	0.02	0.02	0.03	0.56	2.98
			Jul	Aug	Sep	Oct	Nov	Dec
velocity v	[cm/s]	est.	8	8	6	4	4	4
thickness D	[m]	est.	6	6	8	10	10	10
S_{outer}	[psu]	meas.	27.49	17.04	25.43	28.60	31.98	32.05
S_{inner}	[psu]	meas.	(15)	8.44	21.140	(28.60)	(32.23)	(32.23)
S_{sea}	[psu]	meas.	31.75	30.00	30.10	31.00	32.50	33.20
$\delta^{18}O_{outer}$	[‰]	meas.	-3.91	-9.36	-6.11	-3.84	-1.32	-0.95
$\delta^{18}O_{inner}$	[‰]	meas.	(-12)	-16.56	-10.20	(-3.84)	(-1.64)	(-1.64)
$\delta^{18}O_{sea}$	[‰]	meas.	-2.20	-3.10	-2.90	-2.30	-1.50	-0.80
$\delta^{18}O_{run-off}$	[‰]	mod.	-13.00	-14.50	-15.87	-17.95	-19.98	-23.88
run-off $_{MAR}$	[km ³ /mo]	mod.	5.99	5.23	0.95	0.08	0.05	0.03

6.2 Box Model

A box model is applied to calculate all the incoming and outgoing fluxes from the different sources. One box is representing the surface layer, which is taken to be mixed homogeneously [Mortensen et al., 2013, 2011]. In-flowing fluxes are glacial meltwater $q_{ice,in}$ (calving, frontal melt, basal melt and melange melt), run-off $q_{run-off,in}$ (surface melt and precipitation on land and ice), and incoming seawater $q_{sea,in}$ (see Figure 6.3). Freshwater entering the fjord is composed of meltwater and precipitation.

Here, some simplifying assumptions are made. It is assumed that all freshwater,

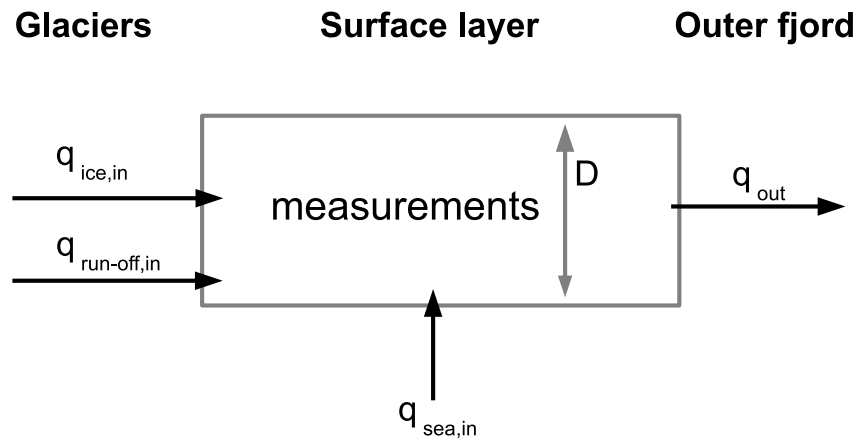


Figure 6.3: A box model with the surface layer as one box, three incoming fluxes (glacial meltwater q_{ice} (basal melt, front melt, calving and melange melt), run-off $q_{run-off}$ (run-off and surface melt) and seawater q_{sea}) and the outgoing flux q_{out} . Salinity and $\delta^{18}\text{O}$ are the measured quantities in the inner fjord region.

coming from run-off and glacial meltwater, is transported to the surface layer because freshwater is buoyant. Also, all meltwater of calved ice bergs enters the surface layer. A negligible amount of ice bergs is leaving the inner fjord region or is melted in the deeper layers. During the winter months sea ice and a melange are covering the inner fjord region, which consists of former calved ice bergs and frozen seawater. Some of the melange survives until summer. The outgoing seawater is replaced by incoming seawater from the deeper layers [Mortensen et al., 2013, 2011].

The following equations for the salinity S and $\delta^{18}O$ changes:

$$V \cdot \frac{dS}{dt} = q_{sea,in}S_{sea} + q_{fresh,in}S_{fresh} - q_{out}S - \frac{dV}{dt}S \quad \text{and} \quad (6.1)$$

$$\begin{aligned} V \cdot \frac{d\delta^{18}O}{dt} &= q_{sea,in}\delta^{18}O_{sea} + q_{ice,in}\delta^{18}O_{ice} + q_{run-off,in}\delta^{18}O_{run-off} \\ &\quad - q_{out}\delta^{18}O - \frac{dV}{dt}\delta^{18}O, \end{aligned} \quad (6.2)$$

where V denotes the volume. The subscripts indicate the origin of the water masses. The volume V is estimated from the width W and length L of the fjord section (red in Figure 6.1) and the thickness of the considered surface layer D using $V = WLD$. From mass conservation, the total incoming flux is

$$q_{in} = q_{fresh,in} + q_{sea,in} = q_{ice,in} + q_{run-off,in} + q_{sea,in}. \quad (6.3)$$

The change in the surface layer thickness is due to changes in the incoming flux and, hence, it is

$$q_{out} = q_{in} - \frac{dV}{dt} = q_{fresh,in} + q_{sea,in} - \frac{dV}{dt}. \quad (6.4)$$

The total outgoing flux is estimated using the geometry of the fjord and an estimate for the surface layer velocity v , namely

$$q_{out} = W \cdot D \cdot v. \quad (6.5)$$

Combining Equations (6.4) and (6.5) gives

$$q_{sea,in} = W \cdot D \cdot v - q_{fresh,in} + \frac{dV}{dt}. \quad (6.6)$$

The incoming freshwater flux is then calculated by combining Equations (6.1), (6.5) and (6.6), which gives

$$q_{fresh,in} = \left[V \frac{dS}{dt} + \left(W D v + \frac{dV}{dt} \right) \cdot (S - S_{sea}) \right] \cdot (S_{fresh} - S_{sea})^{-1}. \quad (6.7)$$

From Equations (6.2), (6.5) and (6.6), $q_{ice,in}$ is calculated as a function of $q_{fresh,in}$

$$\begin{aligned} q_{ice,in} &= \left[V \frac{d\delta^{18}O}{dt} + \left(W D v + \frac{dV}{dt} \right) \cdot (\delta^{18}O - \delta^{18}O_{sea}) \right. \\ &\quad \left. + q_{fresh,in} (\delta^{18}O_{sea} - \delta^{18}O_{run-off}) \right] \\ &\quad \cdot (\delta^{18}O_{ice} - \delta^{18}O_{run-off})^{-1}. \end{aligned} \quad (6.8)$$

Equations (6.7) and (6.8) are then solved numerically for incoming freshwater and glacial meltwater fluxes.

6.2.1 Downscaling

The width, terminus height and InSAR velocity [Joughin et al., 2010] for each of the glaciers are used to downscale the total glacial meltwater contribution to a glacier specific estimate. The MAR run-off distribution is used to split up the run-off calculated here.

6.3 Salinity and $\delta^{18}\text{O}$ Estimates

Assumptions have to be made for the salinity and $\delta^{18}\text{O}$ of the different contributors (see Table 6.1). The measured $\delta^{18}\text{O}$ in the surface layer is, like salinity, taken to be constant with respect to depth in the surface layer and month of the year [Mortensen et al., 2013, 2011].

The bottom water salinity and $\delta^{18}\text{O}$ are taken from depth measurements from a station at the fjord entrance and vary with the month of the year. The depth profiles for that station are shown in Figure 6.4. The salinity of precipitation and glacial meltwater is zero.

The seasonal isotopic signature of the run-off contribution $\delta^{18}\text{O}_{run-off}$ is based

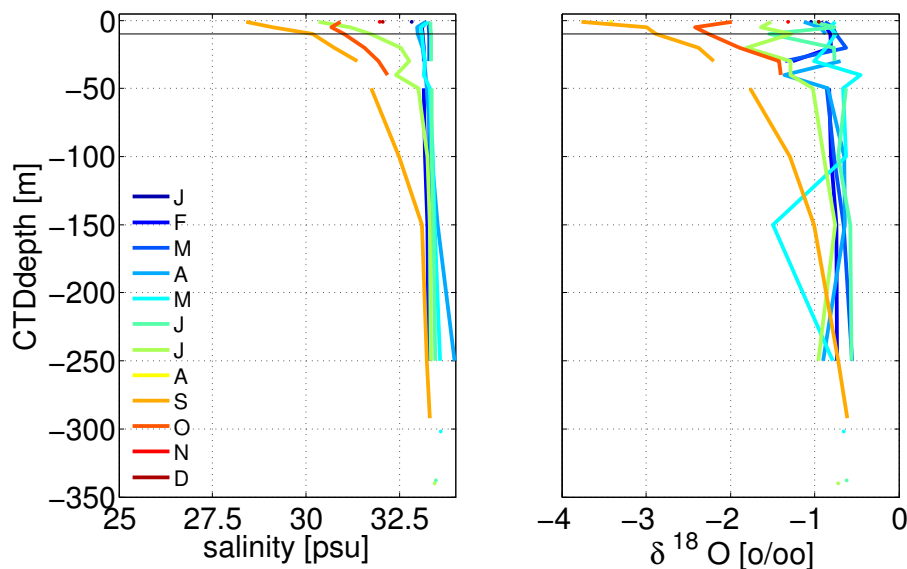


Figure 6.4: The monthly depth profiles of salinity and $\delta^{18}\text{O}$ for a station at the fjord entrance (blue in Figure 6.1). The monthly mean values at 10 m depth (black line) are used as base values for the analysis.

on precipitation output from the isotopic regional climate model REMO-iso. The

model performance for Greenland is tested using the Global Network In Precipitation (GNIP) and ice cores by comparing the modeled and observed isotope values [Sjolte et al., 2011]. REMO-iso captures a significant part of the $\delta^{18}\text{O}$ variability at the coast, i.e. tested for Danmarkshavn.

$\delta^{18}\text{O}$ for glacial meltwater is generally unknown, and it is estimated as follows. There have been $\delta^{18}\text{O}$ measurements of ice bergs conducted in Godthåbsfjord to constrain the isotope value of glacial ice. In total there are 200 measurements that range from -30.04 ‰ to -17.91 ‰ with a median of $\delta^{18}\text{O} = -28.08 \text{ ‰}$ (*Rysgaard, private communication*). Dansgaard [1964] measured ice bergs in West Greenland, and $\delta^{18}\text{O}$ values as low as -30 ‰ and smaller where found. Also, Bhatia [2011] show that water that has been stored under a glacier has $\delta^{18}\text{O}$ values around -30 ‰ . Ice core records from Dye-3, which is located in South Greenland, show that $\delta^{18}\text{O}$ for glacial ice can be smaller than -30 ‰ [Johnsen et al., 2001]. Marginal surface ice studies close to KNS in Reeh et al. [2002] suggest $\delta^{18}\text{O}$ values between -28 ‰ and -34 ‰ . In this analysis, $\delta^{18}\text{O}_{ice} = -28 \text{ ‰}$ is used, based on the local ice berg measurements. Also the sensitivity to the choice of $\delta^{18}\text{O}_{sea}$ and $\delta^{18}\text{O}_{run-off}$, are discussed later.

6.4 Results

Using the salinity records only, the incoming freshwater flux is calculated using Equation (6.7). The total amount of incoming freshwater is $q_{fresh} = (11.5 \pm 2.3) \text{ km}^3/\text{yr}$ and the monthly variation is shown in Figure 6.5. During the winter, there is a minor freshwater inflow (less than $0.2 \text{ km}^3/\text{mo}$) and during the summer, all incoming water in the surface layer is freshwater. Note, that there is no data during winter time. The implications are discussed below.

The glacial meltwater flux is calculated using Equation (6.8). This is the sum of basal melt, frontal melt, calving and sub-melange melt. Surface melt is included in the run-off. The chosen isotope value for the glacial ice, as discussed in Section 6.3, is $\delta^{18}\text{O}_{ice} = -28 \text{ ‰}$. Figure 6.6 shows the monthly variation of glacial meltwater and run-off. In this case, there is $q_{ice} = (7.8 \pm 6.4) \text{ km}^3/\text{yr}$ glacial meltwater, and $q_{run-off} = (3.8 \pm 8.7) \text{ km}^3/\text{yr}$ run-off (precipitation and surface melt), which is smaller than the run-off computed by MAR ($q_{run-off, MAR} = (13.1 \pm 5.5) \text{ km}^3/\text{yr}$). This is due to the assumption that the run-off has the same isotopic composition as the precipitation given by REMO-iso. However, surface melt also occurs in the ablation zone that might have a smaller isotopic signature than the precipitation. In reality, some of the surface meltwater (that is included in the MAR run-off) per-

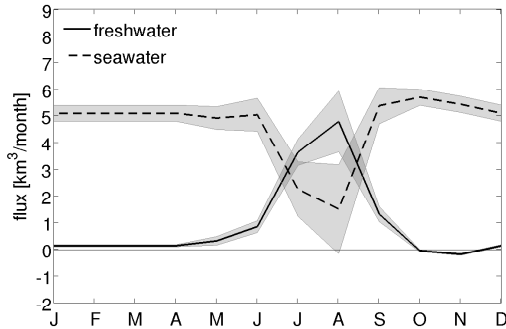


Figure 6.5: The modeled monthly amount of incoming freshwater q_{fresh} (solid line) and seawater q_{sea} (dashed line) calculated from the salinity records in the inner fjord. The shaded area indicates the uncertainty on the quantities.

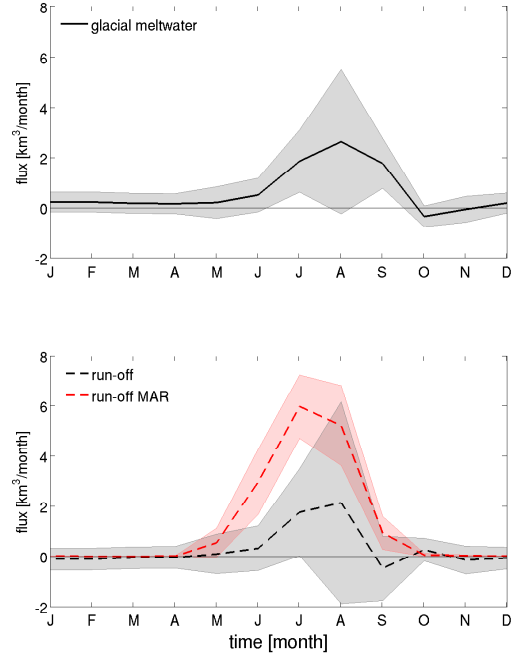


Figure 6.6: The modeled monthly variation of glacial meltwater (being basal melt, front melt, calving and melange melt; black solid line) and run-off (being precipitation and surface melt; black dashed) for $\delta^{18}\text{O}_{ice} = -28 \text{ ‰}$.

colate through the ice sheet via moulin and is therefore included in the estimate for glacial melt and not in the run-off. According to the MAR based surface run-off estimates, around 70% of the meltwater produced in the ablation zone seems to reach the bedrock before reaching the ocean.

There is a small negative flux in the autumn, that lies within the uncertainties where measurements are sparse.

Speculatively, one could assume that there is negligible calving in the winter time (October to April) and sub-melange melt is considered to be a minor contributor. In the case that both can be neglected during winter, it is possible to isolate the basal meltwater component from winter conditions. Here basal meltwater is melt that occurs under the glaciers and enters the fjord at the grounding line and melt of the glacier faces. The basal meltwater contribution is $0.25 \text{ km}^3/\text{mo}$ in the winter from all glaciers. Basal melt and glacier speed are connected: more friction due to high velocities increase basal melt, and basal meltwater engages lubrication and hence higher velocities. Summer surface velocities at KNS increase by 30 % with

Table 6.2: Run-off (precipitation and surface melt) and glacial meltwater (being basal melt, front melt, calving and melange melt) flux for all glaciers terminating into the inner part of Godthåbsfjord and for each glacier individually. The width, terminus height and InSAR velocity (Joughin, 2010) for each of the glaciers are used to downscale the total glacial meltwater contribution to a glacier specific estimate. The MAR run-off distribution is used to split up the run-off calculated here.

	glacier contribution [%]	glacial meltwater [km ³ /yr]	run-off MAR [%]	run-off MAR [km ³ /yr]	run-off contribution [km ³ /yr]	total freshwater [km ³ /yr]
total	<i>100</i>	7.8	<i>100</i>	13.0	3.8	11.5
KNS	<i>62</i>	4.8	<i>37</i>	4.8	1.4	6.2
AS	<i>5</i>	0.4	<i>15</i>	1.9	0.5	0.9
QS	<i>1</i>	0.1	<i>10</i>	1.4	0.4	0.5
NS	<i>31</i>	2.4	<i>26</i>	3.4	1.0	3.4
KS	<i>1</i>	0.1	<i>12</i>	1.5	0.5	0.5

respect to the winter velocity [Ahlstrøm et al., 2013], so the basal melt water flux is scaled equally. The summer basal meltwater flux is then 0.32 km³/mo, and the total basal meltwater contribution for all glaciers, including frontal melt, is 3.3 km³/yr. This value has to be interpreted as an upper limit, since there is calving detected also in the winter month and hence ice bergs and melange are melting all year.

6.4.1 Downscaling

Table 6.2 shows the modeled downscaled yearly contributions for all the tidewater and land-terminating glaciers in the inner part of Godthåbsfjord. For the largest glacier KNS, there is 4.8 km³/yr glacial meltwater and 1.4 km³/yr run-off, and hence the modeled total freshwater coming from KNS only is 6.2 km³/yr. The basal meltwater, including frontal melt, coming from KNS is 2.1 km³/yr assuming no calving and melange melt in the winter.

6.5 Discussion

In this study, it is assumed that all freshwater rises to the surface layer due to its buoyancy. However, the melted glacial water is mixing during its rise, and some freshwater is staying in the deeper layers as shown in [Mortensen et al., 2013]. From the measurements used in Mortensen et al. [2013], the freshwater content during summer in the surface layer is 58% in 2009 and 51% in 2010. This is ignored in this

Table 6.3: Sensitivity to isotopic composition, surface layer thickness and velocity (see Figure 6.7).

	default	reasonable changes	resulting glacial meltwater flux change
summer velocity	8 cm/s	± 2.5 cm/s	± 2.3 km ³ /yr
$\delta^{18}\text{O}_{ice}$	-28‰	-2 ‰	-1.4 km ³ /yr
$\delta^{18}\text{O}_{sea}$	see Table 6.1	± 0.1 ‰	± 0.9 km ³ /yr
$\delta^{18}\text{O}_{run-off}$	see Table 6.1	± 1 ‰	± 0.3 km ³ /yr

simplified analysis, and hence the total freshwater is underestimated.

Calculating the analytic uncertainties is done in a very rigorous way. The large uncertainties arise from the sparse available measurements in the inner part of the fjord. With more measurements in the inner part of the fjord of the surface layer velocity, the isotopic signature of the run-off and glacial meltwater, the uncertainties can be reduced. However, accessing the inner part of the fjord during the winter time is difficult due to the melange.

Also, the estimation of $\delta^{18}\text{O}_{ice}$ is challenging.

6.5.1 Sensitivity

The sensitivity to the velocity in the surface layer is shown in Figure 6.7a. The Greenlandic outlet glaciers are accelerating and the Greenland ice sheet is melting at increased rates. Higher velocities will increase the freshwater influx and therefore the glacial meltwater contribution [Rignot et al., 2010]. Assuming a change in the summer surface layer velocity of 30%, meaning ± 2.5 cm/s, the resulting change in the glacial water flux is ± 2.3 km³/yr.

The choice of the isotopic value for glacial ice is of significance to make a distinction between run-off and glacial melt. Figure 6.7d shows yearly contributions for varying $\delta^{18}\text{O}_{ice}$. With decreasing $\delta^{18}\text{O}$ -signature for ice, the glacial meltwater contribution decreases and the run-off increases. At higher $\delta^{18}\text{O}_{ice}$ -values, the isotopic signature of run-off and glacial ice is similar and the model does not give physical results. Assuming that the value is overestimated and the ice has an isotopic signature of -30 ‰, as discussed in Section 4, the glacial meltwater is be decreased by -1.4 km³/yr.

Shifting the seasonal variation of $\delta^{18}\text{O}_{sea}$ (see Figure 6.7b) results in small change

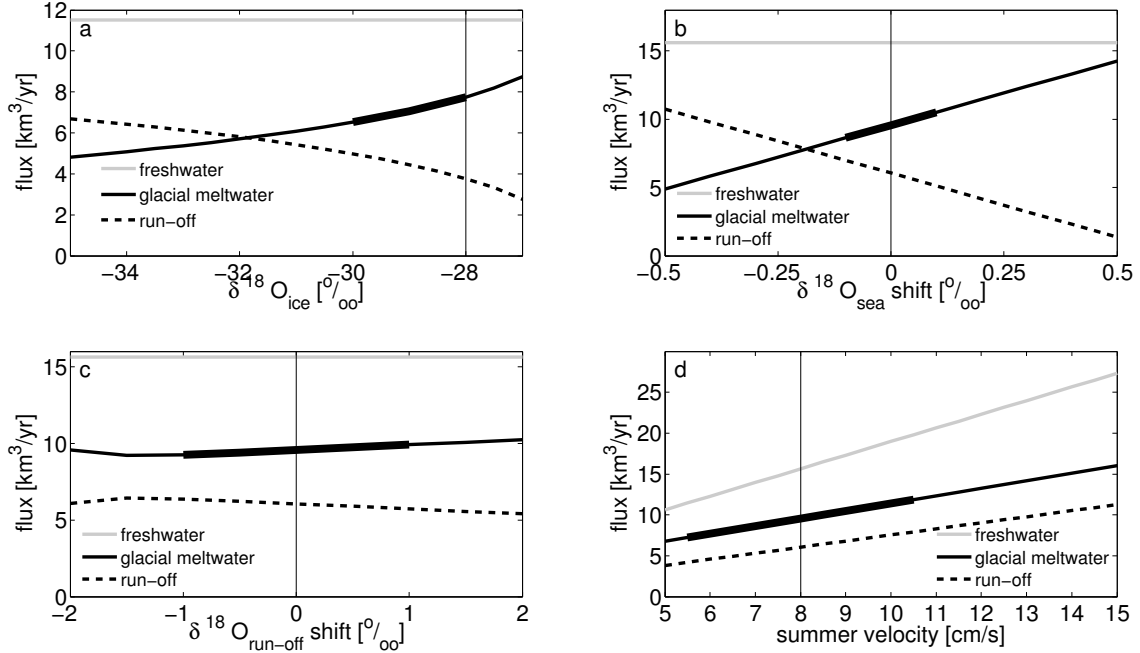


Figure 6.7: Sensitivity to the choice of the isotopic value for glacial ice (a), a shift in $\delta^{18}\text{O}_{sea}$ (b), a shift in the isotopic signature of the modeled run-off (c) and the summer velocity in the surface layer (d). The freshwater influx is shown in grey, the thin vertical line shows the value used in the analysis, and thick black line indicates sensitivity test range, cf. Table 6.3.

in the glacial meltwater influx. A possible shift of $\pm 0.1 \text{ ‰}$ will result in glacial meltwater flux change of $\pm 0.9 \text{ km}^3/\text{yr}$.

Altering the isotopic signature of the modeled run-off (see Figure 6.7c) by $\pm 1 \text{ ‰}$ (about 5%) results in small change of $\pm 0.3 \text{ km}^3/\text{yr}$.

Summarizing, within the plotted domains the glacial meltwater flux is less sensitive to the isotopic value of the run-off and the winter surface layer thickness. The result depends strongly on the modeled isotopic signature of seawater and also the estimated summer velocity of the surface layer. The result also shows a sensitivity to the isotopic value of the glacial meltwater $\delta^{18}\text{O}_{ice}$.

6.6 Conclusion

Water samples have been taken in Godthåbsfjord between 2007 and 2010 and were analyzed for salinity and for the first time for stable oxygen isotopes. Both quantities show a seasonal variation with extrema in August. The delay between the inner

and outer part of the fjord is one month.

Using $\delta^{18}O$ in addition to salinity makes it possible to distinguish between several freshwater sources. There is (11.5 ± 2.3) km³/yr freshwater entering the fjord, (7.8 ± 6.4) km³/yr of which is from glacial meltwater (basal melt, frontal melt, calving and melange melt) and (3.8 ± 8.7) from run-off (precipitation and surface melt). KNS contributes 1.4 km³/yr run-off and 4.8 km³/yr glacial melt. Earlier estimates for the KNS discharge flux are (5.5 ± 1) km³/yr w.e. (*Podrasky, private communication*, from winter velocities), and (8.3 ± 1.6) km³/yr w.e. [Mortensen et al., 2013, without subglacial discharge]. As shown earlier, more than half of the freshwater is actually present in the surface layer.

The sparse measurements in the inner part of the fjord, especially in June and July, are limiting the precision of the results as seen in the uncertainties.

The sensitivity study performed shows that the glacial meltwater flux depends strongly on the estimated summer velocity of the surface layer. The result also shows a sensitivity to the isotopic value of the glacial meltwater $\delta^{18}O_{ice}$. With a better knowledge of the discussed parameters, such as the velocity in the surface layer and the isotopic signature of glacial ice, the uncertainties in the estimates of the various freshwater sources can be reduced significantly.

With this method, it is possible to calculate the freshwater contributions from the glaciers from oceanographic measurements in the surface layer of the fjord. With year around measurements, it would be possible to study the seasonal response of the fjord to the glacial meltwater influx in more detail.

7 | Conclusions and Outlook

In this chapter the conclusions and the impact of the changing climate on the area are presented. Finally, an outlook with potential future work is shown.

In Chapter 4, it is shown that PISM reproduces the present behavior of KNS, with a good agreement between modeled and observed quantities such as solid ice flux, surface velocities and total mass flux. KNS is currently losing mass and will continue to lose mass in the future. Present mean modeled mass loss for the period covered by ICESat (2003–2008) is (3.84 ± 3.18) km³/yr of ice.

The driving stress is below 100 kPa for the largest part of the ice stream. In the last 30 km, the driving stress increases to several hundreds of kPa. According to Truffer and Echelmeyer [2003], KNS belongs to the *isbræ type*. *Isbræ type* ice streams, such as Jakobshavn Isbræ, have deep bedrock troughs and steep surface slopes with high driving stresses (~ 200 kPa). The other extreme is the so-called *ice stream type* with small surface slopes and hence low driving stresses (10 kPa). Its location is not strongly controlled by the bedrock elevation, but probably forms due to its basal conditions such as a slippery bed or weak till [Truffer and Echelmeyer, 2003]. From the available bed elevation maps only, one would expect that KNS is an *ice stream type*, however high driving stresses near the terminus suggest the contrary.

Using present day climate without additional warming, the KNS drainage basin will likely suffer a mass loss of (4.6 ± 3.1) km³/yr of ice. The best model run suggests a mass loss of 3.3 km³/yr until 2050. The conservative prognostic run, using the repeated 2002–2011 climate, suggests a mean mass loss of (4.59 ± 3.18) km³/yr of ice until 2050. Using the RCP scenarios, the modeled mean mass loss for all four scenarios increases significantly to (11.21 ± 2.87) km³/yr of ice, which corresponds to (10.28 ± 2.63) km³/yr water equivalent and (0.03 ± 0.01) mm sea level rise.

The iterative inversion for bed elevation presented in Chapter 5 is tested on Jakobs-

havn Isbræ. It is possible to retrieve the bed elevation in the proximity of the terminus, for which surface velocity measurements are available. This approach is applied to KNS, since there are no bed elevation measurements close to the terminus. Here, a trough in the bed is emerging.

Stable oxygen isotope analysis carried out in Chapter 6, makes it possible to distinguish between several freshwater sources when using $\delta^{18}O$ and salinity measurements. There is (11.5 ± 2.3) km³/yr freshwater entering the fjord, (7.8 ± 6.4) km³/yr of which is from glacial meltwater (basal melt, frontal melt, calving and melange melt) and (3.8 ± 8.7) km³/yr from run-off (precipitation and surface melt). KNS contributes 1.4 km³/yr run-off and 4.8 km³/yr glacial melt, and hence 6.2 km³/yr of freshwater.

Table 7.1 shows a collection of mass balance estimates for the region in comparison to the values computed here and prognostic estimates. All values are converted to the ice equivalent mass balance.

The total mass balance is the sum of iceberg calving, basal melt and surface mass balance. The amount of melt at the base of KNS is unknown. The results in Chapter 4 suggest a mean basal melt rate of (0.36 ± 0.16) km³/yr of ice. Chapter 6 suggests a much larger value of about 2.2 km³/yr of ice.

7.1 Outlook

The PISM version used here has a very simple basal hydrology model with local basal melt, but without transport between grid cells. However, the most recent PISM version (stable0.6) does have a basal hydrology model [Bueler and Van Pelt, 2014]. Generally, basal melt accounts for a small amount of the total mass balance, but larger contributions of 5% have been reported for, e.g., Columbia glacier in Alaska [Alexander et al., 2013].

PISM is using ice surface temperature, which is the temperature at the surface of the ice, below the firn, as input parameter. Climate model output is the surface temperature at the actual ice sheet surface, which is used in ice sheet models. A firn model would be needed to account for the temperature difference at each grid cell.

Another improvement would be the coupling of PISM to a climate model, since they influence each other [Quiquet et al., 2012], especially for long model runs with

Table 7.1: Collection of mass balance estimates M_T for the region in comparison to the values determined here and prognostic estimates. Positive values indicate mass gain, and negative values show mass loss. The unit is km^3/yr of ice.

Method	Area covered	Period	Reference	M_T ($\text{km}^3/\text{yr ice}$)	M_T (Gt w.e.)
frontal velocities and fjord bathymetry	KNS		[Mortensen et al., 2013]	-7.6 ± 1.5	-8.2 ± 1.6
ICESat elevation changes	KNS basin	2003–2008	[Sørensen et al., 2011]	-2.49	-2.28
surface velocities	KNS, NS	1958, 1964 and 1996	[Rignot et al., 2008]	-8.1	-7.4
		2000 and 2004	[Rignot et al., 2008]	-9.8	-9.0
surface velocity and ice thickness	KNS	2005–2007	[Rignot et al., 2008]	-12.1	-11.1
SMB and frontal ablation	KNS	2010	Podrasky van As et al. [2014]	-5 ± 1 -4.6-5.5	-4.6 ± 0.9 -5-6
ice sheet modelling	KNS	2003–2008	this thesis	-3.84 ± 3.18	-3.52 ± 2.92
isotope study	KNS, AS, NS	2007–2010	this thesis	-12.5 ± 2.5	-11.5 ± 2.3
isotope study	KNS	2007–2010	this thesis	-6.8	-6.2
ice sheet modelling (conservative)	KNS	2011–2050	this thesis	-4.59 ± 3.18	-4.21 ± 2.92
ice sheet modelling (all RCP)	KNS	2011–2050	this thesis	-11.21 ± 2.87	-10.28 ± 2.63
ice sheet modelling (RCP2.6)	KNS	2011–2050	this thesis	-11.19 ± 2.96	-10.26 ± 2.71
ice sheet modelling (RCP4.5)	KNS	2011–2050	this thesis	-11.22 ± 2.97	-10.29 ± 2.72
ice sheet modelling (RCP6.0)	KNS	2011–2050	this thesis	-11.20 ± 2.96	-10.27 ± 2.71
ice sheet modelling (RCP8.5)	KNS	2011–2050	this thesis	-11.23 ± 2.98	-10.30 ± 2.73

significant changes in the ice sheet geometry [Solgaard and Langen, 2012]. However, for short term runs that have been performed in this thesis, a coupling would not change the outcome significantly.

The pattern of fast flowing arms is not captured well by the PISM model runs. This is a result of the very smooth bedrock elevation grid, especially at the terminus. So, it is difficult to capture KNS only with PISM and a part of the modeled fluxes may actually be from its neighboring glacier, AS. A better bed map would make a distinction easier, and also, one could model all glaciers terminating into Godthåbsfjord.

With more computing power available, it would be possible to perform the runs on a higher resolution, e.g., 1 km or even 500 m. However, the bed elevation map must contain information on the same resolution.

There have been no successful ice thickness measurements using ice penetrating radar in the proximity of the terminus because warm and wet ice conditions absorb the radar signal. Bedrock troughs under the ice would make it possible to model the actual surface velocity pattern. Since there are temperate radars in development, additional data would improve the model results. Since the fjord is very narrow and long, and the measured surface velocity has narrow fast flowing arms, it is likely that there is a bedrock trough underneath KNS. Also, the driving stress in the terminus region is high, which hints to a deep bedrock trough.

The glacial meltwater computation using the isotope analysis is limited by the sparse available. The sensitivity study performed shows that the glacial meltwater flux depends strongly on the estimated summer velocity of the surface layer. With year around measurements, it would be possible to study the seasonal response of the fjord to the glacial meltwater influx in more detail.

Versteegh et al. [2012] showed, that the shell of the blue mussel can be used as a proxy for past oxygen isotopes ($\delta^{18}\text{O}$), when it is collected not too close to the glacier front. Using these, it might be possible to estimate the past glacial melt from the glaciers al well.

7.2 Impact

The ice loss by KNS is small compared to the total mass loss of Jakobshavn Isbræ that has a yearly loss of 25–33 Gt. Godthåbsfjord and its neighboring fjords have a diverse ecosystem, which could be affected by the ongoing changes in the fjord, such as increased freshwater flux. This in turn will affect the local biodiversity, e.g. phytoplankton, which will have impact on the food web in the Arctic. Plankton is eventually feeding most fish, marine birds and mammals in the Arctic [Michel et al., 2012]. Mammals such as the harbour porpoise, are directly affected by warmer ocean temperatures [Heide-Jørgensen et al., 2011]. In addition, the changing environment has an impact on the cod population dynamics, which affects the fishery and hence local economy significantly [Storr-Paulsen et al., 2004]. A very vivid example of the consequences of increased freshwater flux is the following. In 2009, the ice dammed lake Illuliartôk near Narssap Sermia drained into the fjord. A large upwelling of freshwater took redfish, which live close to the glaciers, to the surface. The redfish died of diverse diseases [Kjeldsen et al., 2011], see Figure 7.1.



Figure 7.1: Deceased redfish after an upwelling of freshwater. Picture taken by Jakob Bertelsen.

A | Poster EGU 2012: Modelling
the outlet glaciers terminat-
ing in Godthåbsfjord.

Modelling the outlet glaciers terminating in Godthåb fjord.

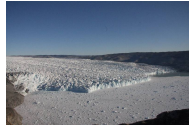
Antje Fitzner and Dorte Dahl-Jensen
Centre for Ice and Climate, Niels Bohr Institute, University of Copenhagen



EGU General Assembly 2012 – EGU2012-205-1 – Board number XY371

Motivation

- ▶ Mass loss of the Greenland ice sheet: surface melting and flow through outlet glaciers.
- ▶ Processes leading to the mass loss through outlet glaciers such as calving and basal melting are not well understood.
- ▶ This study: outlet glaciers terminating in Godthåb fjord.
- ▶ Main contributing glacier: Kangiata Nunaata Sermia.



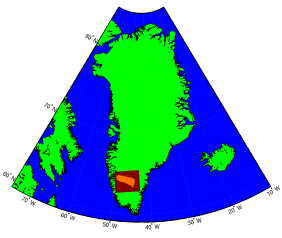
Kangiata Nunaata Sermia
Credit: Peter S. Mikkelsen

Main objective: Estimating fresh water flux from the outlet glaciers contributing to the fresh water in Godthåb fjord.

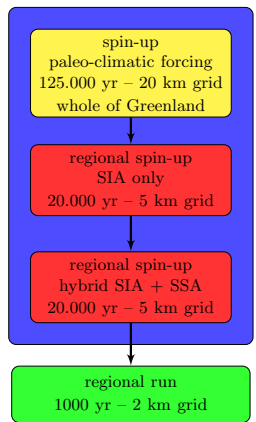
The Parallel Ice Sheet Model

- ▶ PISM is an open source C++ three-dimensional thermomechanically coupled and time-dependent ice sheet model (UAF, www.pism-docs.org).
- ▶ Enthalpy formulation for polythermal conditions (Aschwanden et al. [2012]).
- ▶ Used approximation: SIA with SSA as a sliding law (Bueler and Brown [2009]).

Modelling Region and Spin-up



- ▶ Orange: Drainage basin based on surface gradients (Code from Della-Giustina).
- ▶ Red: Regional modelling domain.
- ▶ Boundary values: from spin-up with paleo-climatic forcing.



Climatic Forcing

- Surface mass balance and 2 m air temperature:
- ▶ **RACMO** RCM output as used in the SeaRISE experiment (Ettema et al. [2009])
 - ▶ **HIRHAM** RCM output from DMI (ECHAM5, A1B scenario, used in this study: mean of 1992) (Mottram et al. [2012, in prep.], Lucas-Picher et al. [2012]).

Digital Elevation Model and Bathymetry

- The new DEM contains:
- ▶ Bathymetry (*unpublished*, Greenland Climate Research Centre).
 - ▶ DEM (based on the 1985 survey) (Natural History Museum of Denmark).
 - ▶ 5 km Greenland data set (Bamber et al. [2001]).
 - ▶ **Coming soon:** Bedrock map of the terminus region by CREStS.

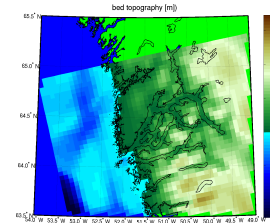


Figure: Bed topography on a 5 km grid from Bamber et al. [2001].

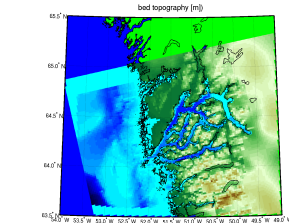


Figure: Combined bed topography on a 2 km grid.

Modelled and Observed Surface Velocities

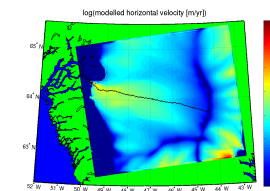


Figure: Modelled surface velocity on a 2 km grid with HIRHAM forcing.

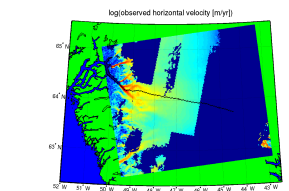


Figure: Observed surface velocity on a 2 km grid [Joughin et al. [2010]].

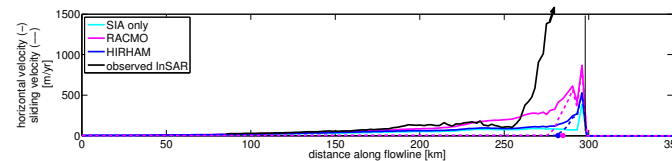
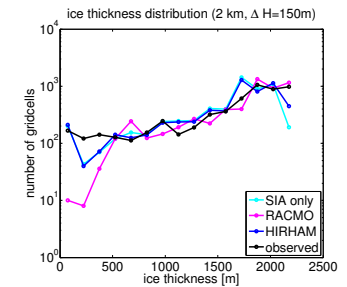
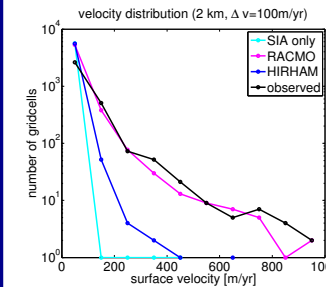


Figure: Observed and modelled surface velocity along an arbitrary flow line (see figures above). The bold dots represent the location where the SSA velocity (sliding) exceeds the SIA velocity.

Quantitative Validation

- ▶ Comparison of the modelled and observed number of grid cells in a certain surface velocity and ice thickness interval in the drainage basin (dominated by low velocities):



- ▶ Absolute difference ice thickness: $\Delta H = H_{\text{observed}} - H_{\text{modelled}}$ for all grid cells in the drainage basin and calculating the mean and standard deviation of the ΔH distribution.

$$(\Delta H_{\text{SIA}})_{\text{mean} \pm \text{std}} = (65.36 \pm 55.20) \text{ m}$$

$$(\Delta H_{\text{RACMO}})_{\text{mean} \pm \text{std}} = (-130.99 \pm 47.49) \text{ m}$$

$$(\Delta H_{\text{HIRHAM}})_{\text{mean} \pm \text{std}} = (39.24 \pm 49.34) \text{ m}$$

- ▶ Relative difference surface velocity: $\Delta V^R = \frac{\Delta V}{V_{\text{observed}}}$
- $(\Delta V_{\text{SIA}}^R)_{\text{mean} \pm \text{std}} = (-0.51 \pm 0.34)$
- $(\Delta V_{\text{RACMO}}^R)_{\text{mean} \pm \text{std}} = (-0.51 \pm 5.62)$
- $(\Delta V_{\text{HIRHAM}}^R)_{\text{mean} \pm \text{std}} = (0.39 \pm 0.51)$
- ▶ The RACMO forcing models the low velocities more accurately.
- ▶ **The HIRHAM forcing shows better results for modelled ice thickness and surface velocities (all magnitudes).**
- ▶ Including sliding and the new bed topography improved results.

Conclusions and Outlook

- ▶ Missing topographical focussing at the terminus.
 - Near terminus bed topography from CREStS.
- ▶ Generation of a floating tongue.
 - Calving model.
- ▶ Estimate freshwater flux into Godthåb fjord.

Take-home message

- ▶ The model captures the high velocities near the terminus qualitatively.
- ▶ The distinct fast flowing arms are not well modelled.

References:

Aschwanden, A. et al. (2012). An enthalpy formulation for glaciers and ice sheets. *Journal of Glaciology*, 58(205):441–457.
 Bamber, J. et al. (2001). A new ice thickness and bed data set for the Greenland ice sheet. I: Measurement, data reduction, and errors. *Journal of Geophysical Research, D, Atmospheres*, 106:33.
 Bueler, E. and Brown, J. (2009). Shallow shelf approximation as a sliding law in a thermomechanically coupled ice sheet model. *Journal of Geophysical Research*, 114(F3):1–21.
 Ettema, J. et al. (2009). Higher surface mass balance of the Greenland ice sheet revealed by high-resolution climate modeling. *Geophysical Research Letters*, 36(12):4–8.
 Joughin, I. et al. (2010). MEaSUREs Greenland Ice Velocity Map from InSAR Data. *Boulder, Colorado, USA: National Snow and Ice Data Center, Digital media*.
 Lucas-Picher, P. et al. (2012). Very high resolution regional climate model simulations over Greenland: Identifying added value. *Journal of Geophysical Research*, 117(D2):1–16.

Acknowledgments:

This study is conducted in affiliation with the Greenland Climate Research Centre in Nuuk. Many thanks to the PISM group for helping setting up the model and answering questions.

Antje Fitzner
fitzner@gfy.ku.dk
www.gfy.ku.dk/~fitzner

B | Poster IGS 2013: Modelling
the outlet glaciers terminat-
ing in Godthåbsfjord.

Modelling the outlet glaciers terminating in Godthåb fjord.

Antje Fitzner and Dorte Dahl-Jensen
Centre for Ice and Climate, Niels Bohr Institute, University of Copenhagen

IGS symposium on glaciers and ice sheets in a warming climate, Fairbanks, Alaska, 25 – 29 June 2012, 63A265

Motivation

- Mass loss of the Greenland ice sheet: surface melting and flow through outlet glaciers.
- Processes leading to the mass loss through outlet glaciers such as calving and basal melting are not well understood.
- This study: outlet glaciers terminating in Godthåb fjord.
- Main contributing glacier: Kangiata Nunaata Sermia.



Kangiata Nunaata Sermia
Credit: Peter S. Mikkelsen

Main objective: Estimating fresh water flux from the outlet glaciers contributing to the fresh water in Godthåb fjord.

Take-home message

- The model captures the high velocities near the terminus qualitatively.
- The distinct fast flowing arms are not well modelled (due to sparse bedrock topography data?).
- The modelled velocities and fluxes are overall lower than than observed.

Digital Elevation Model and Bathymetry

The new DEM contains:

- 5 km Greenland data set (Bamber et al. [2001]).
- DEM (based on the 1985 survey) (Natural History Museum of Denmark).
- Bathymetry (*unpublished*, Greenland Climate Research Centre).

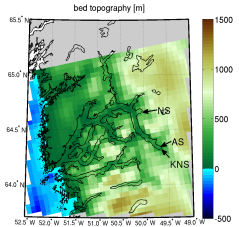


Figure: Bed topography on a 5 km grid from Bamber et al. [2001].

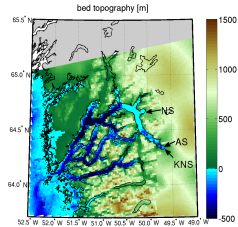


Figure: Combined bed topography on a 2 km grid.

Climatic Forcing

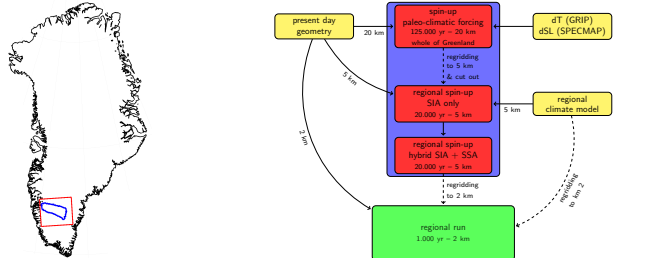
Surface mass balance and 2 m air temperature:

- **RACMO** RCM output as used in the SeaRISE experiment (Ettema et al. [2009])
- **HIRHAM A1B** RCM output from DMI (ECHAM5, A1B scenario, used in this study: mean of 1992) (Mottram et al. [2012, in prep.], Lucas-Picher et al. [2012]).
- **HIRHAM** RCM output from DMI (reanalysis, used in this study: mean of 1990) (Mottram et al. [2012, in prep.], Lucas-Picher et al. [2012]).

The Parallel Ice Sheet Model

- PISM is an open source C++ three-dimensional thermomechanically coupled and time-dependent ice sheet model (UAF, www.pism-docs.org).
- Enthalpy formulation for polythermal conditions (Aschwanden et al. [2012]).
- Used approximation: SIA with SSA as a sliding law (Bueler and Brown [2009]).

Modelling Region and Spin-up



- Blue: Drainage basin based on surface gradients (Code from Della-Giustina).
- Red: Regional modelling domain.
- Boundary values: from spin-up with paleo-climatic forcing.

Modelled and Observed Surface Velocities

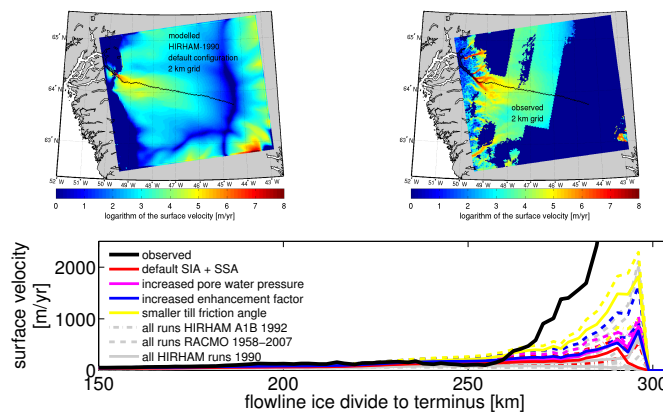
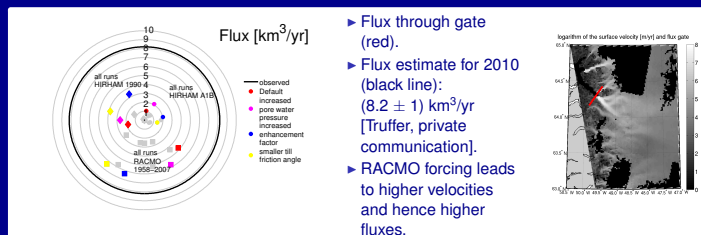


Figure: Observed (Joughin et al. [2010]) and modelled surface velocity along a flow line (v. s.).

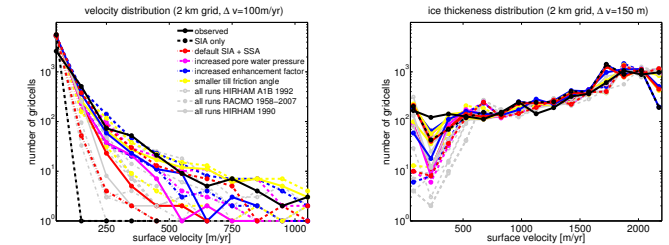
Flux



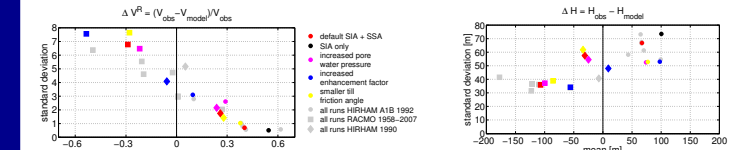
- Flux through gate (red).
- Flux estimate for 2010 (black line): $(8.2 \pm 1) \text{ km}^3/\text{yr}$ [Truffer, private communication].
- RACMO forcing leads to higher velocities and hence higher fluxes.

Quantitative Validation

- Comparison of the modelled and observed number of grid cells in a certain surface velocity and ice thickness interval in the drainage basin (dominated by low velocities):



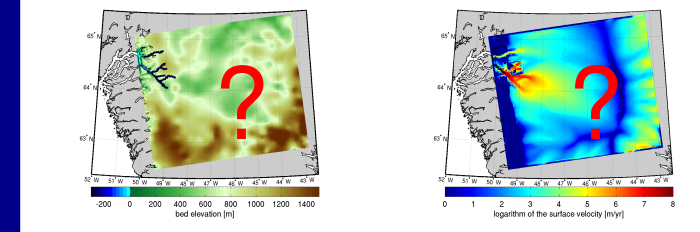
- Absolute difference ice thickness and relative difference surface velocity for all grid cells in the drainage basin and calculating the mean and standard deviation of the difference.



- The RACMO forcing models the velocities distribution more accurately.
- The HIRHAM forcing shows better results for modelled surface velocities compared to the observed velocity pattern.
- Including sliding and the new bed topography result in higher velocities near the terminus.
- Parameter choices such as smaller till friction angle and increased pore water pressure improved the results.

What if...

... there are deep troughs in the bed topography where the surface velocity is very high?



Conclusions and Outlook

- Missing topographical focussing at the terminus. → Near terminus bed topography from CREGIS → Are there deep troughs?
- Generation of a floating tongue. → Calving model.
- Verify ice divide position with more observed velocity data

References:
Aschwanden, A. et al. (2012). An enthalpy formulation for glaciers and ice sheets. *Journal of Glaciology*, 58(209):441–457.
Bamber, J. et al. (2001). A new ice thickness and bed data set for the Greenland ice sheet. I- Measurement, data reduction, and errors. *Journal of Geophysical Research. D. Atmospheres*, 106:33.
Bueler, E. and Brown, J. (2009). Shallow shelf approximation as a sliding law in a thermomechanically coupled ice sheet model. *Journal of Geophysical Research*, 114(F3):1–21.
Ettema, J. et al. (2009). Higher surface mass balance of the Greenland ice sheet revealed by high-resolution climate modeling. *Geophysical Research Letters*, 36(12):4–8.
Joughin, I. et al. (2010). MEASURES Greenland Ice Velocity Map from InSAR Data. *Boulder, Colorado, USA: National Snow and Ice Data Center, Digital media*.
Lucas-Picher, P. et al. (2012). Very high resolution regional climate model simulations over Greenland: Identifying added value. *Journal of Geophysical Research*, 117(D2):1–16.

Acknowledgments:
This study is conducted in affiliation with the Greenland Climate Research Centre in Nuuk.
Many thanks to the PISM group for helping setting up the model and answering questions.

Antje Fitzner
fitzner@gfy.ku.dk
www.gfy.ku.dk/~fitzner



C | Poster EGU 2013: Modeling the present and future behavior of the glaciers terminating into Godthåbsfjord, West Greenland

Modeling the present and future behavior of the glaciers terminating into Godthåbsfjord, West Greenland

Antje Fitzner^{1,2} and Dorte Dahl-Jensen¹

¹Centre for Ice and Climate, Niels Bohr Institute, University of Copenhagen and ²Greenland Climate Research Centre, Nuuk

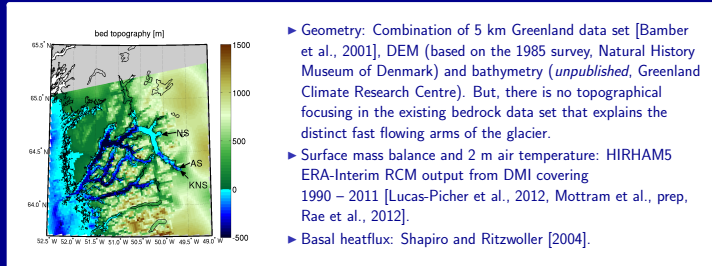
EGU2013-366, EGU General Assembly 2013, board number B663

Motivation

- The mass loss of the Greenland ice sheets is due to changing surface mass balance, direct surface melt, ice flow through outlet glaciers and basal melt.
- Processes leading to the mass loss through outlet glaciers such as calving and basal melting are not well understood.
- This study: Focus on outlet glaciers terminating in Godthåbsfjord with the main contributing glacier Kangiaata Nunāta Sermia (KNS).
- Extensive oceanographic measurements [Mortensen et al., 2011, 2013] and studies covering the behavior of the glaciers [Ahlstrøm et al., subm, van As et al., 2011] are available.
- Freshwater influences the marine and terrestrial ecosystem. Changes in the ecosystem have an effect on local fishery and hence economy.
- Main objective: Estimating current and future freshwater flux from the outlet glaciers.**

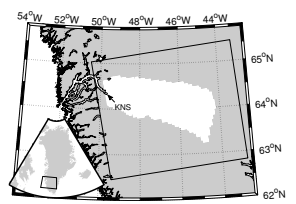


Geometry and Climatic Forcing



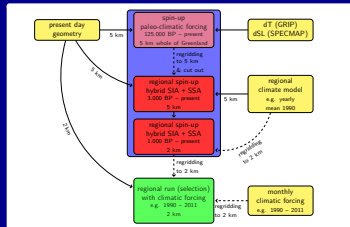
The Parallel Ice Sheet Model

- PISM is an open source c++ three-dimensional thermomechanically coupled and time-dependent ice sheet model (UAF, www.pism-docs.org).
- Enthalpy formulation for polythermal conditions [Aschwandter et al., 2012].
- Used approximations: non-sliding shallow ice approximation (SIA) and the shallow shelf approximation (SSA) as a sliding law [Bueler and Brown, 2009].
- Drainage basin generator using surface gradients [DellaGiustina, 2011]. The modeling region is shown as a black rectangle with the white area being the drainage basin.



► Version used: PISM development 2313605.

Spin-up



Choice of initialization:

- Paleo-climatic spin-up covering one glacial cycle (provided by the PISM group).
- Regional 5 km spin-up from 3000 BP to present using a constant 1990 climate.
- Regional run on 2 km from 1000 BP to present with constant 1990 climate. In this stage the parameters described in the following are altered.
- Regional run with monthly climatic forcing (1990 – 2011) for selected parameter settings.

Parameter Study

Parameter alteration (in red) to fit the modeled and observed surface velocities and ice thickness:

► Flow enhancement factor e in the SIA: $\dot{\epsilon}_{ij} = Ae\tau_{ij}^{n-1}\tau_{ij}$.

with the rate factor A , $n = 3$ the exponent in the flow law and the deviatoric stresses τ , where $\tau_E = \sqrt{\tau_{ij}\tau_{ij}/2}$. The exact value of the enhancement factor is unknown and often varied in ice sheet modelling, but values between 1 and 10 are commonly used.

► Basal shear stress τ_b : $\tau_b = \tau_c \frac{u_b^{q-1}}{u_{thr}^{q-1}} u_b$.

with u_b the modeled sliding velocity, $q = 0.25$ the exponent of the pseudo-plastic basal resistance model, u_{thr} the velocity threshold in the pseudo-plastic basal resistance model and the till yield stress τ_c .

► Basal yield stress τ_c (material strength at the base) described as a Mohr-Coulomb criterion [Cuffey and Paterson, 2010]: $\tau_c = c_0 + \tan(\phi)N$.

with the cohesion factor $c_0=0$, the till friction angle ϕ and the effective pressure $N = \rho gH - p_w$, where p_w is the pore water pressure.

► Till friction angle as a function of the bed elevation:

$$\phi = \begin{cases} \phi_{min} & b \leq b_{min} \\ \phi_{min} + (b(x,y) - b_{min}) \frac{\phi_{max} - \phi_{min}}{b_{max} - b_{min}} & b_{min} < b < b_{max} \\ \phi_{max} & b \geq b_{max} \end{cases}$$

where b_{min} , b_{max} , ϕ_{min} and ϕ_{max} are constant values.

► Pore water pressure: $p_w = \alpha w \rho g H$.

with w the basal water thickness and α a factor controlling the pore water pressure that determines how the effective thickness of basal water affects the pore water pressure. α gives the fraction of the overburden pressure ($\rho g H$) that is the pore water pressure.

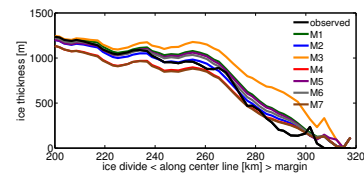
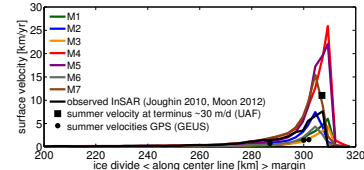
The varied parameter setting are shown in the table. Bold values represent the default values (for Jakobshavn Isbræ). In total all, combinations, 108 model runs with >20000 processor hours, are performed.

flow enhancement factor	e	1	3	5
threshold velocity	u_{thr}	10 m/s	100 m/s	1000 m/s
till friction angle	$[\phi_{min}, \phi_{max}]$	[0,15]	[0,20]	[5,30] [20,45]
pore water pressure fraction	α	0.97	0.98	0.99

Parameter Selection

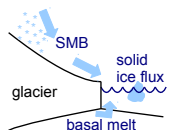
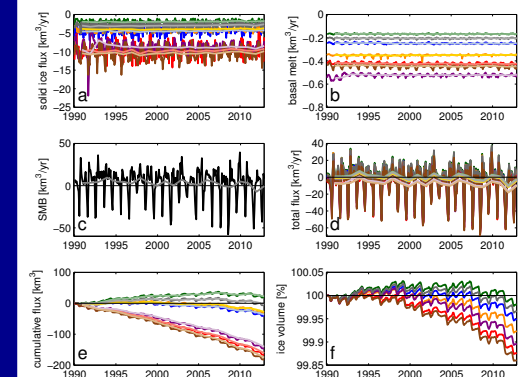
The best seven parameter settings are selected:

- M1** RMS of the modeled and observed surface velocity (from InSAR [Joughin et al., 2010, Moon et al., 2012]) per grid cell.
- M2** Difference in the mean of the modeled and observed surface velocity.
- M3** RMS of the modeled and observed ice thickness per grid cell.
- M4** Difference in the mean of the modeled and observed ice thickness.
- M5** RMS of the modeled and observed surface velocity per velocity interval (interval width of 50 m/yr).
- M6** RMS of the modeled and observed velocity along a center line following the southern arm of KNS.
- M7** Combined ranking of the first six.



best seven	M1	M2	M3	M4	M5	M6	M7
flow enhancement factor	e	1	1	3	1	3	1
threshold velocity	u_{thr} [m/s]	10	10	10	1000	1000	10
till friction angle	$[\phi_{min}, \phi_{max}]$	[5,30]	[0,15]	[20,45]	[5,30]	[0,15]	[20,45]
pore water pressure fraction	α	0.98	0.97	0.98	0.97	0.97	0.98

Monthly Mean Climatic Forcing



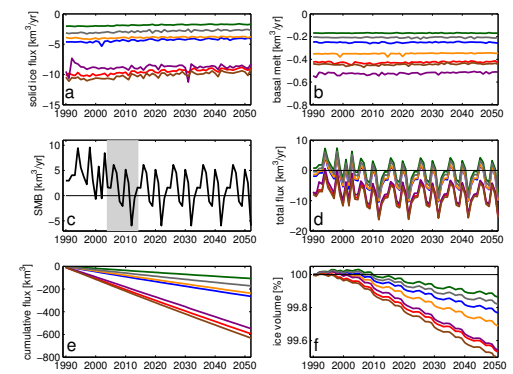
- Seasonal variations.
- Total flux is the sum of solid ice flux, basal melt and SMB.
- Two modes of results, one moderate and one with extreme solid ice mass loss.
- Mass gain in the 1990s and mass loss in the recent years.

- IceSAT mass loss 2003–2008: $-2.49 \text{ km}^3/\text{yr}$ [Sørensen et al., 2011].
- Estimated calving flux: $(-5 \pm 1) \text{ km}^3/\text{yr}$ [Podrasky, private communication].

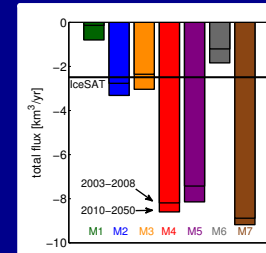
Prognostic Runs

- Record extended using repeated 2002 – 2011 forcing to 2050. No additional warming to present climate.
- Yearly means show continued mass loss.
- Total flux per year averaged for the period 2010 – 2050:

- M1** – $0.80 \text{ km}^3/\text{yr}$
- M2** – $3.31 \text{ km}^3/\text{yr}$
- M3** – $3.04 \text{ km}^3/\text{yr}$
- M4** – $8.60 \text{ km}^3/\text{yr}$
- M5** – $8.14 \text{ km}^3/\text{yr}$
- M6** – $1.84 \text{ km}^3/\text{yr}$
- M7** – $9.18 \text{ km}^3/\text{yr}$



Discussion, Conclusions and Outlook



- PISM reproduces the present behavior of KNS and seasonal variations are modeled.
- Missing bedrock elevation measurements at the terminus.
- KNS is currently losing mass and will continue to lose mass.
- M2** and **M3** match best observed surface velocities and IceSAT mass loss.
- Using present day climate without additional warming, the KNS drainage basin will lose between 3.0 and $3.3 \text{ km}^3/\text{yr}$.
- Small contribution to total mass loss of the Greenland Ice Sheet.
- But large impact on the local ecosystem.

References:

Ahlstrøm, A. et al. (subm). Seasonal velocities of eight major marine-terminating outlet glaciers of the Greenland ice sheet from continuous in situ GPS instruments. Aschwandter, A. et al. (2012). An enthalpy formulation for glaciers and ice sheets. *J. of Glac.*, 58(2009):441–457. Bamber, J. et al. (2001). A new ice thickness and bed data set for the Greenland ice sheet. 1- Measurement, data reduction, and errors. *JGR Atmospheres*, 106:33. Bueler, E. and Brown, J. (2009). Shallow shelf approximation as a sliding law in a thermomechanically coupled ice sheet model. *JGR*, 114(F3):1–21. Cuffey, K. and Paterson, W. (2010). *The Physics of Glaciers*. Butterworth-Heinemann, Elsevier, fourth edition. DellaGiustina, D. (2011). Regional modeling of Greenland's outlet glaciers with the Parallel Ice Sheet Model. Master's thesis, University of Alaska, Fairbanks; M.S. Computational Physics. Joughin, J. et al. (2010). Greenland flow variability from ice-sheet-wide velocity mapping. *J. Of Glac.*, (56):415–430. Lucas-Picher, P. et al. (2012). Very high resolution regional climate model simulations over Greenland: Identifying added value. *JGR*, 117(D2):1–16.

Moon, T. et al. (2012). 21st Century Evolution of Greenland Outlet Glacier Velocities. *Science*, 336:676–678. Mortensen, J. et al. (2011). Heat Sources for glacial meltwater in a Sub-Arctic Fjord (Godthåbsfjord) in Contact with the Greenland Ice Sheet. *JGR*, 116. Mortensen, J. et al. (2013). On the seasonal freshwater stratification in the proximity of fast-flowing tidewater glaciers in a sub-Arctic sill fjord. *JGR*. Mottram, R. et al. (prep). Reconstructing the surface mass balance of the Greenland Ice Sheet with the regional climate model HIRHAM5, 1989–2011. Rae, J. et al. (2012). Greenland ice sheet surface mass balance: evaluating simulations and making projections with regional climate models. *TCD*, 6. Shapiro, N. and Ritzwoller, M. (2004). Inferring surface heat flux distributions guided by a global seismic model: particular application to Antarctica. *Earth and Planetary Science Letters*, 225. Sørensen, L. et al. (2011). Mass balance of the Greenland ice sheet (2003/2008) from ICESat data: the impact of interpolation, sampling and firm density. *TC*, 5(1):173–186. van As, D. et al. (2011). Programme for Monitoring of the Greenland Ice Sheet (PROMICE): first temperature and ablation records. *Geol. Surv. Den. Greenl.*, 23:73–76.

Antje Fitzner
fitzner@gfy.ku.dk
www.gfy.ku.dk/~fitzner

Acknowledgments:
Many thanks to the PISM group for helping setting up the model and answering questions.



D | Poster EGU 2013: Estimating the glacial meltwater contribution to the fresh water budget from salinity and $\delta^{18}\text{O}$ measurements in Godthåbsfjord

Estimating the glacial meltwater contribution to the fresh water budget from salinity and $\delta^{18}\text{O}$ measurements in Godthåbsfjord

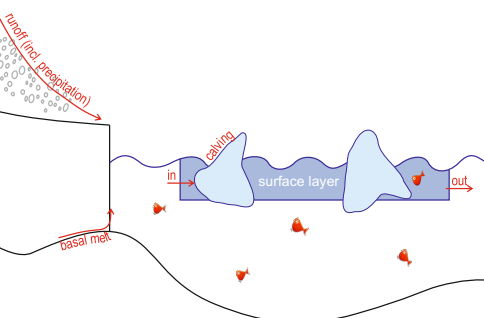
Antje Fitzner^{1,2}, Dirk van As³, Jørgen Bendtsen⁴, Dorthe Dahl-Jensen¹, Xavier Fettweis⁵, John Mortensen², Søren Rysgaard^{2,6,7}
¹ Centre for Ice and Climate, Niels Bohr Institute, Copenhagen University, DK, ² Greenland Climate Research Centre, GL, ³ Geological Survey of Greenland and Denmark, DK, ⁴ VitusLab, DK, ⁵ University of Liège, BE, ⁶ Arctic Research Centre, DK, ⁷ Centre for Earth Observation Science, CA
 EGU2013-364, EGU General Assembly 2013, board number B604



Motivation

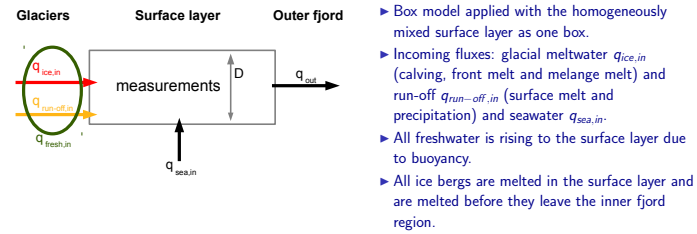
- ▶ Mass loss of the Greenland Ice Sheet increases due to changes in the surface mass balance and ice discharge.
- ▶ All mass loss enters the fjords as freshwater.
- ▶ Freshwater influences the marine and terrestrial ecosystem.
- ▶ Changes in the ecosystem have an effect on local fishery and hence economy.

Concept



- ▶ Freshwater can be quantified using salinity measurements.
- ▶ Between the freshwater origin, being run-off (surface melt and precipitation) or glacial melt (calving and basal melt), cannot be distinguished using salinity only.
- ▶ **New measure: the isotopic signature ($\delta^{18}\text{O}$) of the freshwater sources is different!**

Box Model



- ▶ Box model applied with the homogeneously mixed surface layer as one box.
- ▶ Incoming fluxes: glacial meltwater $q_{ice,in}$ (calving, front melt and melange melt) and run-off $q_{run-off,in}$ (surface melt and precipitation) and seawater $q_{sea,in}$.
- ▶ All freshwater is rising to the surface layer due to buoyancy.
- ▶ All ice bergs are melted in the surface layer and are melted before they leave the inner fjord region.

Governing equations:

$$V \cdot \frac{dS}{dt} = q_{sea,in} S_{sea} + q_{fresh,in} S_{fresh} - q_{out} S - \frac{dV}{dt} S \quad \text{and} \quad (1)$$

$$V \cdot \frac{d\delta^{18}\text{O}}{dt} = q_{sea,in} \delta^{18}\text{O}_{sea} + q_{ice,in} \delta^{18}\text{O}_{ice} + q_{run-off,in} \delta^{18}\text{O}_{run-off} - q_{out} \delta^{18}\text{O} - \frac{dV}{dt} \delta^{18}\text{O}, \quad (2)$$
 with the volume V . The subscripts indicate the origin of the water masses. The volume V is estimated from the width W and length L of the fjord section and the thickness of the considered surface layer D . From mass conservation, the total incoming flux is

$$q_{in} = q_{fresh,in} + q_{sea,in} = q_{ice,in} + q_{run-off,in} + q_{sea,in} \quad (3)$$

The change in the surface layer thickness is due to changes in the incoming flux and hence it is

$$q_{out} = q_{in} - \frac{dV}{dt} = q_{fresh,in} + q_{sea,in} - \frac{dV}{dt} \quad (4)$$

The total outgoing flux is estimated using the geometry of the fjord and an estimate for the surface layer velocity v , namely

$$q_{out} = W \cdot D \cdot v \quad (5)$$

Combining Equations 4 and 5 gives

$$q_{sea,in} = W \cdot D \cdot v - q_{fresh,in} + \frac{dV}{dt} \quad (6)$$

The incoming freshwater flux is then calculated by combining Equations 1, 5 and 6, which gives

$$q_{fresh,in} = \frac{V \frac{dS}{dt} + (WDv + \frac{dV}{dt}) \cdot (S - S_{sea})}{S_{fresh} - S_{sea}} \quad (7)$$

From Equations 2, 5 and 6, $q_{ice,in}$ is calculated as a function of $q_{fresh,in}$

$$q_{ice,in} = \frac{V \frac{d\delta^{18}\text{O}}{dt} + (WDv + \frac{dV}{dt}) \cdot (\delta^{18}\text{O} - \delta^{18}\text{O}_{sea}) + q_{fresh,in} (\delta^{18}\text{O}_{sea} - \delta^{18}\text{O}_{run-off})}{\delta^{18}\text{O}_{ice} - \delta^{18}\text{O}_{run-off}} \quad (8)$$

▶ Equations 7 and 8 are then solved numerically for incoming freshwater and glacial meltwater fluxes. The run-off is then $q_{run-off} = q_{fresh} - q_{ice}$ from mass conservation.

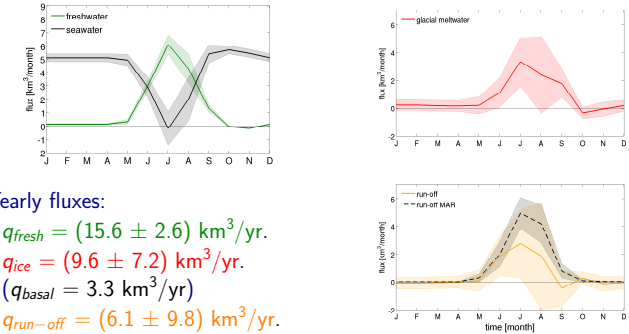
Salinity and $\delta^{18}\text{O}$ Estimates

- ▶ **Seawater:** From a station at the fjord entrance below the surface layer.
- ▶ **Run-off:** $\delta^{18}\text{O}_{run-off}$ from the isotopic regional climate model REMO-iso [Sjolte et al., 2011]. The salinity is zero.
- ▶ **Glacial meltwater:** $\delta^{18}\text{O} = -28 \text{‰}$ from measured ice bergs in Godthåbsfjord (Rysgaard, private communication). The salinity is zero.

Basal Melt

- ▶ Negligible calving and run-off in the winter time (October to April).
- ▶ Isolate the basal meltwater, meaning melt under the glacier and front melt, component from winter conditions.
- ▶ Summer surface velocities at KNS increase by 30 % with respect to the winter velocity [Ahlstrøm et al., subm], so the basal melt water flux is scaled equally.

Result

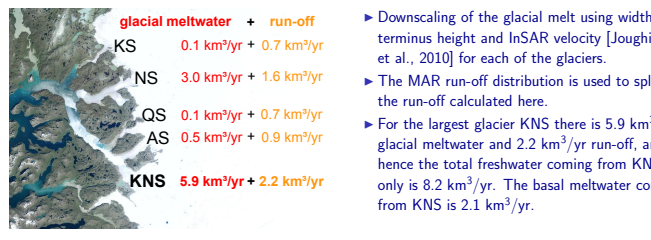


- Yearly fluxes:
 ▶ $q_{fresh} = (15.6 \pm 2.6) \text{ km}^3/\text{yr}$.
 ▶ $q_{ice} = (9.6 \pm 7.2) \text{ km}^3/\text{yr}$.
 ($q_{basal} = 3.3 \text{ km}^3/\text{yr}$)
 ▶ $q_{run-off} = (6.1 \pm 9.8) \text{ km}^3/\text{yr}$.

Sensitivity

- Changes in the glacial water flux due to changes in
Summer surface layer velocity $\pm 2.5 \text{ cm/s} \rightarrow \pm 2.3 \text{ km}^3/\text{yr}$
Winter surface layer thickness $\pm 3 \text{ m} \rightarrow \pm 0.8 \text{ km}^3/\text{yr}$
Isotopic signature of ice to -30‰ $\rightarrow -1.4 \text{ km}^3/\text{yr}$
Shift in $\delta^{18}\text{O}_{sea}$ $\pm 0.3 \text{‰}$ $\rightarrow \pm 2.8 \text{ km}^3/\text{yr}$
Shift in $\delta^{18}\text{O}_{run-off}$ $\pm 1 \text{‰}$ $\rightarrow \pm 0.3 \text{ km}^3/\text{yr}$
- More measurements throughout the year are needed to reduce uncertainties!

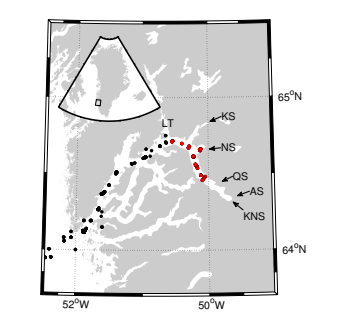
Downscaling



Summary

- ▶ Using $\delta^{18}\text{O}$ in addition to salinity, makes it possible to distinguish between several freshwater sources.
- ▶ There is $(15.6 \pm 2.6) \text{ km}^3/\text{yr}$ freshwater entering the fjord, whereof $(9.6 \pm 7.2) \text{ km}^3/\text{yr}$ is from glacial meltwater (excluding surface melt) and $(6.1 \pm 9.8) \text{ km}^3/\text{yr}$ from run-off.
- ▶ **KNS** contributes $2.2 \text{ km}^3/\text{yr}$ run-off, $5.9 \text{ km}^3/\text{yr}$ glacial meltwater and hence $8.1 \text{ km}^3/\text{yr}$ freshwater. Earlier estimates for the KNS discharge flux of solid ice are be $(5 \pm 1) \text{ km}^3/\text{yr}$ (Podrasky, private communication).

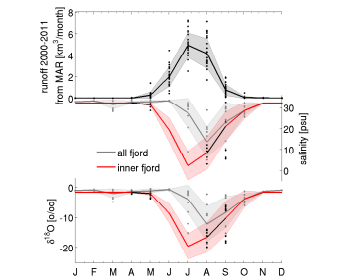
Introduction



- ▶ Two landlocked glaciers (KS, NS) and three tide water glaciers (KNS, AS, NS).
- ▶ Earlier analyses: oceanographic measurements [Mortensen et al., 2011, 2013], glaciological observations [Ahlstrøm et al., subm] and AWS [van As et al., 2011].
- ▶ Surface water (< 10 m depth) samples taken in Godthåbsfjord between 2007 and 2010: Analyzed for salinity and $\delta^{18}\text{O}$.
- ▶ Focus on the inner fjord measurements (red) covering about 40 km of the fjord.

Data Description

- ▶ Seasonal variability of the run-off for all five glaciers. Regional climate model output from MAR [Fettweis et al., 2011]. The shape is used to fill up the missing month in the measurements.
- ▶ All fjord seasonal variability of salinity and $\delta^{18}\text{O}$ in gray.
- ▶ Inner fjord measurements in black. Reconstructed curve, as used in the analysis, in red.



- ▶ Estimated surface layer velocities are 4 cm/s in the winter and 8 cm/s in the summer.
- ▶ Surface layer thickness estimated to be 6 m during summer and 10 m in winter time.

E | Manuscript submitted to The Cryosphere: Modeling Present and Future Behavior of the Tidewater Glacier Kangiata Nunaata Sermia, West Greenland

Modeling Present and Future Behavior of the Tidewater Glacier Kangiata Nunaata Sermia, West Greenland

A. Fitzner^{1,2} and D. Dahl-Jensen¹

¹Centre for Ice and Climate, Niels Bohr Institute, Copenhagen University, Denmark

²Greenland Climate Research Centre, Greenland

Correspondence to: A. Fitzner
(fitzner@nbi.ku.dk)

1

Abstract

The Greenland ice sheet is losing mass due to changing surface mass balance, direct melting on the surface, ice flow through the numerous outlet glaciers, and basal melt. This study focuses on the outlet glaciers terminating in Godthåbsfjord near Nuuk
5 in West Greenland, with Kangiata Nunaata Sermia (KNS) being the main contributing glacier. The mass loss of this glacier forms a small contribution to the total mass loss of the Greenland Ice Sheet, but it will have a large impact on the local ecosystem in the form of freshwater flux into the fjord.

The Parallel Ice Sheet Model is applied to model current and future mass loss. A parameter study is conducted to select the best parameter settings matching observed
10 InSAR surface velocities and observed ice thickness. A monthly mean climatic forcing is applied to these best settings to investigate the individual components of the total fluxes. The model reproduces the present behavior of KNS. Also, seasonal variations are modeled. The modeled solid ice flux, surface velocities, and total mass flux agree
15 well with observations from surface velocities, calving flux estimates and IceSAT elevation changes.

The glacier is currently losing mass and will continue to lose mass. Using present day climate without additional warming, the KNS drainage basin will likely suffer a mass loss of (4.6 ± 3.1) km³/yr. The best model run suggests a mass loss of 3.3 km³/yr until
20 2050.

2

1 Introduction

The mass loss of the Greenland ice sheet is caused by changing surface mass balance, ice flow through the numerous outlet glaciers, and basal melt. Large outlet glaciers, like Jakobshavn Isbræ, are studied in great detail. However, processes leading to their behavior such as calving and basal melting are not well understood. Many smaller glaciers have not been investigated in such great detail.

In this article, we focus on Godthåbsfjord, located near Nuuk in West Greenland, see Figure 1. It is a unique fjord system with a length of about 150 km and a shallow sill at the entrance that protects the fjord. There are several tidewater glaciers contributing to the fresh water content. The largest contributor is Kangiata Nunaata Sermia (KNS). Extensive oceanographic measurements (Mortensen et al., 2011, 2013), surface velocity and weather station studies for these glaciers (Ahlstøm et al., 2013; van As et al., 2011; van As et al., 2014) are available for this region.

Our aim is to describe the present and future behavior of KNS. Section 2 describes the used ice sheet model, PISM, and input data, and Section 3 explains the varied parameters and selection procedure. Results are shown in Section 4 for the current behavior, and in Section 5 for future predictions. Concluding, Section 6 discusses the results found here, and Section 7 contains a short summary and conclusions.

2 Method and Input

For this study, the Parallel Ice Sheet Model, described in more detail in Section 2.1, is used for the KNS drainage basin. The drainage basin is determined using surface gradients under the assumption that the ice flow follows the steepest surface gradient (Budd and Warner, 1996). The modeled region is a rectangle around the drainage basin (see Figure 1).

For Godthåbsfjord there is a high resolution bathymetry available (Rysgaard, private communication), that is combined with a high resolution DEM based on a 1985 sur-

3

vey (Natural History Museum of Denmark, private communication). The bed elevation and ice thickness are taken from the 5 km dataset by Bamber et al. (2001) and the 1 km dataset by Bamber et al. (2013). Unfortunately, availability of ice thickness and bedrock elevation data, especially in the proximity of KNS's terminus, is limited at this point. There is no topographical focusing, such as a deep bedrock trough, in the existing bedrock dataset that explains KNS's distinct fast flowing arms.

Applied climatic forcing and initialization are described in Sections 2.2 and 2.3. Observed surface velocities from InSAR (Joughin et al., 2010; Moon et al., 2012) and GPSs (Ahlstøm et al., 2013) and ice thickness are used to determine the best parameters describing the present state of KNS. Those best parameter settings are then used for future projections (until 2050) to estimate solid ice flux and basal melt that enters the fjord system such as fresh water and total ice volume in the drainage basin.

2.1 PISM

The three-dimensional Parallel Ice Sheet Model (PISM-authors, 2013) uses two shallow approximations: the non-sliding shallow ice approximation (SIA, (Hutter, 1983)) and the shallow shelf approximation (SSA, (Morland et al., 1984; MacAyeal, 1989,b)), which are applied in parallel. For the special case of ice stream flow, both approximations are combined in such a way that the SSA is representing sliding and 'added' to the SIA velocities (Bueler and Brown, 2009). This is referred to as a hybrid run, which is used in this study. Velocities are calculated at each time step from the geometry, temperature and basal strength using the stress momentum equations.

PISM uses an enthalpy formulation for polythermal conditions as described in Aschwanden (2012). This approach allows a better description of temperate ice than achieved when using a temperature formulation. Also, PISM has been part of the Marine Ice Sheet Model Intercomparison Project (Pattyn et al., 2012).

For Antarctic ice shelves, PISM has been improved with a physical two-dimensional calving parametrization based on horizontal strain rates, called eigen-calving, in PISM-PIK ((Winkelmann et al., 2011)). This approach works well for large ice sheets, but

4

cannot be applied to fjord-terminating glaciers because transverse strain rates in a fjord do not allow calving. Also, regional modeling capabilities of PISM have been demonstrated for Jakobshavn Isbræ (DellaGiustina, 2011). This regional approach is used in this study.

5

The used version is PISM development 2313605. In total, there are around 90000 CPU hours performed for PISM model runs in this study.

2.2 Climatic Forcing

Climatic forcing fields required by PISM are surface mass balance and surface temperature. Here, we use high resolution climate model output from HIRHAM5, developed at the Danish Meteorological Institute, and RACMO2 (Regional Atmospheric Climate Model) output. The widely used RACMO2 output (Ettema et al., 2009), as used in the SeaRISE experiment, is applied. The climatic forcing for the 1958–2007 average has been remapped to the PISM 5 km grid by the PISM group.

HIRHAM5 is based on HIRLAM (High Resolution Limited Area Model, (Eerola, 2006)) and ECHAM5 (Roeckner et al., 2003). HIRLAM provides the atmospheric dynamics, and the global ECHAM5 provides the physics. HIRHAM5 is validated through ice cores and automatic weather stations (Dethloff et al., 2002; Box et al., 2003; Kiilsholm et al., 2003; Stendel et al., 2008; Lucas-Picher et al., 2012; Mottram et al., 2012).

20

Recent comparison studies show that HIRHAM5 is generally warmer than RACMO2 due to a lower albedo. Also, the surface mass balance is more negative compared to other discussed models including RACMO2, as shown in Rae et al. (2012).

2.3 Initialization

The initialization process determines the state of the ice sheet at the beginning of the regional runs. For example, an ice sheet remembers past temperatures and hence it

5

does matter whether the ice sheet went through a whole glacial cycle during spin-up or not. Here, two different initializations are used.

On the one hand, a paleo-climatic spin-up, covering one glacial cycle, is performed on a 5 km regular grid (provided by the PISM group), followed by a regional 5 km spin-up from 3000 BP to present. This run uses a constant climate, which is taken to be the first year of the climate record of 1990 for HIRHAM and the 1958–2007 average from RACMO2. The last part of the spin-up is a continuation of the regional run on a 2 km grid from 1000 BP to present, again with a constant climate. In this step, parameters are altered as described in the next sections.

On the other hand, a constant initialization of a 50000 yr long regional run using the SIA, followed by a 50000 yr long hybrid run on a 5 km grid is performed. Then, a 1000 yr regional run on a 2 km grid is performed using the present day climatic forcing only.

Finally, the whole HIRHAM monthly mean climate model output is applied to a subset of model runs, whose selection criteria are described in the following section.

3 Parameter Study

In this section, a description of the altered parameters is given.

One of the often varied parameters is the flow enhancement factor e , which is, for the SIA, incorporated in the strain rate $\dot{\epsilon}_{ij}$. The generalized form of Glen's flow law in index notation is then (Cuffey and Paterson, 2010)

20

$$\dot{\epsilon}_{ij} = Ae\tau_E^{n-1}\tau_{ij}, \quad (1)$$

where A is the rate factor, τ is the deviatoric stress, $n = 3$ is the exponent in the flow law and $\tau_E^2 = \frac{\tau_{ij}\tau_{ij}}{2}$ is the second invariant of the deviatoric stress. The exact value of the enhancement factor is unknown and often varied in ice sheet models. Holocene ice has a value of 2.5 (Cuffey and Paterson, 2010), impure ice at Dye-3 indicates a value of 4 (Dahl-Jensen and Gundestrup, 1987), and at Antarctic shear margins even values

25

of 12 have been estimated (Echelmeyer et al., 1994).

Several parameters control basal strength. Following MacAyeal et al. (1995), the basal shear stress τ_b is given by

$$5 \quad \tau_b = -\beta^2 u_b, \quad (2)$$

where $-\beta^2$ is the drag factor and u_b is the basal velocity. PISM uses a parameterization for the drag factor $-\beta^2$. The basal shear stress τ_b used in PISM is

$$\tau_b = \tau_c \frac{|\mathbf{u}_b|^{q-1}}{u_{thr}^q} \mathbf{u}_b, \quad (3)$$

where \mathbf{u}_b is the modeled sliding velocity, q is the exponent of the pseudo-plastic basal resistance model, u_{thr} is the velocity threshold in the pseudo-plastic basal resistance model and τ_c is the till yield stress. The till yield stress is given by the Mohr-Coulomb criterion (Cuffey and Paterson, 2010), which shows the strength of the material, a mixture of water, ice and till, at the base. Sliding is present when the basal yield stress exceeds the basal shear stress. The basal shear stress is (Schoof, 2006,a, e.g.,)

$$15 \quad \tau_c = c_0 + \tan(\phi)N, \quad (4)$$

where $c_0 = 0$ is the cohesion factor, ϕ is the till friction angle and N is the effective pressure. The effective pressure is $N = \rho g H - p_w$, where p_w is the pore water pressure and $\rho g H$ is the overburden pressure. The pore water pressure is defined as

$$p_w = \alpha w \rho g H, \quad (5)$$

20 where w is the basal water thickness, and α is a factor controlling the pore water pressure that determines how the effective thickness of basal water affects the pore water pressure. Thus, α gives the fraction of the overburden pressure that is the pore water pressure. The basal water thickness depends on the temperature that determines the softness of the ice. Also, dissipation heating and frictional heating at the base are taken

7

into account. However, in the PISM version used here there is no transport of the basal water between grid cells. The till friction angle ϕ can be constant or a function of the bed elevation as follows

$$5 \quad \begin{aligned} \phi &= \phi_{min} & b \leq b_{min} \\ \phi &= \phi_{min} + (b(x,y) - b_{min}) \frac{\phi_{max} - \phi_{min}}{b_{max} - b_{min}} & b_{min} < b < b_{max} \\ \phi &= \phi_{max} & b \geq b_{max} \end{aligned} \quad (6)$$

where b_{min} , b_{max} , ϕ_{min} and ϕ_{max} are constant values.

The parameters altered in the parameter study are climatic forcing and initialization, 10 flow enhancement factor e , pore water pressure fraction α , till friction angle $[\phi_{min}, \phi_{max}]$ and threshold velocity u_{thr} , see Table 1.

3.1 Parameter Selection

The altered parameter values are shown in Table 1. All combinations of possible parameter settings, a total of 108 combinations, are performed for three different climatic forcing and initialization scenarios using the Bamber et al. (2001) ice thickness: HIRHAM5 15 forcing with paleo-climatic spin-up (Hp), HIRHAM5 forcing with constant present day spin-up (Hc), and RACMO2 forcing with paleo-climatic spin-up (Rp). In addition, the model runs using the Bamber et al. (2013) ice thickness are performed for HIRHAM5 and RACMO2 forcing and a paleo-climatic spin-up. This makes a total of 540 model 20 runs with a computing time of about 90000 CPU hours.

The end state of all runs is compared to observed ice thickness and surface velocities. The surface velocity is not an input field for the model; ice thickness, however, is. Five criteria are used to select the best 6 runs: (M1) RMS of the modeled and observed 25 surface velocity per grid cell; (M2) Difference in the mean of the modeled and observed surface velocity; (M3) RMS of the modeled and observed ice thickness per grid cell; (M4) Difference in the mean of the modeled and observed ice thickness; (M5) RMS of

the modeled velocity and observed velocity along a center line following the southern fast flowing arm of KNS; and (M6) the combined ranking of the first five methods. The individual best run is then selected for each method and for the combined best run. The analysis is carried out for the Bamber et al. (2001) and Bamber et al. (2013) datasets separately. The newer dataset is referred to with a star, e.g., M1*.

The parameter setting for those twelve runs is shown in Table 2. Following these criteria, only runs using the HIRHAM5 climatic forcing got selected. The distribution of selected parameters is shown in Figure 2. There is a tendency towards a smaller than pore water fraction α and a smaller threshold velocity u_{thr} for both ice thickness maps. The till friction angle ϕ is smaller than default for Bamber et al. (2001) and larger for Bamber et al. (2013). The enhancement factor e , that matches the observations best, equals 1 for the 2001 and 3 for the 2013 map.

4 Current Velocities and Fluxes

Figure 3 and 4 show the pattern of observed and modeled surface velocities in the modeled region. Note that the pattern of fast flowing arms is not captured by the model. In M6*, where the new ice thickness and bed map by Bamber et al. (2013) is used, there are some features emerging, but not closely as detailed as it is observed. The modeled surface velocities and ice thickness along a center line following the southern fast flowing arm of KNS, see Figure 3, is shown in Figure 5. The selected modeled surface velocities at the terminus range from 0.1 km/yr to 25.9 km/yr. Note that the model runs using the new ice thickness and bed map have retreated about 10 km. This is due to the fact that the bed elevation is below sea level farther inland compared to the map from 2001. Observed surface velocities from InSAR (Joughin et al., 2010; Moon et al., 2012) indicate that M2 captures the InSAR observations at the terminus best. M2, M5, M4* and M5* show a better match to the velocities measured by GEUS GPSs, and M6 matches the estimated summer velocity at the calving front of

9

30 m/day (Podrasky (UAF), private communication). The modeled ice thickness along the center line is captured best by M2 and M2*. As described above, a monthly climatic forcing for the 1990-2011 period covered by the HIRHAM5 model output is applied. PISM is able to output seasonal variability in the modeled fluxes when monthly means of the climatic forcing are applied. The result is shown in Figure 6. The solid ice flux is taken from PISM, which is the amount of ice calved off, corresponding to when it becomes afloat. Modeled fluxes are between zero and 9.7 km³/yr. An estimate based on surface velocities and ice thickness is (5 ± 1) km³/yr (Podrasky (UAF) private communication). Based on this estimate, M2 and M4* match the solid ice flux best, with 4.5 km³/yr and 4.6 km³/yr modeled calving loss. Basal melt in the drainage basin is calculated from model output. The modeled basal melt has to be considered with care, since the PISM version used here does not have a sophisticated basal transport model implemented. Modeled basal melt values range from 0.1 km³/yr to 0.6 km³/yr. There are no estimates for basal melt of KNS available at this point.

The total mass balance M_T , the sum of solid ice flux, basal melt and surface mass balance, is slightly positive in the 1990s and shows a negative trend after 2005. Only model run M1* is gaining mass throughout the whole period. This is due to the fact that in this scenario, KNS has retreated and has lost contact to the fjord. Hence, there is no solid ice flux and the total flux is dominated by the surface mass balance. The modeled total yearly mass balance M_T covering the IceSAT period 2003–2008 is shown in Table 3. Comparison with the IceSAT estimate for the drainage basin (Sørensen et al., 2004), indicates that M2 and M3 imitate the observation of a mass loss of 2.49 km³/yr for the KNS drainage basin best.

The cumulative flux shows that most runs have a continuous mass loss after 1990, whereas M1 has an initial mass increase and as mentioned earlier M1* is gaining mass. Looking at the ice volume as a percentage from the starting volume, all runs with the

exception of M1*, show a smaller ice volume in 2011 compared to 1990. Based on velocity and ice loss observations, M2 simulates the current behavior of KNS best.

5 Future Predictions

5 To extend the climatic forcing to 2050, a conservative approach is applied. The 2002–
2011 interval is extracted and is then repeated following the existing record to 2050. No
additional warming is added to the forcing, which means that the future estimate shown
here accounts for a minimal mass loss until 2050. Additional warming as proposed in
several scenarios of the IPCC report (IPCC, 2007), would increase the mass loss due
10 to warmer temperatures and lower surface mass balance.
The annual variation of the same quantities and parameter setting as in the previous
section are shown in Figure 7. Solid ice flux and basal melt are decreasing slightly over
time because of the reduced ice volume in the drainage basin. The surface mass bal-
ance between 2002 and 2011 is repeated until 2050. Total flux averages after 2010 are
15 as shown in Table 3 in the right column. The modeled mass loss after 2010 is larger
than during the IceSAT period. Cumulative flux and ice volume show a steady mass
loss in the extended period.

Using the run that performed best to model the current behavior, M2, the continued
20 mass loss after the year 2010 is $3.3 \text{ km}^3/\text{yr}$, which is about 0.2% of its volume with
respect to 1990. The remaining selected model runs, excluding M1 and M1*, have a
mass loss of $2.6 \text{ km}^3/\text{yr}$ and $9.0 \text{ km}^3/\text{yr}$, corresponding to a volume loss of 0.01% to
0.7%. The mean mass loss for all twelve runs is $(4.6 \pm 3.1) \text{ km}^3/\text{yr}$.

11

6 Discussion

PISM, in the version used here, has a very simple basal hydrology model with local
basal melt, but without transport between grid cells. The basal melt estimate here is
the total sum in the whole drainage basin assuming that in steady state all liquid basal
5 melt water will exit through KNS. Modeled basal melt for KNS is small compared to es-
timates from other tide water glaciers in Greenland. Due to its small value, it has only
a small influence on the total flux.

The calving criterion used here is the so called ‘floatkill’ option in PISM. Here, all ice is
calved off when it becomes afloat at the terminus. Even though this is not a physical
10 calving criterion, it shows good results in the narrow fjords in Greenland. In this study,
the calving fluxes match the observations well.

As mentioned earlier, the pattern of fast flowing arms is not captured well by the model.
This is a result of the very smooth bedrock elevation grid especially at the terminus.
There have been no successful ice thickness measurements using ice penetrating
15 radar in the proximity of the terminus because warm and wet ice conditions absorb
the radar signal. Bedrock troughs under the ice would make it possible to model the
actual surface velocity pattern.

The climatic forcing applied in the prognostic runs is very conservative. Including addi-
tional emission scenarios, for example the RCP scenarios with a warming, will result in
20 an even larger mass loss until 2050.

7 Conclusions

PISM reproduces the present behavior of KNS and seasonal variations are modeled.
Modeled solid ice flux, surface velocities and total mass flux agree well with observa-
tions from InSAR velocities, calving flux estimates and IceSAT elevation changes.
25 KNS is currently losing mass and will continue to lose mass. Using present day climate
without additional warming, the KNS drainage basin will likely suffer a mass loss of

12

(4.6 ± 3.1) km^3/yr . The best model run suggests a mass loss of $3.3 \text{ km}^3/\text{yr}$ until 2050.

Acknowledgements. The study was financially supported by the Greenland Climate Research Centre and the Niels Bohr Institute, University of Copenhagen.

- 5 We would like to thank the PISM group, especially Andy Aschwanden, Ed Bueler, Daniella Della Giustina and Constantine Khroulev, for the help to set up PISM and answering many questions.

References

- 10 A.P. Ahlström, S.B. Andersen, M.L. Andersen, H. Machguth, F.M. Nick, I. Joughin, C.H. Reijmer, R.S.W. van de Wal, J.P. Merryman Boncori, J.E. Box, M. Citterio, D. van As, R.S. Fausto, A. Hubbard (2013), Seasonal velocities of eight major marine-terminating outlet glaciers of the Greenland ice sheet from continuous in situ GPS instruments, *Earth System Science Data*, 5, 2, 277–287, doi: 10.5194/essd-5-277-2013 .
- 15 D. van As, R.S. Fausto, A.P. Ahlstrom, S.B. Andersen, M.L. Andersen, M. Citterio, K. Edelvang, P. Gravesen, H. Machguth, F.M. Nick, S. Nielsen and A. Weidick (2011), Programme for Monitoring of the Greenland Ice Sheet (PROMICE): first temperature and ablation records, *Geol. Surv. Den. Greenl.*, 23, 73–76.
- D. van As, M.L. Andersen, D. Petersen, X. Fettweis, J.H. van Angelen, J.T.M. Lenaerts, M.R. van den Broeke, J.M. Lea, C.E. Bøggild, A.P. Ahlstrøm and K. Steffen (2014), Increasing meltwater discharge from the Nuuk region of the Greenland ice sheet and implications for mass balance (1960–2012). *J. Glac.*, 60, 220, doi: 10.3189/2014JoG13J065.
- 20 Aschwanden, Andy and Bueler, Ed and Khroulev, Constantine and Blatter, Heinz: An enthalpy formulation for glaciers and ice sheets, *Journal of Glaciology*, 58, 209, doi:10.3189/2012JoG11J088, 2012.
- 25 Bamber, J., Layberry, R., and Gogineni, S. (2001). A new ice thickness and bed data set for the Greenland ice sheet. I- Measurement, data reduction, and errors. *Journal of Geophysical Research. D. Atmospheres*, 106:33.
- Bamber, J. L., Griggs, J. a., Hurkmans, R. T. W. L., Dowdeswell, J. a., Gogineni, S. P., Howat, I., Mougnot, J., Paden, J., Palmer, S., Rignot, E., and Steinhage, D. (2013). A new bed elevation dataset for Greenland. *The Cryosphere*, 7(2):499–510.
- 30

13

- Box, JE and Rinke, A: Evaluation of Greenland ice sheet surface climate in the HIRHAM regional climate model using automatic weather station data, *Journal of climate*, 2003.
- Budd, W.F., and Warner, R.C.: A computer scheme for rapid calculations of balance flux distributions, *Annals of Glaciology* 23, 21-27, 1996.
- 5 Bueler, Ed and Brown, Jed: Shallow shelf approximation as a "sliding law" in a thermomechanically coupled ice sheet model, *Journal of Geophysical Research*, 114, F3, doi:10.1029/2008JF001179, 2009.
- Cuffey, K.M. and Paterson, W.S.B: The Physics of Glaciers, *Butterworth-Heinemann, Elsevier, fourth edition*, 2010.
- 10 Dahl-Jensen, D. and Gundestrup, N.S.: Constitutive properties of ice at Dye 3, Greenland. *The Physical Basis of Ice Sheet Modelling*, 170, 31-43, (1987).
- DellaGiustina, D.: Regional modeling of Greenland's outlet glaciers with the Parallel Ice Sheet Model, Master's thesis, University of Alaska, Fairbanks, 2011. M.S. Computational Physics.
- Dethloff, K. and Schwager, M. and Christensen, J. H. and Kilsholm, S. and Rinke, a. and Dorn, W. and Jung-Rothenhäusler, F. and Fischer, H. and Kipfstuhl, S. and Miller, H.: Recent Greenland Accumulation Estimated from Regional Climate Model Simulations and Ice Core Analysis, *Journal of Climate*, 15,19, doi:10.1175/1520-0442(2002)015<2821:RGAEFR>2.0.CO;2, 2002.
- 15 Echelmeyer, K.A., Harrison, W.D., Larsen, C. and Mitchell, J.E.: The role of the margins in the dynamics of an active ice stream. *J. Glaciol.*, 40, 136, 1994.
- 20 Eerola, Kalle: About the performance of the Hirlam version 7.0, newsletter at www.hirlam.org, 2006.
- Ettema, J., van den Broeke, M. R., van Meijgaard, E., van de Berg, W. J., Bamber, J. L., Box, J. E. and Bales, R. C.: Higher surface mass balance of the Greenland ice sheet revealed by high-resolution climate modeling, *Geophysical Research Letters*, 12, 36, 4–8, doi:10.1029/2009GL038110, 2009.
- Hutter, K.: Theoretical Glaciology: Material Science of Ice and the Mechanics of Glaciers and Ice Sheets, *Theoretical Glaciology: Material Science of Ice and the Mechanics of Glaciers and Ice Sheets*
- 30 IPCC, 2007: Climate Change 2007: The Physical Science Basis. Contribution of Working Group I to the Fourth Assessment Report of the Intergovernmental Panel on Climate Change, Solomon, S., D. Qin, M. Manning, Z. Chen, M. Marquis, K.B. Averyt, M. Tignor and H.L.

- Miller (eds.). *Cambridge University Press, Cambridge, United Kingdom and New York, NY, USA, 996 pp.*
- Joughin, I., Smith, B. E., Howat, I. M., Scambos, T., and Moon, T.: Greenland flow variability from ice-sheet-wide velocity mapping, *Journal Of Glaciology*, 56, 415-430, 2010.
- 5 Kiilsholm, Sissi and Hesselberg Christensen, Jens and Dethloff, Klaus and Rinke, Annette: Net accumulation of the Greenland ice sheet: High resolution modeling of climate changes, *Geophysical Research Letters*, 30, 9, doi:10.1029/2002GL015742, 2003.
- Lucas-Picher, Philippe and Wulff-Nielsen, Maria and Christensen, Jens H. and Adalgeirsdottir, Gudfinna and Mottram, Ruth and Simonsen, Sebastian B.: Very high resolution regional climate model simulations over Greenland: Identifying added value, *Journal of Geophysical Research*, 117, D02108, doi:10.1029/2011JD016267, 2012.
- 10 MacAyeal, D. R.: Large-Scale Ice Flow Over a Viscous Basal Sediment: Theory and Application to Ice Stream B, Antarctica, *Journal of Geophysical Research*, 94, B4, doi:10.1029/JB094iB04p04071, 1989.
- 15 MacAyeal, D. R.: Ice-shelf response to ice-stream discharge fluctuations: iii. the effects of ice-stream imbalance on the ross ice shelf, Antarctica, *Journal of Glaciology*, 35, 119, 38–42, 1989.
- D.R. MacAyeal, R. A. Bindschadler and T. A. Scambos (1995), Basal friction of ice stream E, West Antarctica. *Journal of Glaciology*, Vol. 41, 138, pp. 247–262.
- 20 Moon, T., Joughin, I., Smith, B., and Howat, I.: 21st-Century Evolution of Greenland Outlet Glacier Velocities, *Science*, 336, 576-578, DOI 10.1126/science.1219985, 2012.
- Morland, L.W., Smith, G.D. and Boulton, G.S.: BASAL SLIDING RELATIONS DEDUCED FROM ICE-SHEET DATA, *Journal of Glaciology*, 30, 105, 131–139, 1984.
- Mottram, R., Adalgeirsdottir, G., Bober, F., Lucas-Picher, P., Stendel, M., Christensen, O.B., Christense, J.H.: Reconstructing the surface mass balance of the Greenland Ice Sheet with the regional climate model HIRHAM5, 1989-2011, *The Cryosphere, in preparation*, in prep..
- 25 J. Mortensen, K. Lennert, J. Bendtsen and S. Rysgaard: Heat Sources for glacial meltwater in a Sub-Arctic Fjord (Godthåbsfjord) in Contact with the Greenland Ice Sheet, *J. Geophys. Res.*, 116, C01013, 2011.
- 30 J. Mortensen, J. Bendtsen, R.J. Motyka, K. Lennert, M. Truffer, M. Fahnenstock and S. Rysgaard: On the seasonal freshwater stratification in the proximity of fast-flowing tide-water glaciers in a sub-Arctic sill fjord, *Journal of Geophysical Research: Oceans*, Vol. 118, doi:10.1002/jgrc.20134, 2013.

15

- Pattyn, F., Schoof, C., Perichon, L., Hindmarsh, R. C. A., Bueler, E., de Fleurian, B., Durand, G., Gagliardini, O., Gladstone, R., Goldberg, D., Gudmundsson, G. H., Huybrechts, P., Lee, V., Nick, F. M., Payne, A. J., Pollard, D., Rybak, O., Saito, F., and Vieli, A.: Results of the Marine Ice Sheet Model Intercomparison Project, MISMP, *The Cryosphere*, 6, 573-588, doi:doi:10.5194/tc-6-573-2012, 2012.
- 5 PISM-authors: PISM, a Parallel Ice Sheet Model: User's Manual, 2010.
- Rae, J. G. L., Aalgeirsdóttir, G., Edwards, T. L., Fettweis, X., Gregory, J. M., Hewitt, H. T., Lowe, J. a., Lucas-Picher, P., Mottram, R. H., Payne, A. J., Ridley, J. K., Shannon, S. R., van de Berg, W. J., van de Wal, R. S. W. and van den Broeke, M. R.: Greenland ice sheet surface mass balance: evaluating simulations and making projections with regional climate models, *The Cryosphere Discussions*, 6, doi:10.5194/tcd-6-2059-2012, 2012.
- 10 Roeckner, E , Bäuml, G, Bonaventura, L, Brokopf, R, Esch, M, Giorgetta, M, Hagemann, S, Kirchner, I, Kornblueh, L, Manzini, E, Rhodin, A, Schlese, U, Schulzweida, U and Tompkins, A: The atmospheric general circulation model ECHAM5: Part 1: Model description, *Max-Planck-Institut fur Meteorologie, Hamburg, Germany*, 2003.
- 15 Shapiro, N.M. and Ritzwoller, M.H.: Inferring surface heat flux distributions guided by a global seismic model: particular application to Antarctica, *Earth and Planetary Science Letters*, 223, doi:10.1016/j.epsl.2004.04.011, 2004.
- Schoof, Christian: A variational approach to ice stream flow, *Journal of Fluid Mechanics*, 556, doi:10.1017/S0022112006009591, 2006.
- 20 Schoof, Christian: Variational methods for glacier flow over plastic till, *Journal of Fluid Mechanics*, 555, doi:10.1017/S0022112006009104, 2006.
- L. S. Sørensen, S. B. Simonsen, K. Nielsen, P. Lucas-Picher, G. Spada, G. Adalgeirsdottir, R. Forsberg, and C. S. Hvidberg: Mass balance of the Greenland ice sheet (2003–2008) from ICESat data – the impact of interpolation, sampling and firn density, *The Cryosphere*, vol. 5, pp. 173–186, doi:10.5194/tc-5-173-2011, 2004.
- 25 Stendel, M., J.H. Christensen and D. Petersen (2008): Arctic climate and climate change with a focus on Greenland, *Adv. in Ecol. Res* 40, 13-43, *Elsevier*, 10.1016/S0065-2504(07)00002-5, 2008.
- 30 Winkelmann, R., Martin, M. A., Haseloff, M. , Albrecht, T., Bueler, E., Khroulev, C. and Levermann, A.: The Potsdam Parallel Ice Sheet Model (PISM-PIK) Part 1: Model description, *The Cryosphere*, 5, 715–726, 2011.

16

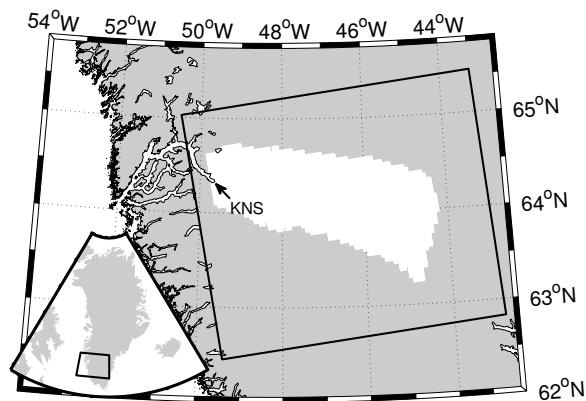


Fig. 1. Godthåbsfjord near Nuuk in West Greenland, with its main contributing tidewater glacier Kangiata Nunaata Sermia (KNS) at the end. The drainage basin is determined using surface gradients only, shown in white. The modeled region is a larger rectangle around this drainage basin, here in black.

17

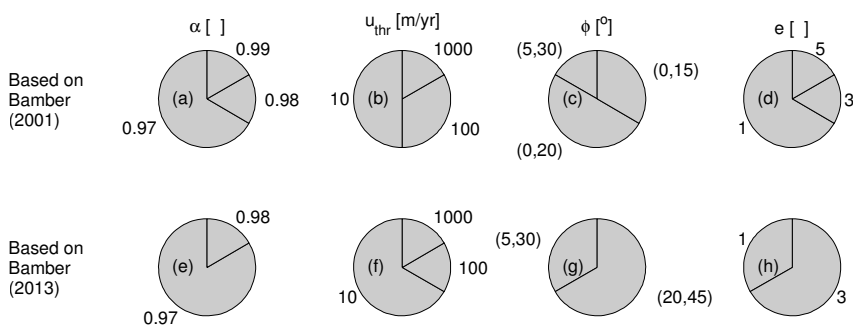


Fig. 2. Distribution of parameters of the selected settings whose model runs match the observations best, i.e., the pore water fraction α (a,e), the threshold velocity u_{thr} (b,f), the till friction angle ϕ (c,g) and the enhancement factor e (d,g).

18

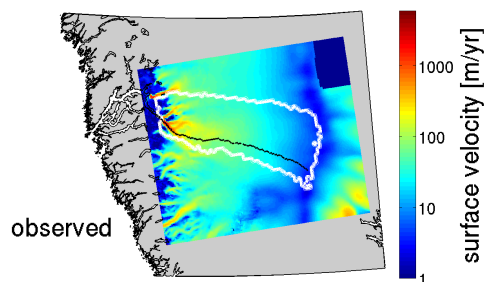


Fig. 3. Observed velocities from InSAR (Joughin et al., 2010; Moon et al., 2012). The black line indicates a center line from the ice divide towards the terminus following the southern fast flowing arm of KNS. See Figure 5 for observed and modeled surface velocities and ice thicknesses along this center line.

19

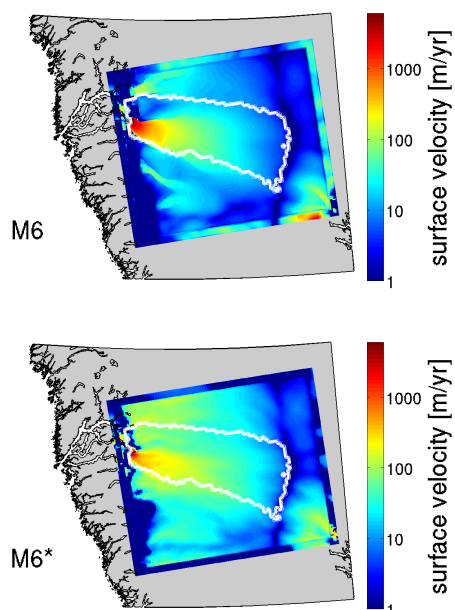


Fig. 4. Modeled surface velocities for selected model runs M6 (using Bamber et al. (2001)) and M6* (using Bamber et al. (2013)). See Figure 5 for surface velocities and ice thicknesses along the center line.

20

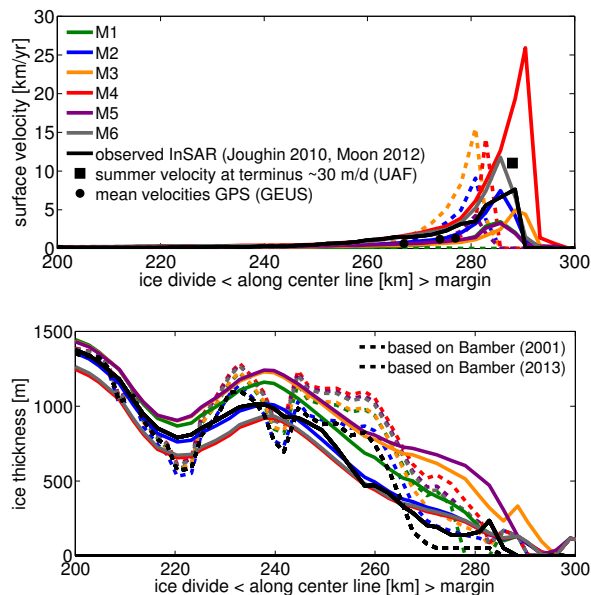


Fig. 5. Modeled surface velocities (top) and ice thickness (bottom) along a center line following the southern fast flowing arm of KNS, see Figure 3. Full lines are the model runs using the Bamber et al. (2001) ice thickness, and dashed lines use the newer ice thickness by Bamber et al. (2013). Observed surface velocities from InSAR (Joughin et al., 2010; Moon et al., 2012), velocities measured by GPSs (Ahlstrom et al., 2013) and summer terminus velocity (Podrasky (UAF), private communication).

For the Bamber et al. (2001) ice thickness, the modeled ice stream appears to be too thick when modeled surface velocities are too small, i.e., M1, M3 and M5. For the new Bamber et al. (2013) ice thickness, all modeled ice streams are thicker than observed close to the terminus.

21

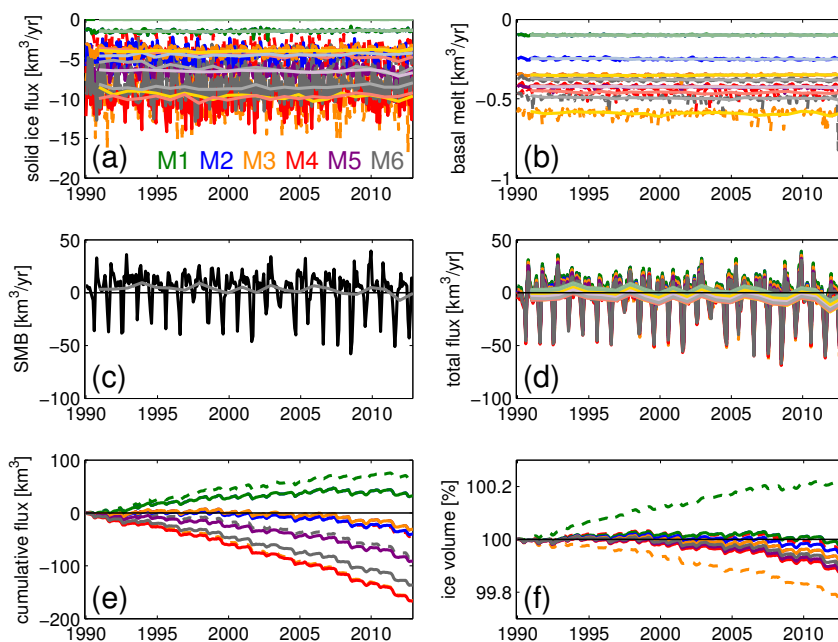


Fig. 6. Monthly variation of solid ice flux (a), basal melt (b), surface mass balance (c), total mass balance M_T (d), cumulative flux (e) and ice volume (f) for the selected parameter settings for the period covered by the HIRHAM5 model output, 1990–2011. Colors correspond to colors used in Figure 2. Full lines are the model runs using the Bamber et al. (2001) ice thickness, and dashed lines use the newer ice thickness by Bamber et al. (2013).

22

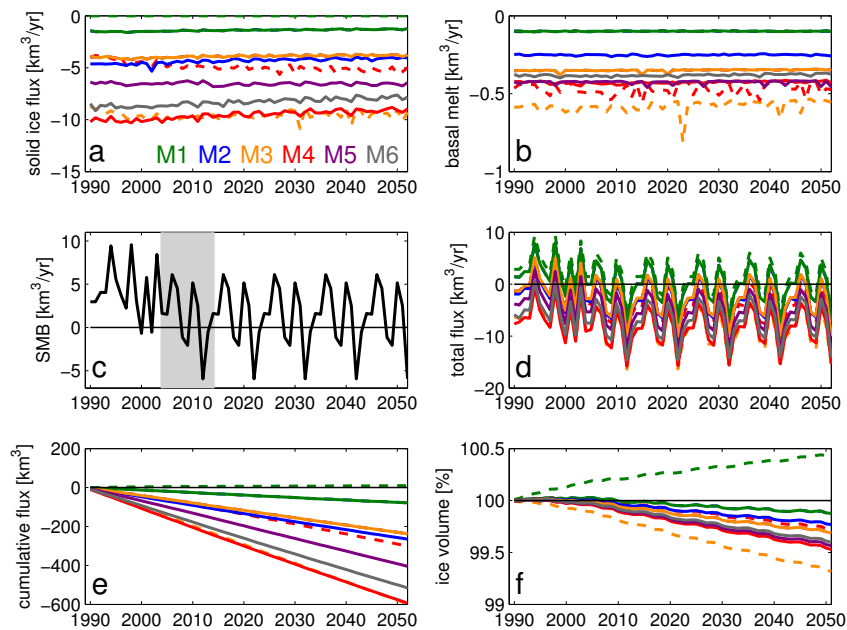


Fig. 7. Yearly means of solid ice flux (a), basal melt (b), surface mass balance (c), total mass balance M_T (d), cumulative flux (e) and ice volume (f) for the selected parameter settings for the extended period, 1990–2050. Full lines are the model runs using the Bamber et al. (2001) ice thickness, and dashed lines use the newer ice thickness by Bamber et al. (2013).

23

Table 1. Parameter space of the runs. Altered parameters are flow enhancement factor e (Equation 1), pore water pressure fraction α (Equation 5), till friction angle (ϕ_{min}, ϕ_{max}) (Equation 4) and threshold velocity u_{thr} (Equation 3). Two different climatic forcings (Section 2.2, H: HIRHAM5 R: RACMO2) and two initializations (Section 2.3, p: paleo climatic spin-up, c: constant spin-up) are tested. Bold numbers are the default value chosen by the PISM group for the regional mode based on Jakobshavn Isbræ.

e []	1	3	5
α []	0.97	0.98	0.99
u_{thr} [m/yr]	10	100	1000
(ϕ_{min}, ϕ_{max}) [degrees]	(0,15)	(0,20)	(5,30) (20,45)
forcing and init.	Hp	Hc	Rp

24

Table 2. Selected individual best run (M1 to M5) for each method and the combined best run M6. The parameter setting for those seven runs are shown here. Altered parameters are flow enhancement factor e , pore water pressure fraction α , till friction angle (ϕ_{min}, ϕ_{max}), threshold velocity u_{thr} , climatic forcing (H: HIRHAM5, R: RACMO2) and initialization (p: paleo climatic spin-up, c: constant spin-up). Bold numbers are the default value chosen by the PISM group for the regional mode based on Jakobshavn Isbræ.

Bamber et al. (2001)	M1	M2	M3	M4	M5	M6
e []	1	1	3	1	5	1
α []	0.97	0.97	0.98	0.97	0.97	0.99
u_{thr} [m/yr]	100	10	10	1000	10	100
(ϕ_{min}, ϕ_{max}) [degrees]	(5,30)	(0,15)	(20,45)	(5,30)	(5,30)	(20,45)
forcing and init.	Hc	Hp	Hp	Hp	Hc	Hp
Bamber et al. (2013)	M1*	M2*	M3*	M4*	M5*	M6*
e []	1	1	3	3	3	3
α []	0.97	0.97	0.97	0.97	0.98	0.97
u_{thr} [m/yr]	10	100	1000	10	10	10
(ϕ_{min}, ϕ_{max}) [degrees]	(20,45)	(5,30)	(20,45)	(20,45)	(20,45)	(5,30)
forcing and init.	Hp	Hp	Hp	Hp	Hp	Hp

25

Table 3. Total modeled mass balance M_T averaged over the periods 2003–2008 when using monthly HIRHAM5 forcing and 2010–2050 for using yearly mean forcing. For comparison the IceSAT mass loss for the period 2003–2008 from Sørensen et al. (2004). Positive values indicate mass gain, and negative values mean mass loss.

	M_T [km ³ /yr] 2003–2008	M_T [km ³ /yr] 2010–2050
M1	+0.39	−0.30
M2	−2.77	−3.31
M3	−2.35	−3.04
M4	−8.19	−8.60
M5	−5.03	−5.58
M6	−6.96	−7.35
M1*	+1.84	+1.05
M2*	−1.91	−2.64
M3*	−8.47	−9.01
M4*	−3.16	−4.43
M5*	−4.46	−5.55
M6*	−5.02	−6.05
mean	−3.84±3.18	−4.59±3.10
IceSAT	−2.49	

26

F | Manuscript submitted to Journal of Geophysical Research Earth Surface: Estimating the glacial meltwater contribution to the freshwater budget from salinity and $\delta^{18}\text{O}$ measurements in Godthåbsfjord

1 **Estimating the glacial meltwater contribution to the**
2 **freshwater budget from salinity and $\delta^{18}\text{O}$**
3 **measurements in Godthåbsfjord**

A. Fitzner,^{1,2} D. van As,³ J. Bendtsen,⁴ D. Dahl-Jensen,¹ X. Fettweis,⁵
S. Rysgaard,^{2,6,7}

D. van As, Geological Survey of Greenland and Denmark (GEUS), Øster Voldgade 10, 1350
Copenhagen, Denmark

J. Bendtsen, ClimateLab, Symbion Science Park, Fruebjergvej 3, 2100 Copenhagen, Denmark

D. Dahl-Jensen, Centre for Ice and Climate, Niels Bohr Institute, Copenhagen University,
Juliane Maries Vej 30, 2100 Copenhagen, Denmark

X. Fettweis, University of Liège, Department of Geography 2, Allée du 6 Août, Bat. B11, 4000
Liège, Belgium

A. Fitzner, Centre for Ice and Climate, Niels Bohr Institute, Copenhagen University, Juliane
Maries Vej 30, 2100 Copenhagen, Denmark and Greenland Climate Research Centre, Greenland
Institute of Natural Resources, Kivioq 2, 3900 Nuuk, Greenland (fitzner@nbi.dk)

S. Rysgaard, Greenland Climate Research Centre, Greenland Institute of Natural Resources,
Kivioq 2, 3900 Nuuk, Greenland; Arctic Research Centre, Aarhus University, 8000, Aarhus,
Denmark and Centre for Earth Observation Science, CHR Faculty of Environment Earth and
Resources, University of Manitoba, 499 Wallace Building, Winnipeg, MB R3T 2N2, Canada

¹Centre for Ice and Climate, Niels Bohr

4 **Abstract.** This study combines available data on freshwater fluxes from
5 land and glaciers and measurements of salinity and stable oxygen isotopes
6 in Godthåbsfjord, taken between 2007 and 2010, in order to determine the
7 relative contribution from the various freshwater sources into the fjord. There-
8 fore, the seasonal signal is analyzed.
9 A box model is used to compute the freshwater contributions from the glaciers
10 from oceanographic measurements. The model identifies critical parameters
11 for quantifying glacial meltwater and run-off to the fjord system. These crit-
12 ical parameters include the stable oxygen isotope composition of glacial ice,
13 run-off and seawater, and transport in the surface layer. With a better knowl-
14 edge of the discussed parameters, such as the velocity in the surface layer

Institute, Copenhagen University, Denmark.

²Greenland Climate Research Centre,
Greenland

³Geological Survey of Greenland and
Denmark, Denmark

⁴VitusLab, Denmark

⁵University of Liège, Belgium

⁶Arctic Research Centre, Denmark

⁷Centre for Earth Observation Science,
Canada

15 and the isotopic signature of glacial ice, the uncertainties in the estimates
16 of the various freshwater sources can be reduced significantly.

17 According to this study, there is (11.5 ± 2.3) km³/yr freshwater entering the
18 fjord, (7.8 ± 6.4) km³/yr of which from glacial meltwater (excluding surface
19 melt) and (3.8 ± 8.7) km³/yr of which from run-off of surface melt water.

20 Downscaling the modeled results allow the estimation of individual glacier
21 contributions. The largest tidewater glacier Kangiata Nunaata Sermia con-
22 tributes 4.8 km³/yr glacial meltwater and 1.4 km³/yr run-off, and, hence,
23 the total freshwater coming from this glacier is 6.2 km³/yr.

1. Introduction

24 The mass loss of the Greenland ice sheet increases due to changes in the surface mass
25 balance and accelerated ice discharge through numerous outlet glaciers at the margins.
26 Calving, surface melt and basal melt contribute to the total discharge into the ocean.
27 Observations and climate models can give estimates for calving and surface melt. Basal
28 melt, however, cannot be observed directly for tidewater glaciers. Even though mass loss
29 by basal melting is neglected on the global scale, it plays an important role in the regional
30 environment. Higher ocean temperatures increase frontal melt, and warmer air tempera-
31 tures increase the production of surface meltwater on the ice sheet, that runs off to the
32 base of the ice. The resulting lubrication accelerates outlet glaciers [*Motyka et al.*, 2003;
33 *Rignot et al.*, 2010; *Holland et al.*, 2008]. All freshwater sources including precipitation
34 regulate the freshwater budget of Godthåbsfjord, which influences the fjord ecosystem.
35 In the fjord, a seasonal variability is measurable in the salinity content. Based on salinity
36 measurements, the freshwater amount can be quantified, but it is not possible to distin-
37 guish between the different freshwater sources. Here salinity and stable oxygen isotope
38 measurements are combined to distinguish between different sources like glacial meltwater,
39 i.e. basal melt, frontal melt, calved ice bergs and melange melt, and run-off, i.e. precipi-
40 tation and surface melt.

41 This study focuses on Godthåbsfjord, a 190 km long and complex fjord system with several
42 tidewater and land-terminating glaciers. Figure 1 shows the fjord and the frontal location
43 of the tidewater glaciers Kangiata Nunaata Sermia (KNS), Akullerssuup Sermia (AS),
44 Narsap Sermia (NS), and the land-terminating glaciers Qamanaarssuup Sermia (QS) and

45 Kangilinnuata Sermia (KS).

46 Extensive oceanographic measurements [*Mortensen et al.*, 2011, 2013], studies covering
47 the behavior of the glaciers [*Ahlstøm et al.*, 2013], and automatic weather station records
48 [*van As et al.*, 2011, 2014], are available for this region.

2. Data Description

49 The studied area with its measurement locations is shown in Figure 1.

50 Water temperature and salinity were measured using a Sea-Bird Electronics SBE 19plus
51 SEACAT Profiler CTD (conductivity, temperature and depth). The SBE 19plus was cali-
52 brated by the manufacturer every 1–2 yr, and uncertainties of the salinity after calibration
53 were typically within the range 0.005–0.010 psu. Temperature uncertainties were near to
54 the initial accuracy of the instrument of 0.005 °C.

55 For oxygen isotope analysis, water samples of 2 mL were collected from each station in
56 gas-tight vials and analyzed on a Picarro Isotopic Water Analyzer, L2120-I (Picarro, Sun-
57 nyvale, CA, USA). Water samples were introduced into the vaporization chamber using
58 an attached PAL autosampler (Leap Technologies, Carrboro, NC, USA). Each sample was
59 analyzed three times (three consecutive replicate injections; $\sigma < 0.005\text{--}0.007\text{ ‰}$) along-
60 side a set of three laboratory reference materials, which had previously been calibrated to
61 the VSMOW (Vienna Standard Mean Ocean Water) scale [*Coplen*, 1994].

62 The ratio of the stable oxygen isotopes in the water ^{16}O and ^{18}O , $\delta^{18}\text{O}$, is calculated.

63

64 In this study, only measurements in the surface layer with a total depth of less than
65 10 m and in the inner part of the fjord are used. Between 2007 and 2010, there were 72
66 samples.

67 The seasonal variation of the surface measurements of salinity and $\delta^{18}\text{O}$ in the outer
68 fjord is shown in Figure 2, with an extreme in August. For the analysis of the glacial
69 meltwater contribution, only the inner fjord measurements are considered. This means
70 that all measurements between the first measuring point and the Lake Tasersuaq inlet
71 (LT in Figure 1) – about 40 km – are taken into account, which cover April, May, August
72 and September only.

73 The mean velocity of the surface layer, measured by drifters during summer, is less than
74 10 cm/s [*Mortensen et al.*, submitted].

75 The thickness of the surface layer, also shown in *Mortensen et al.* [2011, 2013], is 6 to
76 10 m during the summer and about 10 m during winter, and the considered section has
77 typical average velocities of about 4 cm/s in the winter and 8 cm/s during the summer
78 [*Mortensen et al.*, submitted]. The sensitivity to the estimated velocity and surface layer
79 thickness is are discussed later.

80 The monthly means are used in this analysis and are shown in Table 1.

81 RegridDED regional climate model output from MAR (Modele Atmosphérique Regional,
82 *Fettweis et al.* [2011]; *van As et al.* [2014]) for the seasonal variation of the run-off in the
83 same period (2007–2010) is used for comparison of the here calculated run-off contribution.

3. Box Model

84 A box model is applied to calculate all the incoming and outgoing fluxes from the
85 different sources. One box is representing the surface layer, which is taken to be mixed
86 homogeneously [*Mortensen et al.*, 2011, 2013]. In-flowing fluxes are glacial meltwater $q_{ice,in}$
87 (calving, frontal melt, basal melt and melange melt), run-off $q_{run-off,in}$ (surface melt and
88 precipitation on land and ice), and incoming seawater $q_{sea,in}$ (see Figure 3). Freshwater

89 entering the fjord is composed of meltwater and precipitation.

90 Here, some simplifying assumptions are made. It is assumed that all freshwater, coming
 91 from run-off and glacial meltwater, is transported to the surface layer because freshwater
 92 is buoyant. Also, all meltwater of calved ice bergs enters the surface layer. A negligible
 93 amount of ice bergs is leaving the inner fjord region or is melted in the deeper layers.
 94 During the winter months sea ice and a melange are covering the inner fjord region, which
 95 consists of former calved ice bergs and frozen seawater. Some of the melange survives
 96 until summer. The outgoing seawater is replaced by incoming seawater from the deeper
 97 layers [Mortensen *et al.*, 2011, 2013].

98 The following equations for the salinity S and $\delta^{18}O$ changes:

$$V \cdot \frac{dS}{dt} = q_{sea,in}S_{sea} + q_{fresh,in}S_{fresh} - q_{out}S - \frac{dV}{dt}S \quad \text{and} \quad (1)$$

$$V \cdot \frac{d\delta^{18}O}{dt} = q_{sea,in}\delta^{18}O_{sea} + q_{ice,in}\delta^{18}O_{ice} + q_{run-off,in}\delta^{18}O_{run-off} - q_{out}\delta^{18}O - \frac{dV}{dt}\delta^{18}O, \quad (2)$$

99 where V denotes the volume. The subscripts indicate the origin of the water masses.

100 The volume V is estimated from the width W and length L of the fjord section (red in
 101 Figure 1) and the thickness of the considered surface layer D using $V = WLD$.

102 From mass conservation, the total incoming flux is

$$q_{in} = q_{fresh,in} + q_{sea,in} = q_{ice,in} + q_{run-off,in} + q_{sea,in}. \quad (3)$$

103 The change in the surface layer thickness is due to changes in the incoming flux and,

104 hence, it is

$$q_{out} = q_{in} - \frac{dV}{dt} = q_{fresh,in} + q_{sea,in} - \frac{dV}{dt}. \quad (4)$$

105 The total outgoing flux is estimated using the geometry of the fjord and an estimate for
 106 the surface layer velocity v , namely

$$q_{out} = W \cdot D \cdot v. \quad (5)$$

107 Combining Equations (4) and (5) gives

$$q_{sea,in} = W \cdot D \cdot v - q_{fresh,in} + \frac{dV}{dt}. \quad (6)$$

108 The incoming freshwater flux is then calculated by combining Equations (1), (5) and (6),
 109 which gives

$$q_{fresh,in} = \left[V \frac{dS}{dt} + \left(W D v + \frac{dV}{dt} \right) \cdot (S - S_{sea}) \right] \cdot (S_{fresh} - S_{sea})^{-1}. \quad (7)$$

110 From Equations (2), (5) and (6), $q_{ice,in}$ is calculated as a function of $q_{fresh,in}$

$$q_{ice,in} = \left[V \frac{d\delta^{18}O}{dt} + \left(W D v + \frac{dV}{dt} \right) \cdot (\delta^{18}O - \delta^{18}O_{sea}) + q_{fresh,in} (\delta^{18}O_{sea} - \delta^{18}O_{run-off}) \right] \cdot (\delta^{18}O_{ice} - \delta^{18}O_{run-off})^{-1}. \quad (8)$$

111 Equations (7) and (8) are then solved numerically for incoming freshwater and glacial
 112 meltwater fluxes.

113

3.1. Downscaling

114 The width, terminus height and InSAR velocity [Joughin, 2010] for each of the glaciers
 115 are used to downscale the total glacial meltwater contribution to a glacier specific estimate.
 116 The MAR run-off distribution is used to split up the run-off calculated here.

4. Salinity and $\delta^{18}O$ Estimates

117 Assumptions have to be made for the salinity and $\delta^{18}O$ of the different contributors (see
 118 Table 1). The measured $\delta^{18}O$ in the surface layer is, like salinity, taken to be constant with
 D R A F T August 27, 2014, 3:53pm D R A F T

119 respect to depth in the surface layer and month of the year [*Mortensen et al.*, 2011, 2013].
120 The bottom water salinity and $\delta^{18}\text{O}$ are taken from depth measurements from a station
121 at the fjord entrance and vary with the month of the year. The depth profiles for that
122 station are shown in Figure 4. The salinity of precipitation and glacial meltwater is zero.
123 The seasonal isotopic signature of the run-off contribution $\delta^{18}\text{O}_{run-off}$ is based on pre-
124 cipitation output from the isotopic regional climate model REMO-iso. The model per-
125 formance for Greenland is tested using the Global Network In Precipitation (GNIP) and
126 ice cores by comparing the modeled and observed isotope values [*Sjolte et al.*, 2011].
127 REMO-iso captures a significant part of the $\delta^{18}\text{O}$ variability at the coast, i.e. tested for
128 Danmarkshavn.

129 $\delta^{18}\text{O}$ for glacial meltwater is generally unknown, and it is estimated as follows. There
130 have been $\delta^{18}\text{O}$ measurements of ice bergs conducted in Godthåbsfjord to constrain the
131 isotope value of glacial ice. In total there are 200 measurements that range from -30.04 ‰
132 to -17.91 ‰ with a median of $\delta^{18}\text{O} = -28.08\text{ ‰}$ (*Rysgaard, private communication*).
133 *Dansgaard* [1964] measured ice bergs in West Greenland, and $\delta^{18}\text{O}$ values as low as -
134 30 ‰ and smaller where found. Also, *Bhatia et al.* [2011] show that water that has been
135 stored under a glacier has $\delta^{18}\text{O}$ values around -30 ‰ . Ice core records from Dye-3, which
136 is located in South Greenland, show that $\delta^{18}\text{O}$ for glacial ice can be smaller than -30 ‰
137 [*Johnsen et al.*, 2001]. Marginal surface ice studies close to KNS in *Reeh et al.* [2002]
138 suggest $\delta^{18}\text{O}$ values between -28 ‰ and -34 ‰ . In this analysis, $\delta^{18}\text{O}_{ice} = -28\text{ ‰}$ is
139 used, based on the local ice berg measurements.

140 Also the sensitivity to the choice of $\delta^{18}\text{O}_{sea}$ and $\delta^{18}\text{O}_{run-off}$, are discussed later.

5. Results

141 Using the salinity records only, the incoming freshwater flux is calculated using Equa-
142 tion (7). The total amount of incoming freshwater is $q_{fresh}=(11.5 \pm 2.3)$ km³/yr and the
143 monthly variation is shown in Figure 5. During the winter, there is a minor freshwater
144 inflow (less than 0.2 km³/mo) and during the summer, all incoming water in the surface
145 layer is freshwater. Note, that there is no data during winter time. The implications are
146 discussed below.

147 The glacial meltwater flux is calculated using Equation (8). This is the sum of basal melt,
148 frontal melt, calving and sub-melange melt. Surface melt is included in the run-off. The
149 chosen isotope value for the glacial ice, as discussed in Section 4, is $\delta^{18}\text{O}_{ice} = -28$ ‰.
150 Figure 6 shows the monthly variation of glacial meltwater and run-off. In this case, there
151 is $q_{ice}=(7.8 \pm 6.4)$ km³/yr glacial meltwater, and $q_{run-off}=(3.8 \pm 8.7)$ km³/yr run-off
152 (precipitation and surface melt), which is smaller than the run-off computed by MAR
153 ($q_{run-off,MAR}=(13.1 \pm 5.5)$ km³/yr). This is due to the assumption that the run-off has
154 the same isotopic composition as the precipitation given by REMO-iso. However, surface
155 melt also occurs in the ablation zone that might have a smaller isotopic signature than
156 the precipitation. In reality, some of the surface meltwater (that is included in the MAR
157 run-off) percolate through the ice sheet via moulin and is therefore included in the esti-
158 mate for glacial melt and not in the run-off. According to the MAR based surface run-off
159 estimates, around 70% of the meltwater produced in the ablation zone seems to reach the
160 bedrock before reaching the ocean.

161 There is a small negative flux in the autumn, that lies within the uncertainties where
162 measurements are sparse.

163
164 Speculatively, one could assume that there is negligible calving in the winter time (Oc-
165 tober to April) and sub-melange melt is considered to be a minor contributor. In the
166 case that both can be neglected during winter, it is possible to isolate the basal meltwater
167 component from winter conditions. Here basal meltwater is melt that occurs under the
168 glaciers and enters the fjord at the grounding line and melt of the glacier faces. The basal
169 meltwater contribution is $0.25 \text{ km}^3/\text{mo}$ in the winter from all glaciers. Basal melt and
170 glacier speed are connected: more friction due to high velocities increase basal melt, and
171 basal meltwater engages lubrication and hence higher velocities. Summer surface veloci-
172 ties at KNS increase by 30 % with respect to the winter velocity [*Ahlstøm et al., 2013*],
173 so the basal melt water flux is scaled equally. The summer basal meltwater flux is then
174 $0.32 \text{ km}^3/\text{mo}$, and the total basal meltwater contribution for all glaciers, including frontal
175 melt, is $3.3 \text{ km}^3/\text{yr}$.

176 This value has to be interpreted as an upper limit, since there is calving detected also in
177 the winter month and hence ice bergs and melange are melting all year.

5.1. Downscaling

178 Table 2 shows the modeled downscaled yearly contributions for all the tidewater and
179 land-terminating glaciers in the inner part of Godthåbsfjord. For the largest glacier KNS,
180 there is $4.8 \text{ km}^3/\text{yr}$ glacial meltwater and $1.4 \text{ km}^3/\text{yr}$ run-off, and hence the modeled
181 total freshwater coming from KNS only is $6.2 \text{ km}^3/\text{yr}$. The basal meltwater, including

182 frontal melt, coming from KNS is $2.1 \text{ km}^3/\text{yr}$ assuming no calving and melange melt in
183 the winter.

6. Discussion

184 In this study, it is assumed that all freshwater rises to the surface layer due to its buoy-
185 ancy. However, the melted glacial water is mixing during its rise, and some freshwater is
186 staying in the deeper layers as shown in [Mortensen *et al.*, 2013]. From the measurements
187 used in Mortensen *et al.* [2013], the freshwater content during summer in the surface layer
188 is 58% in 2009 and 51% in 2010. This is ignored in this simplified analysis, and hence the
189 total freshwater is underestimated.

190 Calculating the analytic uncertainties is done in a very rigorous way. The large uncer-
191 tainties arise from the sparse available measurements in the inner part of the fjord. With
192 more measurements in the inner part of the fjord of the surface layer velocity, the isotopic
193 signature of the run-off and glacial meltwater, the uncertainties can be reduced. However,
194 accessing the inner part of the fjord during the winter time is difficult due to the melange.
195 Also, the estimation of $\delta^{18}\text{O}_{ice}$ is challenging.

196
197 The sensitivity to several parameters is studied in this section (see also Figure 7 and
198 Table 3).

6.1. Sensitivity

199 The sensitivity to the velocity in the surface layer is shown in Figure 7a. The Green-
200 landic outlet glaciers are accelerating and the Greenland ice sheet is melting at increased
201 rates. Higher velocities will increase the freshwater influx and therefore the glacial melt-

202 water contribution [*Rignot et al.*, 2010]. Assuming a change in the summer surface layer
203 velocity of 30%, meaning ± 2.5 cm/s, the resulting change in the glacial water flux is
204 ± 2.3 km³/yr.

205 The choice of the isotopic value for glacial ice is of significance to make a distinction be-
206 tween run-off and glacial melt. Figure 7d shows yearly contributions for varying $\delta^{18}\text{O}_{ice}$.
207 With decreasing $\delta^{18}\text{O}$ -signature for ice, the glacial meltwater contribution decreases and
208 the run-off increases. At higher $\delta^{18}\text{O}_{ice}$ -values, the isotopic signature of run-off and glacial
209 ice is similar and the model does not give physical results. Assuming that the value is
210 overestimated and the ice has an isotopic signature of -30 ‰, as discussed in Section 4,
211 the glacial meltwater is be decreased by -1.4 km³/yr.

212 Shifting the seasonal variation of $\delta^{18}\text{O}_{sea}$ (see Figure 7b) results in small change in the
213 glacial meltwater influx. A possible shift of ± 0.1 ‰ will result in glacial meltwater flux
214 change of ± 0.9 km³/yr.

215 Altering the isotopic signature of the modeled run-off (see Figure 7c) by ± 1 ‰ (about
216 5%) results in small change of ± 0.3 km³/yr.

217

218 Summarizing, within the plotted domains the glacial meltwater flux is less sensitive to
219 the isotopic value of the run-off and the winter surface layer thickness. The result depends
220 strongly on the modeled isotopic signature of seawater and also the estimated summer
221 velocity of the surface layer. The result also shows a sensitivity to the isotopic value of
222 the glacial meltwater $\delta^{18}\text{O}_{ice}$.

7. Conclusion

223 Water samples have been taken in Godthåbsfjord between 2007 and 2010 and were an-
224 alyzed for salinity and for the first time for stable oxygen isotopes. Both quantities show
225 a seasonal variation with extrema in August. The delay between the inner and outer part
226 of the fjord is one month.

227 Using $\delta^{18}O$ in addition to salinity makes it possible to distinguish between several freshwa-
228 ter sources. There is (11.5 ± 2.3) km³/yr freshwater entering the fjord, (7.8 ± 6.4) km³/yr
229 of which is from glacial meltwater (basal melt, frontal melt, calving and melange melt)
230 and (3.8 ± 8.7) from run-off (precipitation and surface melt). KNS contributes 1.4 km³/yr
231 run-off and 4.8 km³/yr glacial melt. Earlier estimates for the KNS discharge flux of solid
232 ice are be (5 ± 1) km³/yr (*Podrasky, private communication*, from winter velocities), and
233 (7.6 ± 1.5) km³/yr [*Mortensen et al., 2013*, without subglacial discharge]. As shown ear-
234 lier, more than half of the freshwater is actually present in the surface layer.

235 The sparse measurements in the inner part of the fjord, especially in June and July, are
236 limiting the precision of the results as seen in the uncertainties.

237 The sensitivity study performed shows that the glacial meltwater flux depends strongly
238 on the estimated summer velocity of the surface layer. The result also shows a sensitivity
239 to the isotopic value of the glacial meltwater $\delta^{18}O_{ice}$. With a better knowledge of the
240 discussed parameters, such as the velocity in the surface layer and the isotopic signature
241 of glacial ice, the uncertainties in the estimates of the various freshwater sources can be
242 reduced significantly.

243 With this method, it is possible to calculate the freshwater contributions from the glaciers
244 from oceanographic measurements in the surface layer of the fjord. With year around mea-

245 surements, it would be possible to study the seasonal response of the fjord to the glacial
246 meltwater influx in more detail.

247 **Acknowledgments.** This study is part of the Greenland Climate Research Centre
248 activities. SR was funded by the Canada Excellence Research Program (CERC). We
249 would like to thank Jesper Sjolte for providing us with his isotope modeling results.

References

- 250 A.P. Ahlstrøm, S.B. Andersen, M.L. Andersen, H. Machguth, F.M. Nick, I. Joughin, C.H.
251 Reijmer, R.S.W. van de Wal, J.P. Merryman Boncori, J.E. Box, M. Citterio, D. van As,
252 R.S. Fausto, A. Hubbard (2013), Seasonal velocities of eight major marine-terminating
253 outlet glaciers of the Greenland ice sheet from continuous in situ GPS instruments,
254 *Earth System Science Data*, 5, 2, 277–287, doi: 10.5194/essd-5-277-2013 .
- 255 D. van As, M.L. Andersen, D. Petersen, X. Fettweis, J.H. van Angelen, J.T.M. Lenaerts,
256 M.R. van den Broeke, J.M. Lea, C.E. Bøggild, A.P. Ahlstrøm and K. Steffen (2014),
257 Increasing meltwater discharge from the Nuuk region of the Greenland ice sheet and im-
258 plications for mass balance (1960–2012). *J. Glac.*, 60, 220, doi: 10.3189/2014JoG13J065.
- 259 D. van As, R.S. Fausto, A.P. Ahlstrom, S.B. Andersen, M.L. Andersen, M. Citterio, K.
260 Edelvang, P. Gravesen, H. Machguth, F.M. Nick, S. Nielsen and A. Weidick (2011),
261 Programme for Monitoring of the Greenland Ice Sheet (PROMICE): first temperature
262 and ablation records, *Geol. Surv. Den. Greenl.* 23, 7376.
- 263 M.P. Bhatia, S.B. Das, E.B. Kujawinski, P. Henderson, A. Burke, M.A. Charette (2011),
264 Seasonal Evolution of Water Contributions to Discharge from a Greenland Outlet
265 Glacier: Insight from a new Isotope-Mixing Model, *J. Glac.* Vol. 57, No. 205.

- 266 J.O. Blanton and P. Atkinson(1983). Transport and Fate of River Discharge on the
267 Continental Shelf of the Southeastern United States, *J. Geophys. Res.*, 88,C8.
- 268 T.B. Coplen (1994), Reporting of stable hydrogen, carbon, and oxygen isotopic abun-
269 dances, *Pure Appl. Chem.*, 88, 273–276.
- 270 W. Dansgaard (1964), Stable Isotopes in Precipitation, *Tellus XVI*, 4.
- 271 X. Fettweis, M. Tedesco, M. van den Broeke, J. Ettema (2011), Melting trends over the
272 Greenland ice sheet (1958–2009) from spaceborne microwave data and regional climate
273 models, *The Cryosphere*, 5, 359-375, doi:10.5194/tc-5-359-2011.
- 274 D.M. Holland, D. M., R. H. Thomas, B. De Young, M. H. Ribergaard, and B. Lyberth
275 (2008), Acceleration of Jakobshavn Isbr triggered by warm subsurface ocean waters,*Nat.*
276 *Geosci.*, 1, 659664.
- 277 IAEA/WMO (2006), Global Network of Isotopes in Precipitation, The GNIP Database,
278 Accessible at <http://www.iaea.org/water> .
- 279 I. Joughin, I. Howat and T. Scambos: MEaSURES Greenland Ice Velocity Map from
280 InSAR Data, *Boulder, Colorado, USA: National Snow and Ice Data Center, Digital*
281 *media*, 2010.
- 282 S.J. Johnsen, D. Dahl-Jensen, N. Gundestrup, J.P. Steffensen, H.B. Clausen, H. Miller,
283 V. Masson-Delmotte, A.E. Sveinbjörnsdottir and J. White (2001), Oxygen isotope and
284 palaeotemperature records from six Greenland ice-core stations: Camp Century, Dye-
285 3, GRIP, GISP2, Renland and NorthGRIP, *J. Quaternary Sci.*, Vol. 16, pp. 299–307.
286 ISSN 0267-8179.
- 287 J. Mortensen, K. Lennert, J. Bendtsen and S. Rysgaard (2011), Heat Sources for glacial
288 meltwater in a Sub-Arctic Fjord (Godthåbsfjord) in Contact with the Greenland Ice

- 289 Sheet, *J. Geophys. Res.*, *116*, C01013.
- 290 J. Mortensen, J. Bendtsen, R.J. Motyka, K. Lennert, M. Truffer, M. Fahnenstock and
291 S. Rysgaard (2013), On the seasonal freshwater stratification in the proximity of fast-
292 flowing tidewater glaciers in a sub-Arctic sill fjord, *Journal of Geophysical Research:*
293 *Oceans*, *Vol. 118*, doi:10.1002/jgrc.20134.
- 294 J. Mortensen, J. Bendtsen, K. Lennert and S. Rysgaard (submitted), Seasonal variability
295 of the circulation system in a West Greenland tidewater outlet glacier fjord. *Journal of*
296 *Geophysical Research – Earth Surface*.
- 297 R.J. Motyka, L. Hunter, K. A. Echelmeyer, and G. Connor (2003), Sub-marine melting
298 at the terminus of a temperate tidewater glacier, LeConte Glacier, Alaska, U.S.A., *Ann.*
299 *Glaciol.*, *36*, 57-65.
- 300 J.F. Pinder and J.F. Jones (1969), Determination of the Ground-Water Component of
301 Peak Discharge from the Chemistry of Total Runoff, *Water Resour. Res.* *5*(2), 438-445.
- 302 N. Reeh, H. Oerter and H. Thomsen (2002). Comparison between Greenland ice-margin
303 and ice-core oxygen-18 records, *Annals of Glaciology* *35*.
- 304 E. Rignot, M. Koppes, and I. Velicogna (2010), Rapid submarine melting of the calving
305 faces of west Greenland glaciers, *Nat. Geosci.*, *3*, 187191, doi:10.1038/NGEO765.
- 306 J. Sjolte, G. Hoffmann, S. J. Johnsen, B. M. Vinther, V. MassonDelmotte, and C. Sturm
307 (2011). Modeling the water isotopes in Greenland precipitation 19592001 with the
308 mesoscale model REMOiso, *J. Geophys. Res.* *116*, D18105 doi:10.1029/2010JD015287.

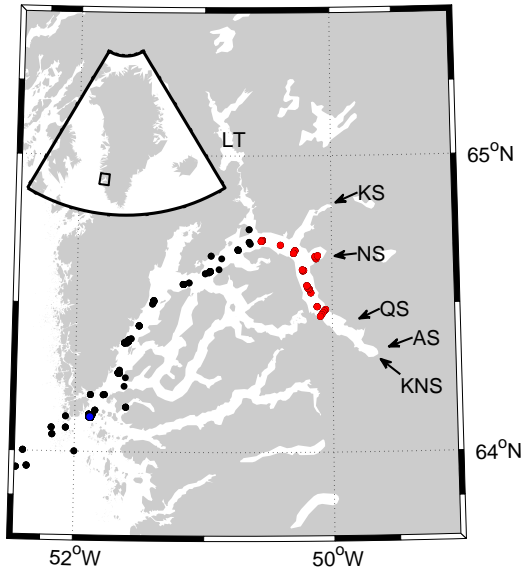


Figure 1. Godthåbsfjord and the location of the tidewater glaciers Kangiata Nunaata Sermia (KNS), Akullerssuup Sermia (AS), Narsap Sermia (NS) and the land-terminating glaciers Qamanaarssuup Sermia (QS) and Kangilinnuata Sermia (KS), and Lake Tasersuaq (LT).

In total, there are 510 surface measurements in Godthåbsfjord (black and red), and 72 of them in the inner part (red). The blue station is used to determine the base values for salinity and $\delta^{18}\text{O}$.

Notation

S	salinity, psu
$\delta^{18}\text{O}$	stable oxygen isotopes, ‰
v	velocity of the surface layer, cm/s
q	volume flux, km^3/yr
D	surface layer thickness, m
W	fjord section width, m
L	fjord section length, m
V	surface layer volume, m^3

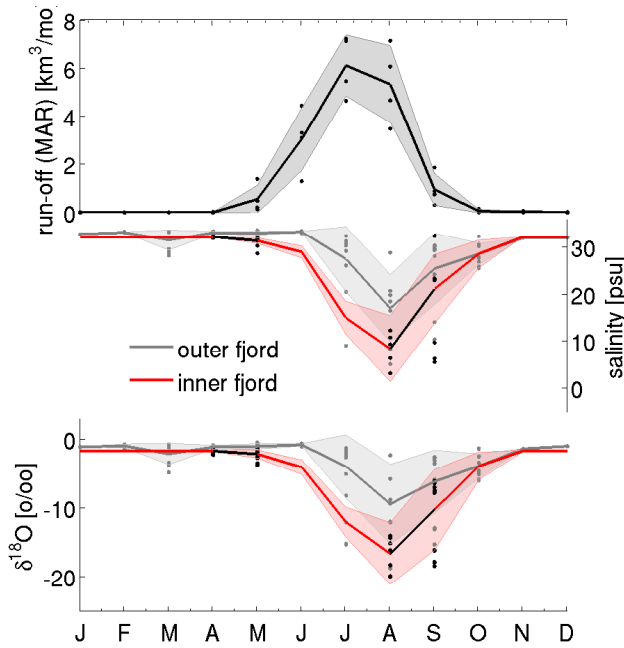


Figure 2. Seasonal variation of modeled MAR run-off and measured salinity and $\delta^{18}\text{O}$. The MAR run-off is shown for the 2007–2010 period (dots), and a monthly mean and standard deviation is calculated (line with shading). Salinity and $\delta^{18}\text{O}$ measurements, taken between 2007 and 2010, are shown for the whole fjord region in gray, which peak in August. The inner fjord region measurements are shown in black and cover April, May, August and September only. Missing data in the remaining month are estimated from the outer fjord variability (red).

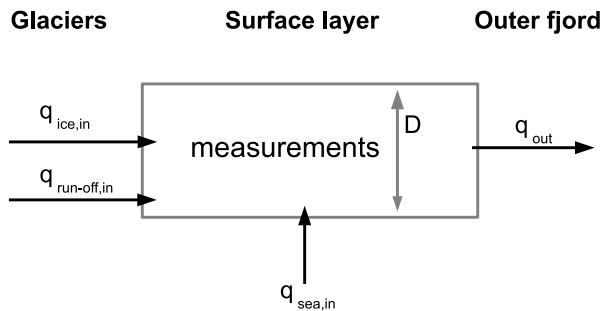


Figure 3. A box model with the surface layer as one box, three incoming fluxes (glacial meltwater q_{ice} (basal melt, front melt, calving and melange melt), run-off $q_{run-off}$ (run-off and surface melt) and seawater q_{sea}) and the outgoing flux q_{out} . Salinity and $\delta^{18}\text{O}$ are the measured quantities in the inner fjord region.

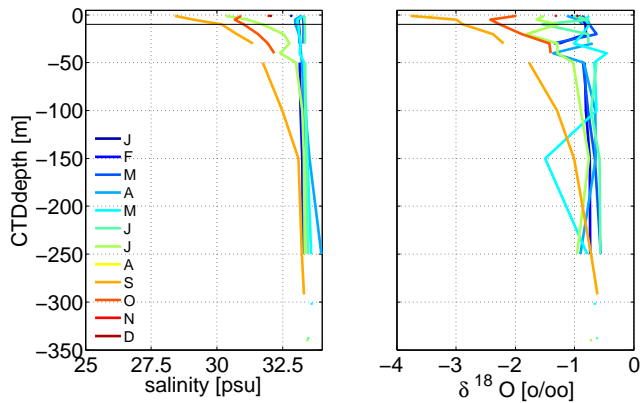


Figure 4. The monthly depth profiles of salinity and $\delta^{18}\text{O}$ for a station at the fjord entrance (blue in Figure 1). The monthly mean values at 10 m depth (black line) are used as base values for the analysis.

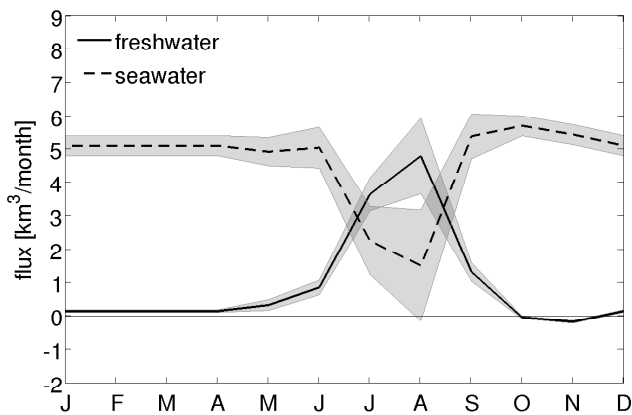


Figure 5. The modeled monthly amount of incoming freshwater q_{fresh} (solid line) and seawater q_{sea} (dashed line) calculated from the salinity records in the inner fjord. The shaded area indicates the uncertainty (SD) on the quantities.

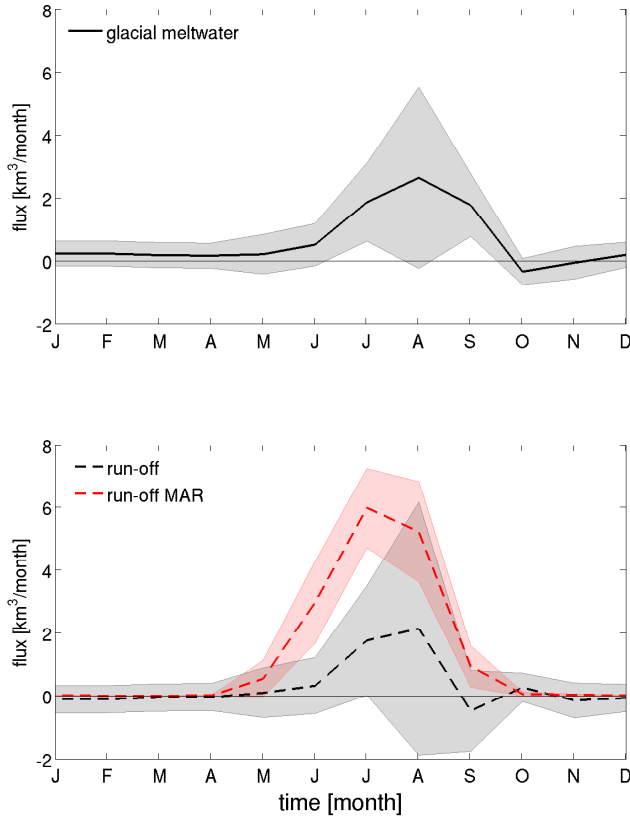


Figure 6. The modeled monthly variation of glacial meltwater (being basal melt, front melt, calving and melange melt; black solid line) in the top and run-off (being precipitation and surface melt; black dashed) in the bottom for $\delta^{18}\text{O}_{ice} = -28 \text{ ‰}$.

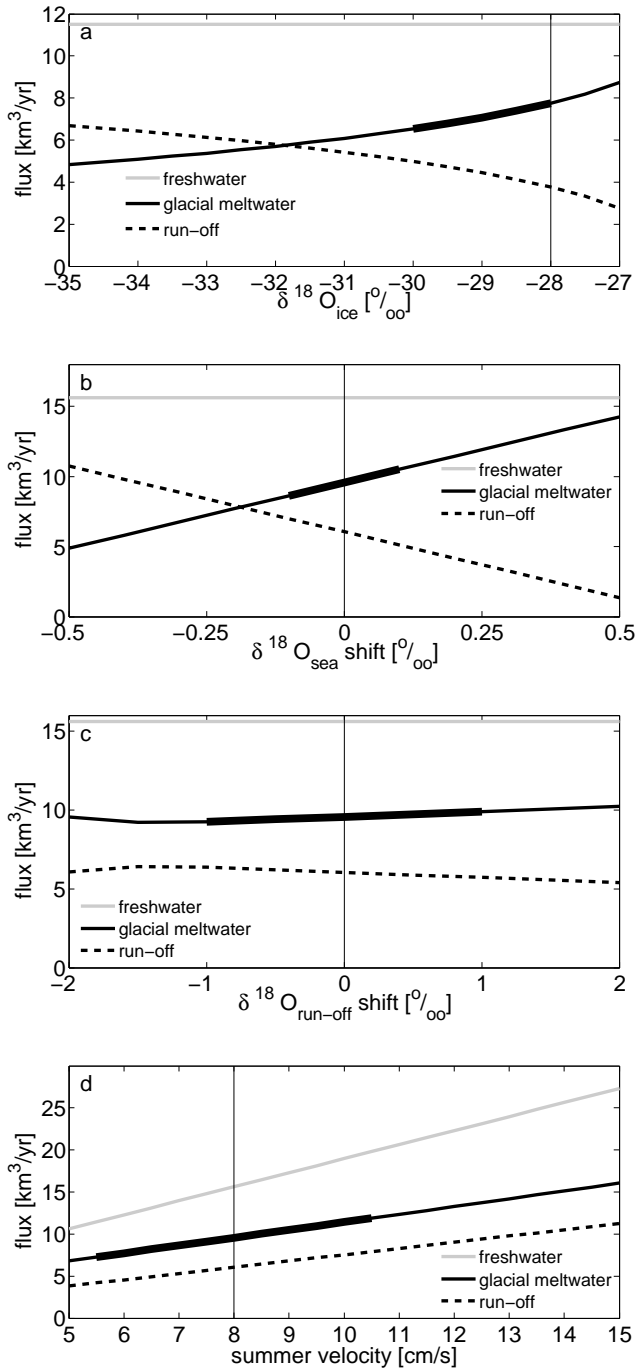


Figure 7. Sensitivity to the choice of the isotopic value for glacial ice (a), a shift in $\delta^{18}\text{O}_{\text{sea}}$ (b), a shift in the isotopic signature of the modeled run-off (c) and the summer velocity in the surface layer (d). The freshwater influx is shown in grey, the thin vertical line shows the value used in the analysis, and thick black line indicates sensitivity test range, cf. Table 3.

Table 1. The monthly variation of all input parameters also indicating the origin of values: estimated, measured or modeled.

Values in brackets show estimated values each month, where no data is available, as shown in Figure 2.

			Jan	Feb	Mar	Apr	May	Jun	Jul	Aug	Sep	Oct	Nov	Dec
velocity v	[cm/s]	est.	4	4	4	4	4	6	8	8	6	4	4	4
thickness D	[m]	est.	10	10	10	10	10	8	6	6	8	10	10	10
S_{outer}	[psu]	meas.	32.83	33.18	31.54	33.12	33.06	33.30	27.49	17.04	25.43	28.60	31.98	32.05
S_{inner}	[psu]	meas.	(32.23)	(32.23)	(32.23)	32.23	31.40	(29)	(15)	8.44	21.140	(28.60)	(32.23)	(32.23)
S_{sea}	[psu]	meas.	33.20	33.20	33.20	33.20	33.20	33.20	31.75	30.00	30.10	31.00	32.50	33.20
$\delta^{18}\text{O}_{outer}$	[‰]	meas.	-1.05	-0.91	-2.06	-1.08	-0.98	-0.75	-3.91	-9.36	-6.11	-3.84	-1.32	-0.95
$\delta^{18}\text{O}_{inner}$	[‰]	meas.	(-1.64)	(-1.64)	(-1.64)	-1.64	-2.09	(-4)	(-12)	-16.56	-10.20	(-3.84)	(-1.64)	(-1.64)
$\delta^{18}\text{O}_{sea}$	[‰]	meas.	-0.80	-0.80	-0.80	-0.80	-0.80	-1.50	-2.20	-3.10	-2.90	-2.30	-1.50	-0.80
$\delta^{18}\text{O}_{run-off}$	[‰]	mod.	-25.62	-25.58	-22.52	-18.57	-15.38	-13.13	-13.00	-14.50	-15.87	-17.95	-19.98	-23.88
run-off $_{MAR}$	[km ³ /mo]	mod.	0.03	0.02	0.02	0.03	0.56	2.98	5.99	5.23	0.95	0.08	0.05	0.03

Table 2. Run-off (precipitation and surface melt) and glacial meltwater (being basal melt, front melt, calving and melange melt) flux for all glaciers terminating into the inner part of Godthåbsfjord and for each glacier individually. The width, terminus height and InSAR velocity (Joughin, 2010) for each of the glaciers are used to downscale the total glacial meltwater contribution to a glacier specific estimate. The MAR run-off distribution is used to split up the run-off calculated here.

	glacier contribution [%]	glacial meltwater [km ³ /yr]	run-off MAR [%]	run-off MAR [km ³ /yr]	run-off contribution [km ³ /yr]	total freshwater [km ³ /yr]
total	100	7.8	100	13.0	3.8	11.5
KNS	62	4.8	37	4.8	1.4	6.2
AS	5	0.4	15	1.9	0.5	0.9
QS	1	0.1	10	1.4	0.4	0.5
NS	31	2.4	26	3.4	1.0	3.4
KS	1	0.1	12	1.5	0.5	0.5

Table 3. Sensitivity to isotopic composition, surface layer thickness and velocity (see Figure 7.

	default	reasonable changes	resulting glacial meltwater flux change
summer velocity	8 cm/s	±2.5 cm/s	±2.3 km ³ /yr
$\delta^{18}\text{O}_{ice}$	-28‰	-2 ‰	-1.4 km ³ /yr
$\delta^{18}\text{O}_{sea}$	see Table 1	±0.1 ‰	±0.9 km ³ /yr
$\delta^{18}\text{O}_{run-off}$	see Table 1	±1 ‰	±0.3 km ³ /yr

APPENDIX F. MANUSCRIPT SUBMITTED TO JOURNAL OF
GEOPHYSICAL RESEARCH EARTH SURFACE: ESTIMATING THE
GLACIAL MELTWATER CONTRIBUTION TO THE FRESHWATER BUDGET
140 FROM SALINITY AND $\delta^{18}\text{O}$ MEASUREMENTS IN GODTHÅBSFJORD

Bibliography

- Ahlstrøm, A. P., Andersen, S. B., Andersen, M. L., Machguth, H., Nick, F. M., Joughin, I., Reijmer, C. H., van de Wal, R. S. W., Merryman Boncori, J. P., Box, J. E., Citterio, M., van As, D., Fausto, R. S., and Hubbard, A. (2013). Seasonal velocities of eight major marine-terminating outlet glaciers of the greenland ice sheet from continuous in situ gps instruments. *Earth System Science Data*, 5(2):277–287.
- Alexander, D., Davies, T., and Shulmeister, J. (2013). Basal melting beneath a fast-flowing temperate tidewater glacier. *Annals of Glaciology*, 54(63):265–271.
- Aschwanden, A., Aðalgeirsdóttir, G., and Khroulev, C. (2012a). Hindcasting to measure ice sheet model sensitivity to initial states. *The Cryosphere Discussions*, 6(6):5069–5094.
- Aschwanden, A., Bueler, E., Khroulev, C., and Blatter, H. (2012b). An enthalpy formulation for glaciers and ice sheets. *Journal of Glaciology*, 58(209):441–457.
- Bamber, J., Layberry, R., and Gogineni, S. (2001). A new ice thickness and bed data set for the Greenland ice sheet. I- Measurement, data reduction, and errors. *Journal of Geophysical Research. D. Atmospheres*, 106:33.
- Bamber, J. L., Griggs, J. a., Hurkmans, R. T. W. L., Dowdeswell, J. a., Gogineni, S. P., Howat, I., Mougintot, J., Paden, J., Palmer, S., Rignot, E., and Steinhage, D. (2013). A new bed elevation dataset for Greenland. *The Cryosphere*, 7(2):499–510.
- Bhatia (2011). Seasonal evolution of water contributions to discharge from a Greenland outlet glacier: insight from a new isotope-mixing model. 57(205):929–941.
- Box, J. and Rinke, A. (2003). Evaluation of Greenland ice sheet surface climate in the HIRHAM regional climate model using automatic weather station data. *Journal of climate*, pages 1302–1319.
- Brown, C., Meier, M., and Post, A. (1982). Calving speed of Alaska tidewater glaciers, with application to Columbia Glacier. Technical report, U.S. Department of the Interior.
- Budd, W. and Warner, R. (1996). A computer scheme for rapid calculations of balance flux distributions. *Annals of Glaciology*.
- Bueller, E. and Brown, J. (2009). Shallow shelf approximation as a “sliding law” in a thermomechanically coupled ice sheet model. *Journal of Geophysical Research*, 114(F3):1–21.

- Bueler, E. and Van Pelt, W. (2014). Mass-conserving subglacial hydrology in the parallel ice sheet model. *Geoscientific Model Development Discussions*, 7(4):4705–4775.
- Cohen, I. and Kundu, P. (2004). *Fluid Mechanics*. Elsevier Science.
- Coplen, T. (1994). Reporting of stable hydrogen, carbon, and oxygen isotopic abundances. *Pure Appl. Chem.*
- Dahl-Jensen, D. and Gundestrup, N. (1987). Constitutive properties of ice at dye 3, greenland. *The Physical Basis of Ice Sheet Modelling*.
- Dansgaard, W. (1964). Stable isotopes in precipitation. *Tellus XVI*.
- Dansgaard, W., Johnson, S., Clausen, H. B., Dahl-Jensen, D., Gundestrup, N., Hammer, C., Hvidberg, C., Steffensen, J., Sveinbjornsdottir, A., Jouzel, J., and Bond, G. (1993). Evidence for general instability of past climate from a 205-kyr ice-core record. *nature*, 364.
- Dansgaard, W., White, J., and Johnson, S. (1989). The abrupt termination of the Younger Dryas climate event. *Nature*, 339.
- DellaGiustina, D. (2011). Regional modeling of greenland’s outlet glaciers with the parallel ice sheet model. Master’s thesis, University of Alaska, Fairbanks, M.S. Computational Physics.
- Dethloff, K., Schwager, M., Christensen, J. H., Kiilsholm, S., Rinke, a., Dorn, W., Jung-Rothenhäusler, F., Fischer, H., Kipfstuhl, S., and Miller, H. (2002). Recent Greenland Accumulation Estimated from Regional Climate Model Simulations and Ice Core Analysis*. *Journal of Climate*, 15(19):2821–2832.
- Durand, G., Gagliardini, O., Favier, L., Zwinger, T., and le Meur, E. (2011). Impact of bedrock description on modeling ice sheet dynamics. *Geophysical Research Letters*, 38(20):6–11.
- Echelmeyer, K.A., H. W. L. C. and Mitchell, J. (1994). The role of the margins in the dynamics of an active ice stream. *J. Glaciol.*
- Eerola, K. (2006). About the performance of the Hirlam version 7.0. *hirlam.org*, (51):93–102.
- Ettema, J., van den Broeke, M. R., van Meijgaard, E., van de Berg, W. J., Bamber, J. L., Box, J. E., and Bales, R. C. (2009). Higher surface mass balance of the Greenland ice sheet revealed by high-resolution climate modeling. *Geophysical Research Letters*, 36(12):4–8.
- Fettweis, X., Tedesco, M., van den Broeke, M., and Ettema, J. (2011). Melting trends over the greenland ice sheet (1958–2009) from spaceborne microwave data and regional climate models. *The Cryosphere*.
- Fischer, P. (1998). simple model for the influence of push-morainial banks on the calving and stability of glacial tidewater termini. (146):31–41.
- Fowler, A. and Larson, D. (1978). On the Flow of Polythermal Glaciers. I. Model and Preliminary Analysis. *Proceedings of the Royal Society of Lonon. Series A, Mathematical and Physical Sciences*, 363(1713):217–242.

- Fowler, A. and Larson, D. (1980a). On the Flow of Polythermal Glaciers. II. Surface Wave Analysis. 370(1741):155–171.
- Fowler, A. and Larson, D. (1980b). The uniqueness of steady state flows of glaciers and ice sheets. *Geophys. J. R. astr. Soc*, 63:333–345.
- Glen, J. W. (1955). The Creep of Polycrystalline Ice. *Proceedings of the Royal Society A: Mathematical, Physical and Engineering Sciences*, 228(1175):519–538.
- Greve, R. and Blatter, H. (2009). *Dynamics of Ice Sheets and Glaciers*. Advances in Geophysical and Environmental Mechanics and Mathematics. Springer Berlin Heidelberg, Berlin, Heidelberg.
- GRIP-Members (1993). climate instability during the last interglacial period recorded in the GRIP ice core. *nature*, 364.
- Groote, P., Stuiver, M., White, J., Johnsen, S. J., and Jouzel, J. (1993). comparison of oxygen isotope records from GISP2 and GRIP Greenland ice cores. *nature*, 366.
- Habermann, M., Maxwell, D., and Truffer, M. (2012). Reconstruction of basal properties in ice sheets using iterative inverse methods. *Journal of Glaciology*, 58(210):795–807.
- Hardy, R., Bamber, J. L., and Orford, S. (2000). The delineation of drainage basins on the Greenland ice sheet for mass-balance analyses using a combined modelling and geographical information system approach. *Hydrological Processes*.
- Heide-Jørgensen, M., Iversen, M., Nielsen, N., Lockyer, C., Stern, H., and Ribergård, M. (2011). Harbour porpoises respond to climate change. *Ecol Evol*.
- Helm, V., Humbert, A., and Miller, H. (2014). Elevation and elevation change of Greenland and Antarctica derived from Cryosat-2. *The Cryosphere*, 8(4):1539–1559.
- Holland, D. M., Thomas, R. H., de Young, B., Ribergaard, M. H., and Lyberth, B. (2008). Acceleration of Jakobshavn Isbræ triggered by warm subsurface ocean waters. *Nature Geoscience*, 1(10):659–664.
- Hooke, R. (2005). *Principles of glacier mechanics*. Cambridge University Press.
- Hutter, K. (1981). The effect of longitudinal strain on the shear stress of an ice sheet: in defence of using stretched coordinates. *Journal of Glaciology*, 27(95).
- Hutter, K. (1983). *Theoretical Glaciology: Material Science of Ice and the Mechanics of Glaciers and Ice Sheets*.
- Hutter, K., Yakowitz, F., and Szidarovszky, F. (1986). A numerical study of plane ice-sheet flow. *Journal of Glaciology*, 32(111).
- Imbrie, John D.; McIntyre, A. (2006). Specmap time scale developed by Imbrie et al., 1984 based on normalized planktonic records (normalized $\delta^{18}O$ vs time, specmap.017).
- IPCC (2007). *Fourth Assessment Report: Climate Change 2007: The AR4 Synthesis Report*. Geneva: IPCC.

- IPCC (2013). *Climate Change 2013: The Physical Science Basis. Contribution of Working Group I to the Fifth Assessment Report of the Intergovernmental Panel on Climate Change*. Cambridge University Press, Cambridge, United Kingdom and New York, NY, USA. 1535pp.
- Johnsen, S., Dahl-Jensen, D., Gundestrup, N., Steffensen, J., Clausen, H., Miller, H., Masson-Delmotte, V., Sveinbjörnsdóttir, A., and White, J. (2001). Oxygen isotope and palaeotemperature records from six greenland ice-core stations: Camp century, dye-3, grip, gisp2, renland and northgrip. *J. Quaternary Sci.*
- Johnson, S., Clausen, H., Dansgaard, W., Gundestrup, N., Hammer, C., Andersen, U., Andersen, K., Hvidberg, C., Dahl-Jensen, D., Steffensen, J., Shoji, H., Sveinbjörnsdóttir, A., White, J., Jouzel, J., and Fisher, D. (1997). The d18O record along the Greenland Ice Core Project deep ice core and the problem of possible Eemian climatic instability. *Journal of Geophysical Research*, 102(C12).
- Joughin, I., Smith, B., Howat, I., Scambos, T., and Moon, T. (2010). Greenland flow variability from ice-sheet-wide velocity mapping. *Journal of Glaciology*, 56(197):415–430.
- Joughin, I., Smith, B. E., Howat, I. M., Floricioiu, D., Alley, R. B., Truffer, M., and Fahnestock, M. (2012). Seasonal to decadal scale variations in the surface velocity of Jakobshavn Isbrae, Greenland: Observation and model-based analysis. *Journal of Geophysical Research*, 117(F2):1–20.
- Khan, S. A., Kjeldsen, K. K., Kjær, K. H., Bevan, S., Luckman, A., Aschwanden, A., Björk, A. A., Korsgaard, N. J., Box, J. E., van den Broeke, M., van Dam, T. M., and Fitzner, A. (2014). Glacier dynamics at helheim and kangerdlugssuaq glaciers, southeast greenland, since the little ice age. *The Cryosphere*, 8(4):1497–1507.
- Kiilsholm, S., Hesselberg Christensen, J., Dethloff, K., and Rinke, A. (2003). Net accumulation of the Greenland ice sheet: High resolution modeling of climate changes. *Geophysical Research Letters*, 30(9):1485.
- Kjeldsen, K., Kjaer, K., Rysgaard, S., and Mortensen, J. (2011). Drainage of ice-dammed lakes and glacier retreat - a link. *American Geophysical Union, Fall Meeting 2011, abstract C23C-0507*, 23:507.
- Lea, J. M., Mair, D. W. F., Nick, F. M., Rea, B. R., van As, D., Morlighem, M., Nienow, P. W., and Weidick, A. (2014a). Fluctuations of a greenlandic tidewater glacier driven by changes in atmospheric forcing: observations and modelling of kangiata nunaata sermia, 1859–present. *The Cryosphere Discussions*, 8(2):2005–2041.
- Lea, J. M., Mair, D. W. F., Nick, F. M., Rea, B. R., Weidick, A., Kjær, K., Morlighem, M., van As, D., and Schofiels, J. (2014b). Terminus-driven retreat of a major southwest greenland tidewater glacier during the early 19th century: insights from glacier reconstructions and numerical modelling. *Journal of Glaciology*.
- Levermann, A., Albrecht, T., Winkelmann, R., Martin, M. a., Haseloff, M., and Joughin, I. (2012). Kinematic first-order calving law implies potential for abrupt ice-shelf retreat. *The Cryosphere*, 6(2):273–286.

- Lliboutry, L. and Duval, P. (1985). Various Isotropic and Anisotropic Ices Found in Glaciers and Polar Ice Caps and their Corresponding Rheologies. *Annales Geophysicae*, 3(2):207–224.
- Lucas-Picher, P., Wulff-Nielsen, M., Christensen, J. H., Aðalgeirsdóttir, G., Mottram, R., and Simonsen, S. B. (2012). Very high resolution regional climate model simulations over Greenland: Identifying added value. *Journal of Geophysical Research*, 117(D2):1–16.
- Luckman, A., Murray, T., de Lange, R., and Hanna, E. (2006). Rapid and synchronous ice-dynamic changes in east greenland. *Geophysical Research Letters*.
- MacAyeal, D. (1989a). Ice-shelf response to ice-stream discharge fluctuations: iii. the effects of ice-stream imbalance on the ross ice shelf, Antarctica. *October*, 35(119):38–42.
- Macayeal, D., Bindschadler, R., and Scambos, T. (1995). Basal friction of ice stream E, West Antarctica. *Journal of Glaciology*.
- MacAyeal, D. R. (1989b). Large-Scale Ice Flow Over a Viscous Basal Sediment: Theory and Application to Ice Stream B, Antarctica. *Journal of Geophysical Research*, 94(B4):4071–4087.
- McNabb, R. W., Hock, R., Rasmussen, L. A., Ahn, Y., Braun, M., Conway, H., Herreid, S., Joughin, I., Pfeffer, W. T., Smith, B. E., and Truffer, M. (2012). Using surface velocities to calculate ice thickness and bed topography: a case study at Columbia Glacier, Alaska, USA. 58(212):1–14.
- Meinshausen, M., Smith, S., Calvin, K., Daniel, J., Kainuma, M., Lamarque, J.-F., Matsumoto, K., Montzka, S., Raper, S., Riahi, K., Thomson, A., Velders, G., and Vuuren, D. (2011). The RCP greenhouse gas concentrations and their extensions from 1765 to 2300. *Climatic Change*, 109(1):213–241.
- Michel, C., Bluhm, B., Gallucci, V., Gaston, A., Gordillo, F., Gradinger, R., Hopcroft, R., Jensen, N., Mustonen, T., Niemi, A., and Nielsen, T. (2012). Biodiversity of arctic marine ecosystems and responses to climate change. *Biodiversity*, 13(3-4):200–214.
- Moon, T. and Joughin, I. (2008). Changes in ice front position on Greenland’s outlet glaciers from 1992 to 2007. *Journal of Geophysical Research*, 113(F2):1–10.
- Moon, T., Joughin, I., Smith, B., and Howat, I. (2012). 21st-century evolution of greenland outlet glacier velocities. *Science*.
- Morland, L., Smith, G. D., and Boulton, G. S. (1984). Basal Sliding Relations Deduced from Ice-Sheet Data. *Journal of Glaciology*, 30(105):131–139.
- Morlighem, M., Rignot, E., Seroussi, H., Larour, E., Ben Dhia, H., and Aubry, D. (2011). A mass conservation approach for mapping glacier ice thickness. *Geophysical Research Letters*, 38(19):1–6.
- Mortensen, J., Bendtsen, J., Lennert, K., and Rysgaard, S. (subm). Seasonal variability of the circulation system in a west greenland tidewater outlet glacier fjord. *Journal of Geophysical Research – Earth Surface*.

- Mortensen, J., Bendtsen, J., Motyka, R. J., Lennert, K., Truffer, M., Fahnestock, M., and Rysgaard, S. (2013). On the seasonal freshwater stratification in the proximity of fast-flowing tidewater outlet glaciers in a sub-Arctic sill fjord. *Journal of Geophysical Research: Oceans*, 118(3):1382–1395.
- Mortensen, J., Lennert, K., Bendtsen, J., and Rysgaard, S. (2011). Heat sources for glacial melt in a sub-Arctic fjord (Godthåbsfjord) in contact with the Greenland Ice Sheet. *Journal of Geophysical Research*, 116(C1):1–13.
- Mottram, R., Aðalgeirsdóttir, G., Bober, F., Lucas-Picher, P., Stendel, M., Christensen, O., and Christense, J. (2012). Reconstructing the surface mass balance of the greenland ice sheet with the regional climate model hirham5, 1989-2011. *The Cryosphere*, in preparation.
- Motyka, R., Hunter, L., Echelmeyer, K., and Connor, C. (2003). Submarine melting at the terminus of a temperate tidewater glacier, leconte glacier, alaska. *Annals Glaciol.*
- Nick, F. and Oerlemans, J. (2006). Dynamics of tidewater glaciers: comparison of three models. *Journal of Glaciology*, 52(177):183–190.
- Nick, F. M., Vieli, A., Andersen, M. L., Joughin, I., Payne, A., Edwards, T. L., Pattyn, F., and van de Wal, R. S. W. (2013). Future sea-level rise from Greenland’s main outlet glaciers in a warming climate. *Nature*, 497(7448):235–8.
- Nye, J. F. (1952). The Mechanics of Glacier Flow. *Journal of Glaciology*, pages 82–93.
- Nye, J. F. (1957). The Distribution of Stress and Velocity in Glaciers and Ice-Sheets. *Proceedings of the Royal Society A: Mathematical, Physical and Engineering Sciences*, 239(1216):113–133.
- Paterson, W. and Budd, W. (1982). Flow parameters for ice sheet modeling. *Cold Regions Science and Technology*, 6:175–177.
- Paterson, W. and Cuffey, K. (2010). *The Physics of glacier*, volume 1969.
- Pattyn, F., Schoof, C., Perichon, L., Hindmarsh, R. C. a., Bueler, E., de Fleurian, B., Durand, G., Gagliardini, O., Gladstone, R., Goldberg, D., Gudmundsson, G. H., Huybrechts, P., Lee, V., Nick, F. M., Payne, a. J., Pollard, D., Rybak, O., Saito, F., and Vieli, a. (2012). Results of the Marine Ice Sheet Model Intercomparison Project, MISMIP. *The Cryosphere Discussions*, 6(1):267–308.
- PISM-authors (2010). PISM, a Parallel Ice Sheet Model: User’s Manual. Technical report.
- Quiquet, a., Punge, H. J., Ritz, C., Fettweis, X., Kageyama, M., Krinner, G., Salas y Mélia, D., and Sjolte, J. (2012). Large sensitivity of a Greenland ice sheet model to atmospheric forcing fields. *The Cryosphere Discussions*, 6(2):1037–1083.
- Rae, J. G. L., Aðalgeirsdóttir, G., Edwards, T. L., Fettweis, X., Gregory, J. M., Hewitt, H. T., Lowe, J. a., Lucas-Picher, P., Mottram, R. H., Payne, a. J., Ridley, J. K., Shannon, S. R., van de Berg, W. J., van de Wal, R. S. W., van den Broeke, M. R., and Lucas-Picher, b. (2012). Greenland ice sheet surface mass balance: evaluating simulations and making projections with regional climate models. *The Cryosphere*, 6(6):1275–1294.

- Reddy, J. (2005). *An Introduction to the Finite Element Method (Engineering Series)*. McGraw-Hill Science/Engineering/Math.
- Reeh, N., Oerter, H., and Thomsen, H. (2002). Comparison between Greenland ice-margin and ice-core oxygen-18 records. *Annals of Glaciology*.
- Rignot, E., Box, J. E., Burgess, E., and Hanna, E. (2008). Mass balance of the Greenland ice sheet from 1958 to 2007. *Geophysical Research Letters*, 35(20):1–5.
- Rignot, E. and Kanagaratnam, P. (2006). Changes in the velocity structure of the Greenland Ice Sheet. *Science (New York, N.Y.)*, 311(5763):986–90.
- Rignot, E., Koppes, M., and Velicogna, I. (2010). Rapid submarine melting of the calving faces of West Greenland glaciers. *Nature Geoscience*, 3(3):187–191.
- Rignot, E. and Mouginot, J. (2012). Ice flow in Greenland for the International Polar Year 2008–2009. *Geophysical Research Letters*, 39(11):1–7.
- Roeckner, E., Bäuml, G., Bonaventura, L., Brokopf, R., Esch, M., Giorgetta, M., Hagemann, S., Kirchner, I., Kornblüeh, L., Manzini, E., Rhodin, A., Schlese, U., Schulzweida, U., and Tompkins, A. (2003). The atmospheric general circulation model ECHAM5: Part 1: Model description. *Max-Planck-Institut für Meteorologie, Hamburg, Germany*, (349).
- Schoof, C. (2006a). A variational approach to ice stream flow. *Journal of Fluid Mechanics*, 556:227.
- Schoof, C. (2006b). Variational methods for glacier flow over plastic till. *Journal of Fluid Mechanics*, 555:299.
- Simonsen, S., Grinsted, A., Aðalgeirsdóttir, G., and Hvidberg, C. (2013). How does the choice of validation data reflect the preferred model-parameters used in initialization of the present-day Greenland ice sheet? *Geophysical Research Abstracts, EGU General Assembly 2013*, 15(EGU2013-8051).
- Sjolte, J., Hoffmann, G., Johnsen, S. J., Vinther, B. M., Masson-Delmotte, V., and Sturm, C. (2011). Modeling the water isotopes in Greenland precipitation 1959–2001 with the meso-scale model REMO-iso. *Journal of Geophysical Research*, 116(D18):D18105.
- Solgaard, A. and Langen, P. (2012). Multistability of the Greenland ice sheet and the effects of an adaptive mass balance formulation. *Climate Dynamics*, 39(7–8):1599–1612.
- Sørensen, L. S., Simonsen, S. B., Nielsen, K., Lucas-Picher, P., Spada, G., Aðalgeirsdóttir, G., Forsberg, R., and Hvidberg, C. S. (2011). Mass balance of the Greenland ice sheet (2003–2008) from ICESat data – the impact of interpolation, sampling and firn density. *The Cryosphere*, 5(1):173–186.
- Stendel, M., Christensen, J. H., and Petersen, D. (2008). Arctic Climate and Climate Change with a Focus on Greenland. *Advances in Ecological Research*, 40(07):2–5.

- Storr-Paulsen, M., Wieland, K., Hovgaard, H., and Raetz, H.-J. (2004). Stock structure of atlantic cod (*gadus morhua*) in west greenland waters: implications of transport and migration. *ICES Journal of Marine Science: Journal du Conseil*, 61(6):972–982.
- Thomas, R., Frederick, E., Krabill, W., Manizade, S., and Martin, C. (2009). Recent changes on Greenland outlet glaciers. *Journal of Glaciology*, 55(189):147–162.
- Truffer, M. and Echelmeyer, K. A. (2003). Of isbræand ice streams. *Annals Of Glaciology*, (1996).
- van As, D. (2011). Warming, glacier melt and surface energy budget from weather station observations in the Melville Bay region of northwest Greenland. 57(202):208–220.
- van As, D., Andersen, M., Petersen, D., Fettweis, X., van Angelen, J., Lenaerts, J., van den Broeke, M., Lea, M., Bøggild, C., Ahlstrøm, A., and Steffen, K. (2014). Increasing meltwater discharge from the nuuk region of the greenland ice sheet and implications for mass balance (1960–2012). *J. Glac.*
- van den Broeke, M., Bamber, J., Ettema, J., Rignot, E., Schrama, E., van de Berg, W. J., van Meijgaard, E., Velicogna, I., and Wouters, B. (2009). Partitioning recent greenland mass loss. *Science*.
- van Pelt, W. J. J., Oerlemans, J., Reijmer, C. H., Pettersson, R., Pohjola, V. a., Isaksson, E., and Divine, D. (2013). An iterative inverse method to estimate basal topography and initialize ice flow models. *The Cryosphere Discussions*, 7(2):873–920.
- Versteegh, E. A. A., Blicher, M. E., Mortensen, J., Rysgaard, S., Als, T. D., and Jr., A. D. W. (2012). Oxygen isotope ratios in the shell of *mytilus edulis*: archives of glacier meltwater in greenland? *Biogeosciences*, 9(12):5231–5241.
- Weertman, J. (1957). Deformation of floating ice shelves. *J. Glaciol.*, 3(21):38–42.
- Winkelmann, R., Martin, M. a., Haseloff, M., Albrecht, T., Bueler, E., Khroulev, C., and Levermann, A. (2011). The Potsdam Parallel Ice Sheet Model (PISM-PIK) - Part 1: Model description. *The Cryosphere*, 5(3):727–740.
- Zwally, H., Abdalati, W., Herring, T., Larson, K., Saba, J., and Steffen, K. (2002). Surface melt-induced acceleration of greenland ice-sheet flow. *Science*.